Department of Communications and Networking

Energy-Efficient Mobility for Small-Cell Overlaid Cellular Networks

Muhammad Tayyab

Aalto University

DOCTORAL DISSERTATIONS

Aalto University publication series
DOCTORAL DISSERTATIONS 43/2021

Energy-Efficient Mobility for Small-Cell Overlaid Cellular Networks

Muhammad Tayyab

A doctoral dissertation completed for the degree of Doctor of Science (Technology) to be defended, with the permission of the Aalto University School of Electrical Engineering, Remote connection link (e.g. Zoom), on 4 May 2021 at 12 o'clock noon.

Aalto University
School of Electrical Engineering
Department of Communications and Networking

Supervising professor
Professor Riku Jäntti, Aalto University, Finland

Thesis advisor
Dr. Xavier Gelabert, Huawei Technologies Sweden AB, Sweden

Preliminary examiners
Professor Sergey Andreev, Tampere University, Finland
Dr. Mads Lauridsen, Nokia Bell Labs, Aalborg, Denmark

Opponents
Professor Erik G. Larsson, Linköping University (LiU), Sweden
Professor Sergey Andreev, Tampere University, Finland

Aalto University publication series
DOCTORAL DISSERTATIONS 43/2021

ISBN 978-952-64-0319-9 (printed)
ISBN 978-952-64-0320-5 (pdf)
ISSN 1799-4934 (printed)
ISSN 1799-4942 (pdf)
http://urn.fi/URN:ISBN:978-952-64-0320-5

Unigrafia Oy
Helsinki 2021

Finland

NORDIC SWAN ECOLABEL
Printed matter
4041-0619

Aalto University

Abstract

Aalto University, P.O. Box 11000, FI-00076 Aalto www.aalto.fi

Author
Muhammad Tayyab

Name of the doctoral dissertation
Energy-Efficient Mobility for Small-Cell Overlaid Cellular Networks

Publisher School of Electrical Engineering

Unit Department of Communications and Networking

Series Aalto University publication series DOCTORAL DISSERTATIONS 43/2021

Field of research Communications Engineering

Manuscript submitted 15 December 2020 **Date of the defence** 4 May 2021

Permission for public defence granted (date) 18 February 2021 **Language** English

☐ **Monograph** ☒ **Article dissertation** ☐ **Essay dissertation**

Abstract

To satisfy the ever-growing demand for enhanced data rate in future cellular networks, an ultra-densification approach is introduced to shrink the coverage of base stations (BSs) and improve frequency reuse. A gain in system capacity is anticipated by increasing the density of BSs; however this gain is expected to come at the expense of a high number of handovers (HOs), increased HO delays, increased HO failures (HOFs), and a high ping pong (PP) rate, which for moderate-to-high-speed users implies significant signaling overhead traffic resulting in an unsatisfactory user experience.

In this thesis, we provide a simulation analysis to study the performance of current 3GPP cellular networks (e.g. Long Term Evolution (LTE)/ New Radio (NR)) with a legacy downlink handover (DL-HO) procedure by taking into account the cell sizes and user mobility. In particular, the potential problems of HOFs are highlighted especially in the case of ultra-densification. Moreover, this work derives a power consumption model and addresses the signaling overhead and power consumption that results from the transmission and reception of HO signaling both at the BS and at the User Equipment (UE) during DL-HO.

The DL-HO analysis exhibits that the measurement report (MeasReport) transmission is the largest contributor to air-interface signaling and its power consumption is higher than random access channel (RACH) signaling and the signaling confirming the HO. In order to cope with the problem of high MeasReport signaling and effectively reduce the associated power consumption, a handover that is based on the uplink (UL) reference signal, referred to here as UL-HO, is proposed that exploits uplink (UL) reference signals (RSs), namely the sounding reference signal (SRS), transmitted by UEs. The performance of UL-HO is compared with DL-HO to quantify the potential benefits in terms of reduction in HO rates, HOFs, PPs, UE, and BS power consumption.

After this, we then highlight another major challenge of today's cellular networks which is the increasing demand for voice and data services in fast-moving public transportation (i.e. bus, tram, train, subway, etc.), especially in urban areas. To this end, we investigate the utilization of mobile relay nodes (MRNs) in vehicles to facilitate efficient group HO and reduce the energy consumption for all on-board UEs. In this thesis, we also address the DL-HO performance of an MRN to identify the causes of MRN HOFs towards the donor BS (DBS) that are more critical for the on-board UEs. To sort out the problem of MRN HOF to the DBS, we extend the applicability of the UL-HO scheme for the MRN to eliminate the MeasReprot signaling during MRN HO to the DBS. Therefore the HO delay can be reduced, decreasing the chances of single point of failure (SPoF) and thus, uninterrupted services can be provided to on-board UEs. Moreover, we analyze the impact of on-board UE cluster size on HO performance and the associated power consumption.

Keywords

ISBN (printed) 978-952-64-0319-9 **ISBN (pdf)** 978-952-64-0320-5

ISSN (printed) 1799-4934 **ISSN (pdf)** 1799-4942

Location of publisher Helsinki **Location of printing** Helsinki **Year** 2021

Pages 102 **urn** http://urn.fi/URN:ISBN:978-952-64-0320-5

Preface

The research work for this thesis was carried out during the years 2018-2020 at Huawei Technologies Oy (Finland) Co. Ltd. This work was funded by the European Union's Horizon 2020 research and innovation program, EU Project SECRET under grant agreement H2020-MSCA-ITN-2016 SECRET-722424. This work was done under the supervision of Dr. Xavier Gelabert, Senior Researcher (thesis advisor), and Dr. George P. Koudouridis, Principal Researcher (thesis co-advisor), at Huawei Technologies Sweden AB, Kista, Sweden. Hence, I wish to express the deepest gratitude to Dr. Xavier Gelabert and Dr. George P. Koudouridis, for the new ideas, useful comments, guidance, valuable insights, engagement through the learning process and indispensable support to finalize this thesis. I would like to express my gratitude to Prof. Riku Jäntti (Supervising Professor) for giving me the opportunity to work as a full-time doctoral student and for providing support and guidance throughout my doctoral studies. It has been a pleasure and a great experience working with all during my doctoral program.

I also wish to thank my thesis preliminary examiners for their valuable reviews and constructive comments that helped to improve the quality of this thesis. The time and effort put in reviewing this dissertation are highly acknowledged. I would also like to express my gratitude to the opponents at the public defense of this thesis.

I would like to thank the EU Horizon 2020 research and innovation program, for the support of funds. The project SECRET was a great opportunity for me to work with many experienced people from Huawei and other project partners from universities and companies, such as Instituto de Telecomunicações, Technische Universität Dresden, University of Bradford, University of Patras, Acticom GmbH, PROEF, and Saras Technology Ltd. I would also like to thank the Nokia Foundation, for providing me with a Nokia Foundation Scholarship 2019, an encouragement grant for doctoral students in Finland.

I would like to thank my parents for supporting me in life and studies. Without that solid base, I wouldn't have made it this far. I would finally, like to thank my loved ones who have supported me throughout the entire process: I will be forever grateful for your endless love, permanent encouragement, and support that was essential during the past years.

Oulu, March 2021
Muhammad Tayyab

Contents

List of Abbreviations

1G/2G/3G	first/second/third generation
3GPP	3rd generation partnership project
AMF	access and mobility management function
BBU	baseband unit
BS	base station
CDMA	code-division multiple access
CRC	cyclic redundancy check
D2D	device to device
DBS	donor base station
DL	downlink
HetNets	heterogeneous networks
HO	handover
HOcmd	handover command
HOconf	handover confirm
HOF	handover failure
HOFR	handover failure ratio
HOR	handover rate
IAB	Integrated Access and Backhaul
ISD	inter-site distance
LTE	long-term evolution
MAC	medium access control
MCS	modulation and coding scheme
MeasReport	measurement report
MME	mobility management entity

MR	mobile relay
MRN	mobile relay node
MSC	mobile small cell
NR	new radio
OPEX	operational expenditure
O-RAN	open radio access network
PPR	ping-pong rate
QAM	quadrature amplitude modulation
QoE	quality of experience
QPSK	quadrature phase-shift keying
RACH	random access channel
RAT	radio access technology
RB	resource block
RE	resource element
RLC	radio link control
RLF	radio link failure
RRU	radio remote unit
RRM	radio resource management
RS	reference signal
RSRP	reference signal received power
s-BS	serving base station
SGW	serving gateway
SPoF	single point of failure
SRS	sounding reference signal
TB	transport block
t-BS	target base station
TTT	time-to-trigger
TS	technical specification
TU	typical urban
UE	user equipment
UCNC	user-centric no-cell

UDG	user data gateway
UL	uplink
UPF	user plane function

List of Symbols

Greek

Δf	subcarrier spacing
$\Delta t_x^s / \Delta T$	duty cycle
ΔT	time period in seconds
η	power amplifier efficiency

Latin

B_{RB}	bandwidth of RB
B_{sys}	system bandwidth
f_c	carrier frequency
$G_{i,j}$	total path gain for i^{th} UE and j^{th} t-BS
$\|h\|^2$	fast fading
I_{MCS}	MCS index
L_{RE}	number of bits in a RE
L_s	size of signaling message
L_{TB}	number of information bits per TB
L_{MR}	MeasReport signaling size in bits
L_{HOcmd}	HOcmd signaling size in bits
L_{HOconf}	HOconf signaling size in bits
N_{symb}^{RB}	number of symbols in an RB
N_{RB}^{DL}	number of DL RBs
N_{RB}^{UL}	number of UL RBs
N_{TB}^{DL}	number of DL TBs
N_{TB}^{UL}	number of UL TBs

N_{TB}^{s}	number of TBs per signaling message *s*
N_s	number of signaling messages
N_{TB}^{MR}	number of TBs per MeasReport signaling message
N_{TB}^{HOconf}	number of TBs per HOconf signaling message
N_{TB}^{HOcmd}	number of TBs per HOcmd signaling message
N_{TB}^{RACH}	number of TBs per RACH signaling message
$P_{x,sup}$	necessary supply power, *x*={*BS*, *UE*}
P_x	output transmitted power, *x*={*BS*, *UE*}
P_{BS}	BS power
P_{UE}	UE power
P_{BS}^{TB}	BS allocated power per TB
P_{UE}^{TB}	UE allocated power per TB
$P_{x,Tx}^{s}$	transmitted power per signaling message *s*, *x*={*BS*, *UE*}
$P_{BS,sup}^{s,Tx}$	BS supply power transmitting signaling *s*
$P_{RF,BS}$	BS RF equipment supply power
$P_{RF,UE}$	UE RF equipment supply power
P'_{BB}	BBU power consumption
$P_{UE,sup}^{s,Tx}$	UE supply power transmitting signaling *s*
P_{TxBB}	UE transmitted BBU power
$P_{x,sup}^{s,Tx}$	"peak" supply power, *x*={*BS*, *UE*}
$\bar{P}_{x,sup}^{s,Tx}$	transmitted time-averaged supply power, *x*={*BS*, *UE*}
P_{Rx}	received power
$P_{x,Rx}^{s}$	received power per signaling message, *x*={*BS*, *UE*}
P_n^s	additive white Gaussian noise
$P_{x,sup}^{s,Rx}$	supply power of signaling *s* reception, *x*={*BS*, *UE*}
P_{RxBB}	UE received BBU power
R_{Rx}	received data rate
Q_{in}	in-sync threshold

Q_{out}	out-of-sync threshold
R	cell radius in km
R_x^S	signaling rate
T_{slot}	time duration of one slot
T_{RB}	time duration of one RB
T_{symb}	symbol length
T_x^S	signaling s duration
T_{BS}^{HOcmd}	HOcmd signaling transmission time
T_{UE}^{MR}	MeasReport signaling transmission time
T_{UE}^{HOconf}	HOconf signaling transmission time
T_{UE}^{RACH}	RACH signaling transmission time

List of Publications

This doctoral dissertation consists of a summary of the following publications which are referred to in the text by their Roman numerals.

I M. Tayyab, X. Gelabert, and R. Jäntti. A Survey on Handover Management: From LTE to NR. *IEEE Access Journal*, Vol. 7, Issue 1, pp. 118907-118930, August 2019.

II M. Tayyab, G. P. Koudouridis, and X. Gelabert. A Simulation Study on LTE Handover and the Impact of Cell Size. Springer, *Broadnets Conference* 2018, LNICST 263, pp. 398-408, 2019.

III M. Tayyab, X. Gelabert, and R. Jäntti. A Simulation Study on Handover in LTE Ultra-Small Cell Deployment: A 5G Challenge. IEEE 5G World Forum Conference, pp. 388-392, Dresden, Germany, 2019.

IV M. Tayyab, G. P. Koudouridis, X. Gelabert, and R. Jäntti. Signaling Overhead and Power Consumption during Handover in LTE. IEEE Wireless Communications and Networking Conference (WCNC), Marrakech, Morocco, 2019.

V M. Tayyab, G. P. Koudouridis, X. Gelabert, and R. Jäntti. Receiver Power Consumption during Handover in LTE. IEEE 5G World Forum Conference, pp. 74-79, Dresden, Germany, 2019.

VI M. Tayyab, G. P. Koudouridis, X. Gelabert, and R. Jäntti. Handover Performance and Power Consumption Analysis of LTE Mobile Relays. *IEEE Vehicular Technology Conference (VTC) Conference*, Victoria, Canada, Dec 2020.

VII M. Tayyab, G. P. Koudouridis, X. Gelabert, and R. Jäntti. Uplink Reference Signals for Energy-Efficient Handover. *IEEE Access Journal*, Vol. 8, PP. 163060-163079, September 2020.

VIII M. Tayyab, G. P. Koudouridis, X. Gelabert, and R. Jäntti. Uplink Reference Signal Based Handover with Mobile Relay Node Assisted User Clustering. *IEEE Global Communications Conference (GLOBECOM)*, Taipei, Taiwan, Dec 2020.

IX M. Tayyab, G. P. Koudouridis, X. Gelabert, and R. Jäntti. Uplink Reference Signals for Power Efficient Handover in Cellular Networks with Mobile Relays. *IEEE Access Journal*, Vol. 9, PP. 24446-24461, Feb 2021.

Author's Contribution

Publication I : "A Survey on Handover Management: From LTE to NR"

The author reviewed the literature, organized it, and wrote the manuscript. The remaining authors also provided valuable insights and feedback that improved the paper.

Publication II : "A Simulation Study on LTE Handover and the Impact of Cell Size"

The author of this thesis had the main responsibility for planning and writing. The basic purpose of this paper was to understand the currently available version of the in-house MATLAB-based LTE System-Level simulator. Dr. Gelabert performed the simulations, provided his input to the system model and performance evaluation sections. Dr. George also provided valuable personal feedback.

Publication III : "A Simulation Study on Handover in LTE Ultra-Small Cell Deployment: A 5G Challenge"

The author of this thesis had the main responsibility for generating and analyzing the simulation results, planning, and writing the paper. The rest of the authors also provided valuable insights.

Publication IV : "Signaling Overhead and Power Consumption during Handover in LTE"

The author of this thesis had the main responsibility for generating and analyzing the simulation results, planning, and writing the paper. The author included the new metrics in the system-level simulator to find the signaling rate and power consumption due to the transmission of air-interface signaling messages

during handover (HO) in LTE. The other authors also provided valuable insights and support for finishing the paper.

Publication V : "Receiver Power Consumption during Handover in LTE"

The author of this thesis had the main responsibility for generating simulation results and writing the paper. The author included the new metrics in the system-level simulator to find the power consumption due to the reception of air-interface signaling messages during HO. The rest of the authors also provided valuable insights and support for finishing the paper.

Publication VI : "Handover Performance and Power Consumption Analysis of LTE Mobile Relays"

The author implemented the system-level simulation model required for studying Mobile Relays. The author of this thesis had the main responsibility for generating simulation results and writing the paper. The remaining authors provided valuable insights that improved the paper.

Publication VII : "Uplink Reference Signals for Energy-Efficient Handover"

The author implemented the system-level simulation model by integrating an in-house "Sounding Reference Signal (SRS) module" with the MATLAB-based system-level simulator (to use SRS for HO measurement). The author formulated the problems of HO and proposed an Uplink reference signal (UL RS) based HO method to overcome the problem of high signaling rate and power consumption due to Measurement Report signaling. The author derived the power consumption model, performed the simulation analysis, and wrote the paper. The rest of the authors also provided valuable insights.

Publication VIII : "Uplink Reference Signal Based Handover with Mobile Relay Node Assisted User Clustering Article"

The author implemented the system-level simulation model required for studying the impact of MR-assisted user clustering. The author of this thesis had the main responsibility for generating simulation results and writing the paper. The rest of the authors also provided valuable insights.

Publication IX : "Uplink Reference Signals for Power-Efficient Handover in Cellular Networks with Mobile Relays"

The author implemented the system-level simulation model to use SRS for the HO measurement of mobile relays. The author developed the UL RS-based HO method for mobile relays to improve the quality of experience of the users on-board. The author organized the manuscript and performed simulations and compared the UL-HO performance with legacy DL-HO schemes. The remaining authors also provided valuable insights.

1. Introduction

1.1 Background and Motivation

Cellular systems have seen massive growth in mobile data usage for the last few decades. There has been a rapid increase in mobile data usage over recent years (over 400 million fold from 2000-2015 [1]) that is anticipated to go up by almost 6-fold from 2017-2022 approaching 77 Exabytes per month in 2022 [2]. To satisfy these high data traffic demands, the ultra-cell-densification approach is introduced for current and future cellular networks. Small cells are, technically, a way to cope with high data demands. This approach improves the spectral efficiency of the cellular networks by squeezing the coverage area of base stations (BSs), thus reducing the number of UEs served by each BS and improving the frequency reuse. However, the ultra-densification approach increases the handover (HO) rate especially for moderate-to-high mobility UEs, i.e. the successive change of the handling BS for a moving user. In short, this approach increases the capacity of the network but at the cost of increased HO rates, higher signaling overheads, and power consumption caused by the HO procedure. The signaling overheads interrupt the data flow and thus reduce the throughput of the UEs [3]. High signaling traffic leads towards high power consumption which needs to be examined carefully. Furthermore, failure in the signaling system increases the outages and system latency resulting in potential loss of the operator's revenues.

In addition to supporting high data rates, future cellular networks should provide a reliable HO mechanism to improve the perceived quality of experience (QoE) for the end-user. The majority of current research works are focused on improving the capacity and throughput in small cell deployments, with fewer studies devoted to HO management. However, the challenge remains the building of reliable HO schemes which provide high data rates for moderate-to-high speed users in urban environments.

Another challenge for mobile operators is to provide energy-efficient network designs to support a large number of UEs and their high data traffic. The telecommunications industry is responsible for 0.4% of worldwide CO_2 emissions and data traffic is expected to increase ten times every five years, which will result in a 20 percent increase in energy consumption [4][5][6]. This directly impacts the environment through a significant contribution to global warming. A novel HO solution to reduce the HO rates and signaling overheads is a step forward to diminish energy consumption which has a direct impact on the operational expenditure (OPEX) of the operator and associated CO_2 emissions.

The above-mentioned HO challenges become more exacerbated for advanced mobility deployments such as on-demand Mobile Small Cells (MSCs) for further densification and energy off-loading. An on-demand MSC is a low power node providing small cell coverage when and where needed. In such deployments, MSCs can be implemented by Mobile Relay Nodes (MRNs) or by individual UEs via Device-to-Device (D2D) communication in order to provide network coverage on the move. MRNs can be roof-mounted on vehicles and trains to provide an MSC servicing on-board UEs while avoiding the associated HO overhead via group mobility. A future MSC vision in [7] shows that MSC based complex mobility scenarios essentially require robust signaling, and power-efficient HO schemes that should provide high data rates without interruptions.

1.1.1 Problem Formulation

The design of future ultra-dense networks implies a denser deployment of radio access infrastructure creating a larger number of smaller covering areas. As a result, mobility procedures will be invoked more often for mobile users moving across these smaller cells. In such dense radio access environments, the mobility requirements are becoming more challenging in terms of limiting the signaling overheads and power consumption in conjunction with improved robustness against HO failures (HOFs). In the 3rd Generation Partnership Project (3GPP) current cellular networks, i.e. Long Term Evolution (LTE) and New Radio (NR), downlink (DL) HO schemes (henceforth DL-HO), are used in which the serving and neighboring BSs transmit DL reference signals (RSs) so that UEs can measure and report back such measurements to the network. As we will discuss in this thesis, for future ultra-dense networks, the DL-HO is problematic in terms of HO performance, signaling overhead and energy consumption. In deployment scenarios where the serving BSs rapidly vary, e.g. in ultra-dense cellular networks or on-demand MSCs, reducing the measurement of DL RSs and other HO-related signaling has a great potential for improving the user's device battery lifetime.

In addition, the MSCs implemented through MRNs can still fail to HO to a new donor BS (DBS[1]) when moving at moderate-to-high speeds. Consequently, the connection of on-board UEs with the MRN will be lost, resulting in a bad user experience and high HO rates for the on-board UEs. This poses strict reliability requirements on the backhaul link to avoid becoming a single point of failure (SPoF) for the handover of multiple UEs.

Among the various problems arising in such DL-HO schemes, this thesis is concerned with the following three problems, namely P1, P2, and P3, along with the corresponding sub-problems:

P1) To identify the main DL-HO drawbacks and pitfalls, i.e. the main causes of DL-HOFs, the highest contributor to signaling overhead and power consumption.

The problem P1 can be further divided into the following five sub-problems:

[1] An MRN wirelessly connects to a serving BS called a DBS.

P1.1) What are the DL-HO challenges?

P1.2) What are the main causes of DL-HO failures?

P1.3) What are the major contributors to air-interface signaling overhead and associated transmitted power consumption due to HO signaling?

P1.4) What are the major contributors to received power consumption due to HO signaling?

P1.5) How to analyze the DL-HO performance in the presence of MSCs (implemented through MRNs) and what are the main causes of MRN HOF towards the DBSs?

P2) How to improve the existing DL-HO scheme by reducing HOF and signaling overheads?

P3) How to improve the HO procedure in MSC deployments implemented through MRNs, in terms of HO reliability (reduced HOFs) and energy efficiency?

In turn, problem P3 consists of one sub-problem:

P3.1) What is the impact of the on-board UEs cluster size on the HO performance and the associated power consumption?

To find the solution to the above-mentioned problems, we adopt system-level simulations which is deemed a good option, being well suited to the nature of the problem of this thesis.

1.2 Objective and Contribution of the Dissertation

Motivated by the importance of a reliable HO scheme for both stationary and MSCs deployment in fulfilling the future cellular network challenges, this thesis provides an uplink reference signal (UL RS) based mobility solution (termed UL-HO) that will improve HO and power-saving performance through the reduction of HO signaling overhead.

The main objective of this dissertation is to analyze and improve the HO performance in the current and future cellular networks, such as 4G, 5G, and B5G. This dissertation addresses a new HO solution and enhancements for achieving better mobility support in cellular systems. With the focus discussed in the last section, the goal of this dissertation is to provide solutions to the aforementioned problems and sub-problems with the adopted UL-HO scheme. A MATLAB based system-level simulator is used for performance evaluation. The main contributions of the dissertation, addressing the problems stated above, are summarized hereafter. Each contribution is supported by a specific publication, conveniently numbered using Roman numerals.

P1.C1) A brief literature survey is conducted for LTE and NR mobility management schemes to identify the DL-HO challenges, enhancing techniques, and key points for formulating an efficient HO scheme. This contribution is presented in Publication I and Chapter 2.

P1.C2) The main causes of DL-HOFs are identified through system-level simulations. It is observed that the measurement report transmission errors are the highest among others for both low (i.e. small cells) and high inter-site distances (ISDs). This contribution is linked to Publication II, Chapter 3, Section 3.4.1, and for ultra-small cell deployment see Publication III.

P1.C3) The system-level simulations are utilized to identify the main contributor to the air-interface signaling overhead. It is found that the measurement report transmission signaling has the highest contribution over the air-interface among other signaling transmissions. A transmitted power consumption model for both the UE and BS is derived to identify the main power consuming signaling message during transmission. This contribution is covered in Publication IV, and Chapter 3, Section 3.4.2, and Section 3.4.3.

P1.C4) Complementing P1.C3, a receiver power consumption model is developed to determine the power consumption due to the reception of HO signaling. It is observed that the major contributor to receiver power consumption is the reception of the measurement report by the BS. This contribution is presented in Publication V, and Chapter 3, Section 3.4.4.

P1.C5) The DL-HO performance in the presence of an MRN is analyzed using the system-level simulator to identify the main causes of MRN HOF towards the DBSs. This contribution is covered in Publication VI and Chapter 3, Section 3.4.5.

P2.C1) An UL RS-based HO (coined as UL-HO) solution is utilized to cope with the problem of high Measurement Report signaling. Using the UL-HO method, no measurement report transmission is required during the HO procedure and this feature eliminates the largest contributor to HOFs in Publications Publication II and Publication III, the major contributor to air-interface signaling in Publication IV and highest contributor to receiver power consumption in Publication V. The power consumption of DL-HO and UL-HO schemes is compared to quantify the potential benefits of the proposed technique. This contribution is linked to Publication VII and Chapter 4.

P3.C1) The impact of varying MRN on-board UEs cluster size on the UL-HO performance and the associated power consumption is analyzed using a system-level simulator. This contribution is enclosed in Publication VIII and Chapter 5, Section 5.2.1.

P3.C2) The proposed UL-HO solution is applied to MSCs implemented using MRNs to cope with the problem of MSCs HOF to a DBS, to reduce the

SPoF cases and provide uninterrupted services to on-board UEs. Also, the impact of varying UL-HO parameters (namely UL RS periodicity, and UL time-to-trigger) on the associated power consumption is studied. This contribution is covered in Publication IX and Chapter 5, Section 5.2.2, Section 5.2.3, Section 5.2.4, and Section 5.2.5.

1.3 Structure of the Thesis

This dissertation is organized as follows. In Chapter 2, a brief literature survey of HO management techniques for LTE and NR are presented. In Chapter 3, the performance of legacy DL-HO methods in terms of signaling cost and energy efficiency is described. The concepts of the DL-HO procedure, system model, and power consumption model implemented for the simulations are presented. Chapter 4 presents the proposed UL RS-based energy-efficient HO procedure. The concepts of the relevant UL-HO procedure, system model and UL RS model implemented for the simulations are described. The performance of the UL-HO procedure is compared with the legacy DL-HO procedure in terms of signaling and power consumption costs. Chapter 5 extends the discussion to show how the UL-HO scheme can be applied to implement MSCs through MRNs. This Chapter also evaluates the impact of MRN-assisted user clustering. Finally, Chapter 6 summarizes the outcomes of this thesis and provides future research directions towards 6G.

1.4 Summary of the Publications

A brief overview of the original publications Publication I to Publication IX is given next.

In Publication I, a survey on HO management in cellular networks, with special emphasis on LTE and NR deployments is presented. Some general concepts of radio access mobility in cellular networks are expressed to highlight the challenges and current research focuses in these areas. In addition, an overview of HO management in LTE and NR is presented to highlight the main differences. A brief analysis of the HO techniques available in the literature for CONNECTED_MODE mobility shows the benefits and drawbacks of each scheme. HO management challenges and enhancing techniques, key points for formulating an efficient HO scheme and future research directions are also described.

In Publication II, the impact of varying cell size and user speed on the DL-HO procedure is addressed. System-level simulations are provided using a MATLAB-based network simulator accounting for multiple points-of-failure and channel modeling compliant with LTE standards. The results show that the measurement report transmission errors are the highest among others for both low and high ISDs.

In Publication III, the performance of an LTE ultra-small cell network deployment is studied by taking into account the user mobility. The analysis exhibits that the measurement report transmission errors are the highest among others

for ultra-small cell deployments. This study is beneficial to realize the problem of HO in a standalone network deployment constituted only by small cells.

In Publication IV, the signaling overhead and the average supply power consumption that results from the transmission of HO-related signaling over the air-interface is studied to identify which part of the HO procedure is more power-consuming. A breakdown of the different signaling transmission contributions is provided, studying the impact of user speed, cell densification and HO parameter selection. The results show that the measurement report transmission signaling has the largest contribution over the air-interface among other signaling.

In Publication V, the average supply power consumption that results from the reception of HO-related signaling messages over the air-interface is studied for LTE, to identify those individual processes of the HO procedure that are more power-consuming. The simulation analysis reveals that the highest contributor to the receiver power consumption is the reception of the measurement report by the BS.

In Publication VI, an analysis of the DL-HO performance in the presence of an MRN and the associated power consumption is studied based on a scenario where a group of users is traveling on a bus. The bus moves along the cell edges of the macro BSs at speeds pertinent to those of an urban city environment. The causes of MRN HOFs towards the DBSs are identified. The analysis indicates that the dominant MRN SPoF cases are due to radio link control (RLC) HO confirmation transmission errors.

In Publication VII, the power consumption associated with DL-HO signaling in 3GPP cellular networks (i.e. LTE/NR) is investigated to define a power-efficient HO scheme for future releases of 3GPP. A detailed mathematical model of transmitted and received power consumption for HO signaling is presented. Based on the model, transmitted and received power consumption values due to signaling overheads during DL-HO are obtained. It is found that Measurement Report transmission is the major contributor to air-interface signaling. An energy-efficient UL RS-based solution to cope with the problem of high signaling overhead and power consumption due to Measurement Report signaling is presented. The simulation evaluation reveals that the proposed UL-HO method is power efficient at both UE and BS side by an almost one-third reduction in power consumption in comparison to legacy DL-HO.

In Publication VIII, the power consumption associated with HO signaling is investigated in a network with mobile relays (MRs) roof-mounted on buses, to study UE clustering aspects. The impact of varying the on-board UEs cluster size on the UL-HO performance and the associated power consumption is analyzed. The simulation evaluation shows that the MRs-based group HO solution is more beneficial when the number of UEs belonging to the bus is higher (i.e. 12 UEs or more per bus).

In Publication IX, the HO performance of 3GPP cellular networks (i.e. LTE/NR) in the presence of an MRN and the associated power consumption is presented in a scenario where a group of users is traveling on a bus along a fixed-trajectory. The UL-HO method is extended for MRNs to provide a solution to

the problem of MRN HOF to a DBS and provide uninterrupted services to on-board UEs. UL reference signals (RS) used for UL-HO are implemented through existing Sounding Reference Signals (SRS) in LTE/NR. The simulation analysis is performed to find the optimum SRS periodicity values as a function of UE/MRN speed, and the impact of varying UL-HO parameters (namely UL RS periodicity and UL-time-to-trigger) on the power consumption. The analysis shows that the UL-HO method can significantly reduce the SPoF cases of the MRNs.

2. Related Work on Handover Management: From LTE to NR

This section provides a brief overview of the related work on radio access mobility in LTE and NR. A detailed literature survey is covered in Publication I.

2.1 Introduction

The trends of HO design published in 1996 [8] recognized that the demand for increased capacity, leading to smaller cell sizes, would increase the number of HOs. The first generation (1G) HO procedure was tested in 1978 [9] with a cell size of tens of kilometres. It was a UE-assisted HO procedure in which the measurements are reported by the UE followed by network decision-making. The decreasing cell size in 2G networks increased the HO issues. To overcome 2G HO challenges, distributed HO decision-making was used [10] which had a high signaling overhead cost during HO. Also, in the decision-making phase, a hysteresis value was added to address the high ping-pong problem. In 3G code-division multiple access (CDMA) networks, soft HO algorithms were used [11] that followed the make-before-break idea to improve the link gains but at the cost of high interference to other users [12]. In the make-before-break HO, the UE is able to be simultaneously connected to two BSs for a while, thus minimizing and practically eliminating any interruption time during the communication. The CDMA networks operate on a single frequency, allowing two BSs to communicate with the user simultaneously, with some signal combination at the receiver end. The 4G and 5G technologies have a larger number of small BSs (in comparison to 1G, 2G, and 3G) to cover the same geographical area that leads to small HO areas and no time for extensive HO signaling. Such limitations demand simplified and efficient signaling HO procedures for future ultra-dense networks.

We now define the HO performance metrics to understand the prior art. The HO rate (HOR) is defined as the total number of triggered HO events divided by the simulation time. An HO event is defined as the initiation of the HO procedure upon fulfilling a so-called entry condition (i.e. A3 offset and time-to-trigger (TTT) conditions successfully completed). The HOR is measured in HO events/s. The HOF ratio (HOFR), measured in %, is defined as the total number of HO failure events divided by the total number of triggered HO events, i.e. the percentage of those HOs which for one reason or another experienced problems

and could not be completed seamlessly. Finally, the ping pong rate (PPR) is defined as the number of ping pong events during a given period of time. In turn, we define a ping pong event as the occurrence of an HO between a serving BS and a target BS, followed by another HO to the original serving BS, all this happening under a predefined time. The details of the DL-HO procedure for LTE/NR can be seen in Section 3.1 and the UL-HO procedure in Section 4.1.

2.2 Handover Management in LTE

When addressing HO in LTE, existing works are usually divided into targeting the reduction of radio link failure (RLF) [13], reduction of ping-pong rate (PPR) [14], or a combination of both [15][16][17], the reduction of HO rate (HOR) [18][19][20], reduction of HO failures (HOFs) [18][21][22], and to assess energy-saving [15].

In [13], HO optimization parameters (i.e. time-to-trigger (TTT) and offset) are adjusted through the proposed distributed mobility robustness optimization algorithm to minimize the HOFs. In [14], the proposed solution can reduce the PPR by selecting a target BS based on orientation match, received signal strength, and current load. A reduced early HO scheme in [15], a fuzzy multiple criteria cell selection scheme in [16], and an HO detection with reinforcement learning concept in [17] reduce both the RLFs and PPR. A distance-based HO scheme in [18] minimizes the HOFs and unnecessary HOs. In [19], a reactive HO technique postpones the HO until the most probable location of a UE arrives thus reducing the HOR. In [20], the HOR is reduced by proposing HO from macro to femtocell only when the available data volume of the femto is larger than the macro cell and the time user stay in the femtocell is greater than a certain threshold. In [21], radio link proactive HO was proposed for UEs with poor radio link conditions in which the HO optimization parameters are reduced to trigger the HO early. For other UEs with good radio link conditions, early HO preparation reduces the HOFs and the HO execution was triggered only when the HO is needed, to avoid high PPR. Ericsson has published a study on HO [22] that shows that HOF rate increases with UE speed, i.e. at UE speed 250 km/h, 97% of HOFs are associated with MeasReport. The works in [15] utilized the reduced early HO scheme to achieve high energy efficiencies.

When addressing HO in LTE heterogeneous networks (HetNets), existing works are usually divided into the following: the HOR reduction [23], joint reduction of PPs and HOFs [24], joint reduction of HOR, HOFs and PPs [25], assessing the energy-saving [26][27][28], load balancing [29][30], improving user capacity or QoE [31][32][33][34][35][36], reducing the HO signaling [37], and user mobility state estimation for the HO decision [38][39].

An SINR-based HOR analysis is presented in [23] to show the effect of interference on the HO procedure. The results show a clear effect of interference on the HO procedure as the SINR-based HO has an HOR which is a “gap” lower than the SINR-free case. In [24], the mobility-based inter-cell-interference-coordination (MB-ICIC) technique reduces both PPs and HOF rates using a com-

bination of HO parameter optimization along with enhanced ICIC. A joint reduction of HOR, HOFs and PPs is achieved using the fuzzy-logic-based scheme [25] in which the user speed and radio channel quality are used to choose a hysteresis margin for the HO decision. The techniques in [26][27][28] reduce energy consumption in the LTE HetNets scenario. In [26], the macrocell power-off approach is found to be suitable for low-speed users and high small-cell densities in HetNets scenarios to save energy. The work in [27] used a constrained Markov decision process to propose the HO in overlapping areas of the cells only if the expected energy saving through the HO is greater than the energy loss at the BS during the HO execution phase to avoid frequent HOs. The work in [28] suitably chooses the HO hysteresis margin to reduce energy consumption and interference at the cost of increased HO execution events. The works in [29][30] propose load balancing techniques. The work in [29] used a centralized self-organizing network to continuously estimate the load status of the cells and decide an HO from a heavily loaded cell to the nearest neighboring cells. In [30], a randomized RRM model is used for the macro to Femto offloading in case of congestion with twenty times higher data rates for the Femto BSs authorized users, compared to non-authorized users. The works in [31][32][33][34][35][36] improve the user capacity or QoE. In [31], the context-aware Markov-based HO model is used to characterize the performance of the mobile user as a function of the neighboring cell power profile, traffic load, and user mobility to improve the user capacity. A machine-learning-based HO management scheme is proposed in [32] that learns from the past HO experiences of the user to improve the QoE. The algorithm proposed in [33] used the QoS metrics to obtain a utility function for each macro and Femto cell to determine the necessity of HO. The analytical model in [34] derived closed-form expressions for HO performance metrics as a function of BS density, user mobility and TTT that helps to reduce the HOR, PPs and HOFs and thus improve the QoE. The work in [35] proposed a frequent HO mitigation algorithm that connects the fast-moving users to macro BSs and adjusts the HO parameters of PP users to avoid PPs and thus improves the QoE. An analytical model in [36] analyzed PP rate and HOFs under varying channel conditions to see the effect of shadowing and fading and thus suggest another way to improve the QoE. A control/data separation architecture proposed in [37] reduced the HO signaling overhead in comparison to conventional networks. Finally, the works in [38][39] estimate the user mobility state to categorize users into low, medium and high-speed users for an early HO decision.

2.3 Handover Management in NR

When addressing the HO in 5G, existing works are usually divided into targeting the following: the reduction of HOFs [40][41], reduction of HOR [3][42][43][44], or a combination of both [45][46], the reduction of PPR and RLF [47], the reduction of HO signaling [43][48][49] and to assess the energy saving [50]. In [40], the HO optimization parameters are scaled by estimating the user mobility state (i.e. low, medium, and high-speed user) to reduce the

HOFs. A cashing technique is proposed in [41] that can store the future data contents in advance, to use when wireless resources are not sufficient thus improves the user QoE. In [3], an HO skipping technique is introduced to skip a few HOs along a high-speed user trajectory considering location-aware, cell-size-aware and hybrid-HO skipping. An anchor-based multi-connectivity architecture was proposed in [42] to reduce the HOR. In [43], the distance between the small cell and the UE along with the movement angle of the UE is used to reduce unnecessary HOs and signaling overhead. In [44], a spatial and temporal contextual multi-armed bandit HO procedure for mmWave cellular networks is proposed to reduce unnecessary HOs by carefully deciding the next target BS, such that the UE connection with the new target BS can last longer. A multi-armed bandit framework is used to exploit the empirical distribution of the user's post-HO trajectory and line-of-sight blockage. In [45], a trade-off between unnecessary HOs, and HOFs is found using a time metric and the estimated time-of-stay of the user. In [46], a grey-rational-analysis-based algorithm is proposed to rank the best available target cells for HO to reduce the frequent HOs and HOFs. In [47], the HO procedure is modelled with geometric elements (Apollonian circles and the straight line) to provide optimum HO parameters for reducing both the RLFs and PPR. A control and user plane separation architecture was proposed in [48] to reduce the HO signaling. In [49], a prediction-based conditional HO scheme is proposed that uses deep-learning to overcome the weaknesses of conditional HO in 5G (i.e. blockages, sudden changes in signal reception power). This scheme uses the former blockage information to predict the best target BS and thus it reduces the HO signaling overheads. In [50], based on UE measurements, a direct HO request from the UE to target BS is proposed bypassing the role of the source BS for faster HO to improve the energy efficiency and HO delay.

2.4 Handover Management in High-Speed Scenarios

The future cellular networks are targeted at providing high data rates for users moving at very high-speeds (e.g. in high-speed train and highway scenarios) with high availability and reliability [51]. The main challenges for high mobility scenarios include accurate channel estimation, advanced signal processing, optimized network deployments, and effective mobility management [52]. It is difficult to accurately predict the channel due to the large Doppler spread at high speeds. Although many channel models are proposed in literature such as [53][54][55] for a high-speed train scenario, more research is still required. New coding, diversity techniques, precoding, modulation, and waveforms are required to overcome the challenges of advanced signal processing in future cellular networks. Furthermore, optimized network deployment also has an important role (see enhancing video QoE in [56] and adaptive optimization in [57]). Finally, out of all the above mentioned challenges, mobility management has special importance. Efficient HO algorithms and techniques are required to reduce the number of HOs, HOFs, latency, and power consumption to effectively manage high-mobility scenarios.

In high-speed scenarios (i.e. train, public and private vehicles, etc.), an MRN can be installed in the rooftop to relay the signal between the DBS and the on-board user [52] and thus reduce the HOR, HOFs, and HO latencies through group HO [58][59]. However, at moderate-to-high speeds, the on-board UEs can still suffer from frequent HOs due to the MRN failing to HO to a new DBS. As a consequence, the MRN connection towards all associated mobile users will be lost creating an SPoF for the on-board UEs. Some other techniques are also available to overcome the mobility management challenges in high-speed scenarios, i.e. deployment optimization with the Radio Remote Unit (RRU) [60], overlapping coverage between the neighboring cells [61], multi-connection [52], and geo-aided fast HO [62].

A mathematical model for an MR HO procedure in a train is described in [63] to weigh up the signaling overheads between 3G and 4G networks. Therein, the results show that the HO cost, HO delay, and drop calls can be reduced by using MRs in the LTE-A network. Furthermore, the work in [64] shows that the MRN can notably lower the end-to-end outage probability at moderate-to-high vehicular penetration loss. In addition, the work in [65] exhibits the outage probability performance of an MRN in the presence of co-channel interference considering the effect of path loss and small-scale fading. An adaptive beamforming scheme for LTE with dynamic adjustment of the HO optimization parameters was proposed in [67] to improve the HO performance of high-speed railways. In [68], a moving cell concept is introduced at 60 GHz that utilizes the radio-over-fiber technique to switch the serving cell in unison with the train and provide uninterrupted transmission to the users. A passive roadside unit detection-based proactive HO scheme for vehicular networks is proposed in [69] to increase the HO success rate, reduce the HO overhead, and improve energy efficiency.

2.5 Uplink Handover Management

Unlike current DL-HO schemes in both LTE and NR, the network could track and locate the mobile user measuring an UL RS [89]. The UE sends the UL RSs that are received at the network to decide which BS shall serve a given UE. The UL-HO scheme improves mobility performance through the reduction of HO signaling overhead. When users are moving in a group, they can jointly be tracked using one UL RS (instead of multiple RSs) potentially minimizing the signaling overhead [70].

In [71], the results show that UL-HO can save UE power consumption by up to 63% in comparison to traditional DL-HO. Similarly, in [91] it is found that UL-HO provides a high gain in terms of UE power consumption especially for “Rural with high-speed UEs” and “high-speed train” scenarios. In [92], the results show that UL-HO can reduce both the HOFs and UE power consumption.

2.6 Discussion and Conclusion

A brief literature survey on HO management in LTE and NR shows that an HO scheme that can optimize all the HO performance metrics (i.e. HOFs, HOR, PPR, signaling overhead, and the power consumption) is still missing. Most of the research works discussed only the trade-offs between HO performance metrics. In addition, a proper solution to the problem of MRN HOF to a DBS (causing an SPoF to the on-board UEs) has largely been overlooked in the literature. Furthermore, UL-HO can reduce the signaling overhead and the UE power consumption as described in [71][91][92] but still further investigations are required to determine if UL-HO is suitable to improve the other HO performance metrics, i.e. HOR, PPR, and BS power consumption.

3. Downlink Reference-Signal-Based Handover

This section provides an overview of the DL-HO procedure for both the UE and MR. A model is formulated to calculate the power consumption due to the transmission and reception of air-interface signaling during the HO procedure. Furthermore, this section reports on the performance of legacy DL-HO procedure in terms of signaling cost and energy efficiency while at the same time it highlights the pitfalls of the legacy DL-HO scheme. Also, this section describes the DL-HO issues for MRs.

3.1 Overview of the Downlink Handover Procedure

An overview of the DL-HO procedure in 3GPP current cellular networks is shown in Figure 1 [72][73]. As per 3GPP technical specification (TS) 36.300 [72] and TS 38.300 [73], both LTE and NR are relying on DL measurement-based HO schemes. In fact, the legacy DL-HO procedures in both NR and LTE follow the same principles with only minor nomenclature differences, see Publication I for details. Henceforth, we will use a generic naming convention to refer to both NR and LTE use cases. For example, the centralized entity in Figure 1 could represent the Access and Mobility Management Function (AMF) in NR or the Mobility Management Entity (MME) in LTE. Identically, the user data gateway (UDG) in Figure 1 could identify the User Plane Function (UPF) in NR or the serving gateway (SGW) in LTE. Lastly, the generic term BS may refer to either an NR gNB or an LTE eNB.

The DL-HO process is divided into four phases: measurements, HO preparation, HO execution, and HO completion. In the first phase, the UE receives the DL RSs transmitted by the serving BS (s-BS) and the nearby BSs to perform the signal strength measurements and computes the reference signal received power (RSRP). These measurements are processed at the UE side including filtering at layers L1 and L3 as shown in Figure 2. Upon fulfilling an entry condition, the UE sends a measurement report (MeasReport) to the s-BS. The A3 event and time to trigger (TTT) are used to check and fulfill the entry condition respectively, i.e. if the RSRP of the t-BS is higher than the s-BS plus a hysteresis margin (called A3 offset) and this condition is maintained by a time defined by TTT [72] (see Figure 2). Upon receiving the MeasReport, the s-BS takes the HO decision and sends the HO request to the t-BS in the HO preparation phase (second phase). Once the t-BS successfully performs the admission control, the t-

BS sends the HO request acknowledgment to the s-BS and prepares for HO. Subsequently, the s-BS sends the HO command (HOcmd) to the UE (third phase). Now, the HO execution starts and the UE starts accessing the t-BS using the Random Access Channel (RACH). Upon successful synchronization with the t-BS, the UE transmits an HO confirmation (HOconf) message to the t-BS. In the fourth, and last, phase, the HO completion phase starts in which the DL path is switched toward the t-BS. Finally, the t-BS sends an HO complete message to the s-BS then the s-BS releases the allocated resources.

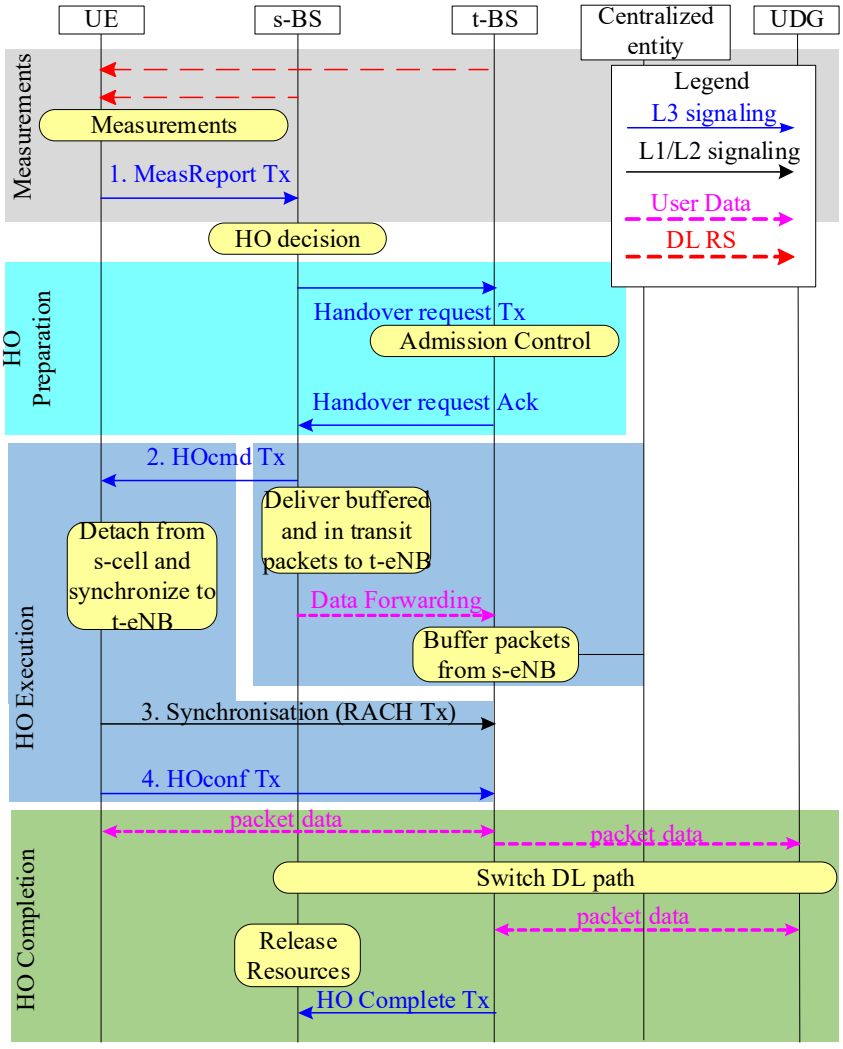

Figure 1. Current cellular networks HO procedure (adapted from [72][73]).

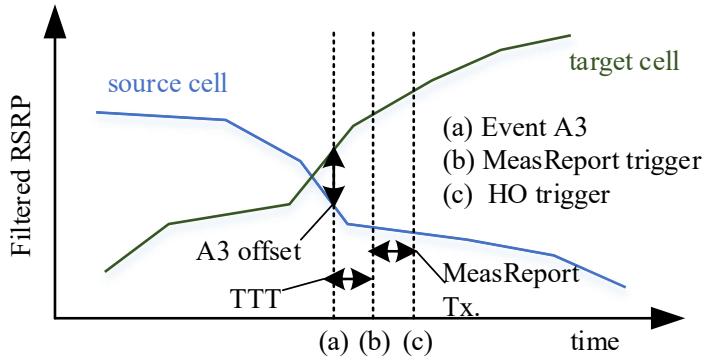

Figure 2. UE measurement processing [26].

3.1.1 Downlink Handover Procedure for Mobile Relays

An MRN is a BS/access point mounted on vehicles (i.e public transport, self-driving vehicles, and drones etc.). The MRN is wirelessly connected to a DBS through the Un radio interface to offer indoor wireless connectivity to on-board users. The on-board users are serviced by the MRN via the Uu interface. Specifically, the MRs support both a subset of UE and BS functionalities to connect with the DBS. As per the 3GPP, there are four different MR architecture alternatives (namely Alt.1 to Alt.4) [74]. The MRN inter-DBS HO process under architecture Alt.1 is the same for UE inter-gNB mobility in NR [73] and UE inter-eNB mobility in LTE [72]. We select the architecture Alt 1 for the simulation evaluation as this is more simplified and its latency analysis shows better performance [75].

The architecture Alt 1 DL-HO procedure for the MRs is illustrated in Figure 3 for 3GPP cellular networks [72][73][74]. The HO procedure for the MRN is the same as we described in section 3.1 and Figure 1 except an MRN is introduced between the UE and the s-BS. The details of the MRN DL-HO procedure can be seen in Publication VI and Publication IX. Notably, in the case of the MRN, the measurements part can be divided into two phases: the MRN measurement and UE measurement. For DL-HO with MRN, we assume that the on-board UEs will not perform DL RS measurements from neighboring BSs as the MRN will perform the measurements from DBSs on their behalf. In the case of MRN HOF to a DBS, the on-board UEs will perform their individual HO procedure with the nearby BSs. The off-board UEs are directly connected to BSs through their individual HO procedure (see Figure 1). The cell selection method is explained in [76] for load balancing of UEs directly connecting to the BS and UEs connecting via the MRN.

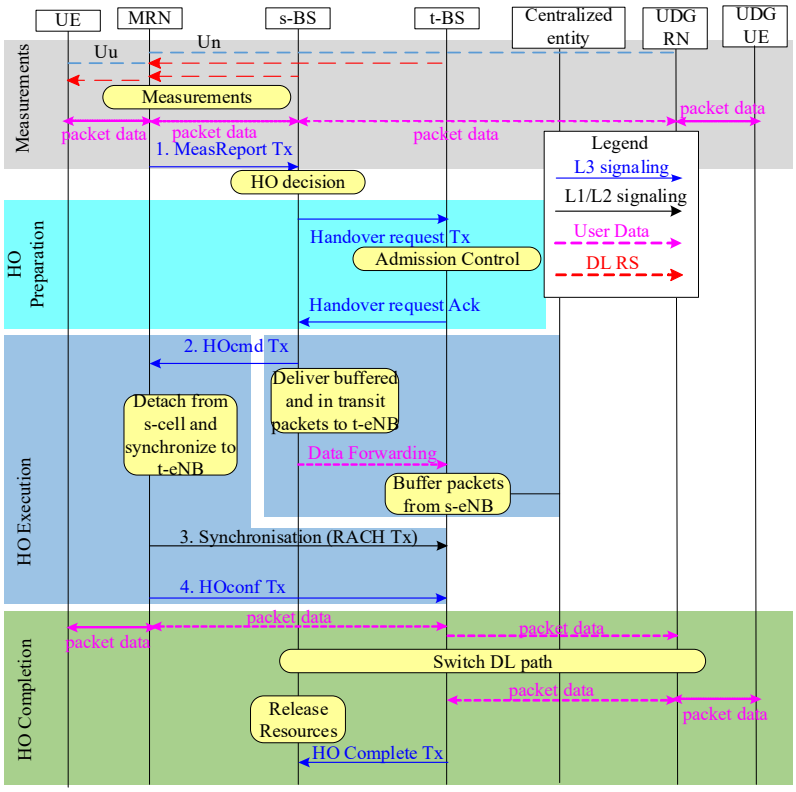

Figure 3. Architecture Alt 1 MRN DL-HO procedure (adapted from [72][73][74]).

3.2 System Model

The evaluation of cellular networks is crucial for understanding their performance and feasibility in the real world. Different methodologies can be used to evaluate their system performance, including: (1) testbeds, (2) measurements with real systems and prototypes, (3) analytical analysis, and (4) simulation [77]. All these methods have their strengths and weaknesses. However, simulation is a popular technique to estimate the performance of cellular systems on a large scale with a highly dynamic environment and properties that are difficult to capture using other methods. A system-level simulator offers a controlled environment to investigate different parameter sets and scenarios with comparably little effort. Thus, a system-level simulator is a powerful method to visualize and analyze the behavior of a user and compare different approaches in cellular networks.

For simulation evaluation, a MATLAB-based system-level simulator is used with a hexagonal grid of sixteen tri-sectored BSs. The simulator is calibrated against a 3GPP calibrated simulator in order to obtain reliable simulation results (see Appendix A1.6 for details). The cell wrap-around feature is included in the simulator to have fair interference conditions across the scenario. A set of 100 UEs with random directions [0°, 360°] and fixed speed are randomly deployed over the scenario. From the available traffic models at the IP level (see

Appendix A1.1, for details), the "full buffer" traffic model is used herein. The initial positions of UEs, mobility patterns, and traffic follow a random distribution. This random distribution is controlled by a seed value, initialized to a given known value at the beginning of each simulation run. When comparing different schemes/algorithms, the same initial seed is used and we also ensure that any newly introduced random process does not alter the setup. Then, the initial positions, mobility patterns, and traffic characteristics are the same for each simulation run. In this sense, the simulation setup is deterministic. Specifically, the simulator is based on LTE standards. However, given the same nature of NR and LTE DL-HO procedures, the NR simulator will approximately give the same outcomes. A detailed description of the HO model and the simulator's features are provided in Publication II and Appendix A1. Herein, the main simulation parameters and assumptions are elaborated in Table 1. The carrier frequency is set to 2.1 GHz with a system bandwidth of 5 MHz, i.e. 25 resource blocks (RBs) and six RBs in each transport block (TB) as per LTE standards. The BS power is 43 dBm whereas the UE and MRN powers are set to 23 dBm. Each sector of a site uses a directional antenna whereas the UEs are using an omnidirectional antennas pattern as described in [78]. The channel model is Typical Urban (TU) with a six-tap model. The information from the channel response vector is extracted for each link and tap and multiplied by the power value of the tap and, using the delay values of the tap, we calculate the frequency response from each of the active links. To generate the shadow fading of the different UEs that have a specific correlation in the area, a correlated log-normal map is generated with a mean of 0 dB and a standard deviation of 8 dB. The distance-dependent path loss models used in the simulator are described in [78]. To detect a radio link failure (RLF), timer T310 is set to 1 second with in-sync counter N311 set to 1, out-of-sync counter N310 set to 1, in-sync threshold Q_{in} to -4.8 dB and out-of-sync threshold Q_{out} to -7.2 dB [79][80]. Radio link monitoring enables the UE to determine whether it is in-sync or out-of-sync with respect to its s-BS. On getting N310 consecutive out-of-sync events, the UE starts the RLF timer T310 as shown in Figure 4. The timer stops when N311 indications are reported (case 2 in Figure 4). If T310 expires, RLF occurs and the UE turns off its transmission to avoid interference and tries to re-establish a connection within a UE connection re-establishment delay (case 1 in Figure 4). The different inter-site distances (ISDs), UE and MRN speeds, and various HO triggering parameters (i.e. TTT and A3 offset) are simulated to find an optimum performance case for the DL-HO procedure. The simulation results are averaged over time (see Section 3.4.1 for details). We fix the simulation time to 60 seconds for both the DL-HO and UL-HO for a fair comparison. The simulation time of 60 seconds was taken "by inspection" after noting that, with 120 seconds simulations, the changes in the results were barely noticeable.

3.2.1 Considered Cellular Deployments for Mobile Relays

In this sub-section, two different simulation scenarios for MRN deployment are presented that we will use in this Chapter and Chapter 5.

Table 1. Simulation parameters and assumptions

Feature	Implementation
Network topology	A hexagonal grid of 16x3=48 cells (wrap-around included)
Inter-site distance	From the set {125, 250, 375, 500, 625, 750, 1000, 1250} m
System Bandwidth	B_{sys} =5 MHz (paired FDD), with $N_{RB}^{DL} = N_{RB}^{UL} = 25$ RBs at carrier frequency f_c =2.1GHz, 1TB=6 RBs, $N_{TB}^{DL} = N_{TB}^{UL} = \lfloor 25/6 \rfloor$
BS DL power (P_{BS})	43 dBm
UE and MRN Power	P_{UE}=P_{MRN}=23 dBm
Antenna patterns	3D model specified in [78], Table A.2.1.1.2-2
Channel model	6 tap model, Typical Urban (TU)
Shadowing	Log-normal Shadowing Mean 0 dB, Standard deviation: 8dB
Propagation model	$L = 130.5 + 37.6 \log_{10}(R)$, R in km $L = 140.7 + 36.7 \log_{10}(R)$ R in km, MRN [78]
UE speed	{3, 30, 60, 90,120} km/h
RLF detection by L1 of UE	T310=1s, N310=1, N311=1 as specified in [79] Q_{in}=-4.8 dB; Q_{out}=-7.2 dB as specified in [80]
HO parameters	TTT= {32, 64, 128, 256} ms, A3 offset = {1, 3, 5} dB.

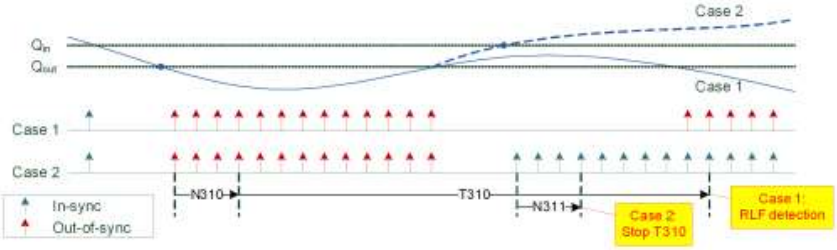

Figure 4. RLF detection.

Scenario 1

A hexagonal grid deployment of 16 tri-sectored BSs with a wrap-around feature is included in the system-level simulator. A total of 200 UEs are randomly deployed across the scenario. It is assumed that the first 12% of UEs (twenty-four UEs) are on board a bus, moving at a constant speed and a specified trajectory. The other 88% of UEs (176 UEs) are off-board (randomly placed outside the bus over the entire simulation area), following a constant speed and random directions uniformly distributed between [0°, 360°]. The MRN scenario with an illustration of on-board and off-board UEs is presented in Figure 5. The bus contains an MRN deployed at the roof-top to enhance the radio link quality of the on-board UEs and decrease the associated HO signaling overhead through group mobility (i.e. only the MRN performs the HO procedure on the behalf of the group of on-board UEs). The MRN is connected to a DBS via a wireless backhaul operating over the same bandwidth as the access link (i.e. in-band wireless backhaul is assumed). The on-board UEs receive cellular services from the MRN and the off-board UEs are connected directly to the macro BSs. Another assumption is that the bus is moving along a trajectory located at the cell edge of the DBSs. The motivation behind this is to reduce the interference of the MRN on the DBSs (because the DBSs and MRN share the same access band) and thus increase the MRN cell coverage area. Furthermore, the UEs at the cell edge experiencing poor radio link conditions can benefit from the MRN following a trajectory along the DBSs cell edges. The considered simulation scenario is shown

in Figure 6 which is used in Publication VI and Publication IX and the main simulation assumptions are summarized in Table 1.

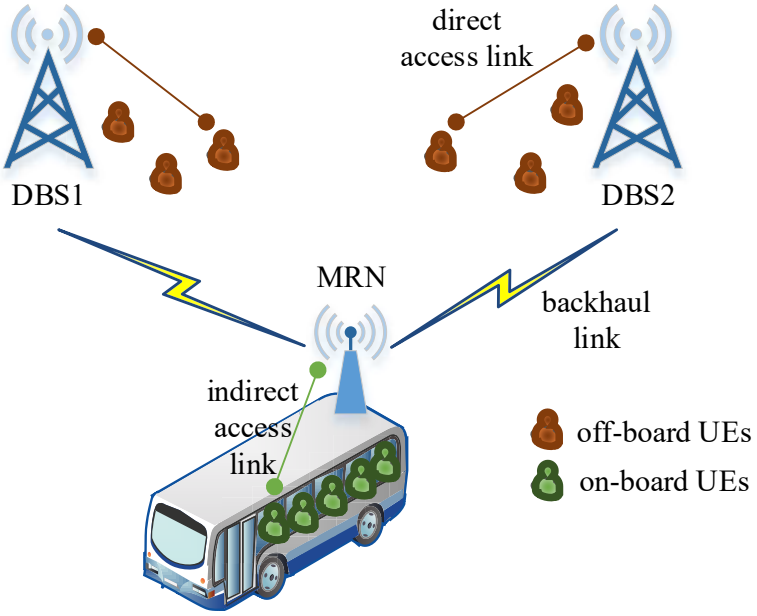

Figure 5. MRN scenario.

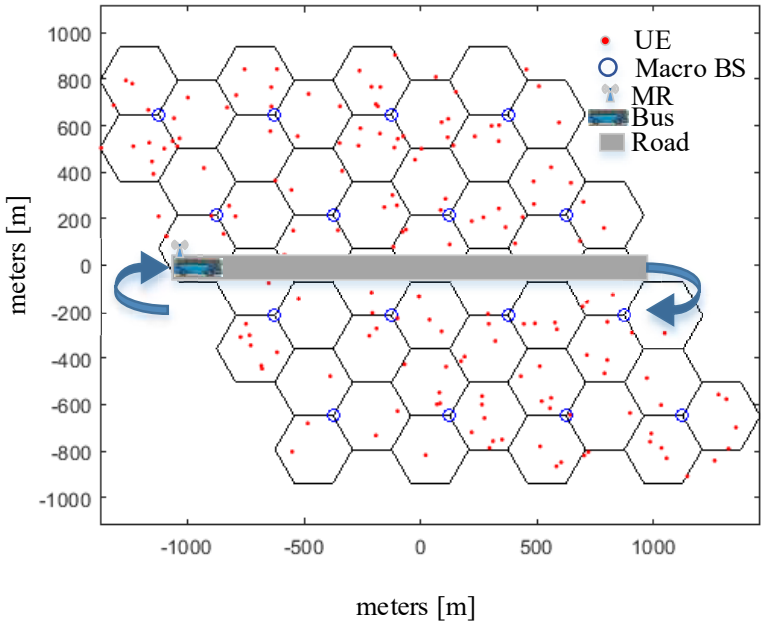

Figure 6. The considered simulation Scenario 1, with the bus following a wrap-around trajectory over the specified trajectory once it hits the rightmost border (used in Publication VI and Publication IX).

Scenario 2

Another MRN deployment scenario considered for the Publication VIII evaluation is shown in Figure 7. In this deployment, a total of 100 UEs is randomly placed over the scenario. Three buses moving on a specified trajectory (located at the cell edge of the DBSs) with a constant speed are placed across the scenario. Each bus contains a set of {12%, 24%, 36%, 48%} on-board UEs resulting in a set of {4, 8, 12, 16} UEs on board. The remaining off-board UEs deployed outside the buses follow rectilinear motion at a fixed speed and random directions uniformly distributed between [0°, 360°]. The buses follow a wrap-around path over the specified trajectory once hitting the rightmost border of the simulated area. The remaining assumptions are the same as described in Scenario 1 and Table 1.

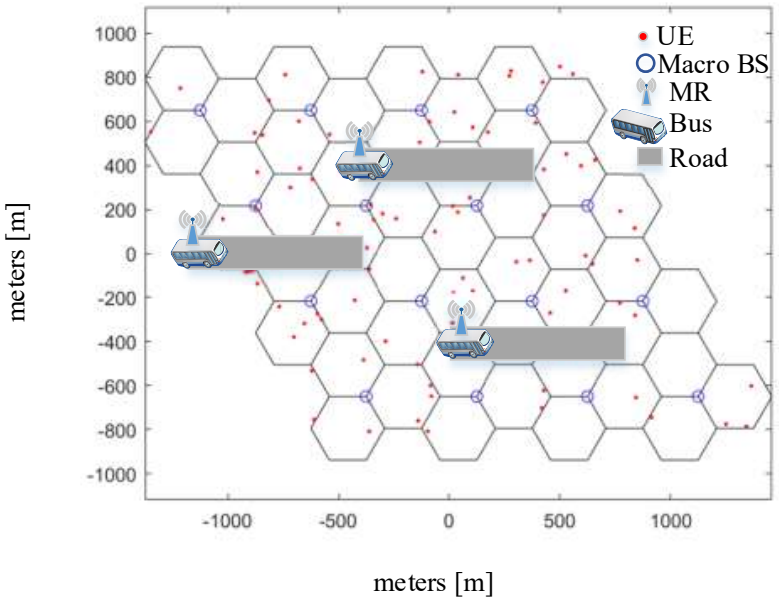

Figure 7. The considered simulation Scenario 2, with the buses following a wrap-around path over the specified trajectory once hit the rightmost border (used in Publication VIII).

3.3 Power Consumption Model

This section presents both the transmitted and received power consumption model for the air-interface signaling that occurs during HO to analyze which part of the HO procedure is more power-consuming. The power consumption model will provide the supplied power to the BS or UE that are necessary to either transmit or receive HO signaling messages.

3.3.1 Transmitted Power Consumption Model

In the BS, the radio equipment can be largely divided into the Base-Band Unit (BBU) and the Remote Radio Unit (RRU). Figure 8 presents a simplified over-

view of the BS and UE components included in the transmitted power consumption model, where $P_{x,sup}$ denotes the necessary supply power to produce an output (transmitted) power P_x, where x={*BS*, *UE*} to denote the BS and UE respectively. Herein, the contribution of the HO mechanism towards supply power is $P_{x,sup}$.

Specifically, the HO signaling over the air interface in both UE and BS transmissions are considered, namely: the HOcmd transmission from the BS side, along with the MeasReport, the RACH, and the HOconf transmission from the UE side. To derive the power consumption of the above-mentioned signaling messages transmissions, first the size of such messages, then the amount of frequency resources (RBs) needed to transmit these messages, and next the output transmitted power allocated to these resources are found. Finally, the time duration of these messages (or duty cycle) is used to compute the time-averaged supply power consumption.

In LTE, the smallest time-frequency unit allocated to a user is an RB. For a subcarrier spacing of $\Delta f = 15$ kHz, an RB has a bandwidth of B_{RB} =180 kHz (i.e. N_{sc}^{RB} =12 subcarriers) and a time duration of one slot, $T_{RB} = T_{slot} = 0.5$ ms [81]. Alternatively, the RB (or slot) duration can be expressed in terms of the number of symbols it contains, i.e. $N_{symb}^{RB} = 7$, times the symbol length T_{symb}. A resource element (RE) is the smallest resource unit consisting of one symbol and one subcarrier. According to the available modulation schemes in LTE, the number of carried bits in a single RE is $L_{RE} \in \{2,4,6\}$ bits for QPSK, 16-QAM, and 64-QAM modulation respectively. A transport block (TB) is the amount of data that the upper layer (MAC layer) provides to the PHY layer depending on the modulation and coding scheme (MCS) and the cyclic redundancy check (CRC).

It is worthwhile noting that, because HOs occur mostly at the cell edge where the RSRP is low, selecting QPSK as the modulation scheme is suitable for the transmission of signaling messages (see Table 2 for details). To transmit the MeasReport data bits in one TB, a 1-ms subframe is assumed with 6 RBs and 2 slots, see Publication VII for details. The modulation and coding scheme (MCS) index is also assumed very low (i.e. I_{MCS} =0) as a bottleneck slowing down the flow of HO messages. The size of each signaling message (in bits) is denoted by L_s, with subindex $s = \{MR, HOcmd, HOcnf\}$ reflecting the different HO signaling messages. Now, the number of information bits per TB ($L_{TB} = 152\ bits$) is found using [82] that include 128 bits of the MeasReport Tx and 24 CRC bits.

With the above in mind, the required number of TBs for each signaling message s, N_{TB}^{s}, can be obtained by:

$$N_{TB}^{s} = \left\lceil \frac{L_s}{L_{TB}} \right\rceil, \text{with } s = \{MR, HOcmd, HOcnf\}, \quad (1)$$

where $\lceil x \rceil$ denotes the smallest integer larger than or equal to x, and, hence it is assumed herein that a signaling message requires an integer number of TBs.

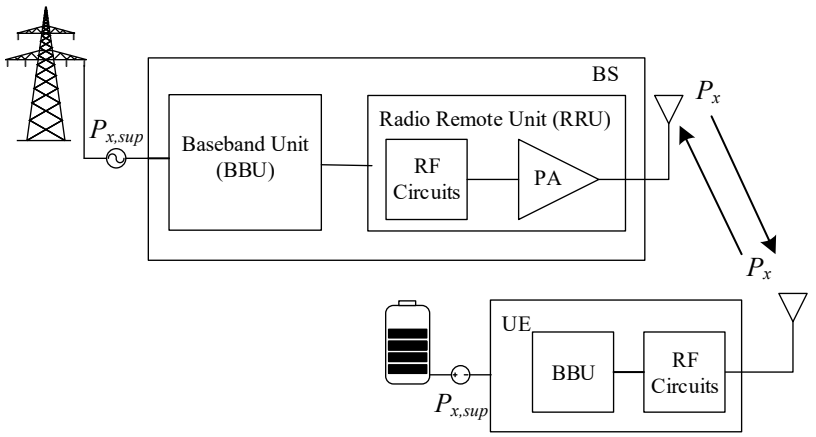

Figure 8. A simplified overview of the BS and UE components included in the transmitted power model.

In addition, for the RACH signaling message transmission, since it carries an unmodulated preamble sequence, the standard specifications are directly referred to which provide the value of N_{TB}^{RA} [81] (see Table 2). For the case of an equal power allocation algorithm, the allocated power per TB at the BS and UE can be formulated as:

$$P_{BS}^{TB} = P_{BS}/N_{TB}^{DL} \text{ , and} \tag{2}$$

$$P_{UE}^{TB} = P_{UE}/N_{TB}^{UL}, \tag{3}$$

where N_{TB}^{DL} (N_{TB}^{UL}) is the total number of TBs in the DL (UL) given a system bandwidth B_{sys}.

The allocated transmitted power (in W) per signaling message s is:

$$P_{x,Tx}^{s} = P_{x}^{TB} \cdot N_{TB}^{s}\,, \tag{4}$$

where x={*BS*, *UE*} and, accordingly, the appropriate number of DL or UL signaling messages should be reflected in N_{TB}^{s}.

Now, some well-known power consumption models are applied for both the BS and UE [83][84][86] in order to obtain the supply power necessary to produce the required transmitted power for each of the signaling messages. In particular, the supply power for the BS transmitting signaling s, $P_{BS,sup}^{s,Tx}$, can be written as:

$$P_{BS,sup}^{s,Tx} = P_{BS,Tx}^{s}/\eta + N_{TB}^{s}/N_{TB}^{DL}\,.\,(P_{RF,BS} + P'_{BB}), \tag{5}$$

where $P_{BS,Tx}^{s}$ is the output transmitted power given by (4) and η is the power amplifier efficiency. $P_{RF,BS}$ denotes the supply power contribution of the RF equipment, which is conveniently scaled by the portion of the utilized resources of signaling message s. Similarly, P'_{BB} is the basic BBU consumption in W (see Table 2).

Equally, the supply power required for the UE to transmit a signaling message s, $P_{UE,sup}^{s,Tx}$, is given by:

$$P_{UE,sup}^{s,Tx} = P_{UE,Tx}^{s} + N_{TB}^{s}/N_{TB}^{UL}\,.\,(P_{RF,UE} + P_{TxBB}), \tag{6}$$

where, $P_{UE,Tx}^{s}$ is the output transmitted power given by (4), and where the supply power contribution to the RF and BB part is also scaled by the portion of

utilized resources by signaling s. P_{TxBB} is the transmitted UE BBU power (see Table 2).

The time-averaged supply power is defined in (7) to capture the time-domain system dynamics during transmission and possible retransmissions of signaling messages,

$$\bar{P}_{x,sup}^{s,Tx} = P_{x,sup}^{s,Tx} \cdot (\Delta t_x^s / \Delta T)\,, \tag{7}$$

where $P_{x,sup}^{s,Tx}$ (x={*BS*, *UE*}) is the "peak" supply power defined in (5)-(6), and $(\Delta t_x^s/\Delta T)$ represents the duty cycle or percentage of time where the signaling is actually transmitted. Assuming that the signaling s has a duration of T_x^s seconds (refer to Table 2 for details) and that a number of N_s signaling messages are transmitted over a period of ΔT seconds, obtaining $\Delta t_x^s = T_x^s \cdot N_s$. Finally, we can rewrite (7) as:

$$\bar{P}_{x,sup}^{s,Tx} = P_{x,sup}^{s,Tx} \cdot T_x^s \cdot (N_s/\Delta T) = P_{x,sup}^{s,Tx} \cdot T_x^s \cdot R_x^s\,, \tag{8}$$

where $R_x^s \triangleq (N_s/\Delta T)$ is defined as the signaling rate which will be obtained from system-level simulations. The main numerical parameters used in the simulations are shown in Table 2.

Table 2. Power consumption parameters and values

Feature	Values
Signaling message sizes	$L_{MR} = 128$ bits; $L_{HOcmd} = 296$ bits; $L_{HOconf} = 96$ bits ([85])
Carried bits in a TB	$L_{TB} = 152$ bits (with QPSK modulation, $L_{RE} = 2$, MCS index=0) [82]
Number of TBs per signaling message	$N_{TB}^{MR} = 1$ TB; $N_{TB}^{HOconf} = 1$ TB; $N_{TB}^{HOcmd} = 2$ TBs; $N_{TB}^{RACH} = 1$ TB.
Power Amplifier efficiency	$\eta = 0.311$ (31.1%) [83]
RF supply power	$P_{RF,BS} = 12.9$ W [83] and $P_{RF,UE} = 2.35$ W [84]
BBU power	$P'_{BB} = 29.4\ W$ [86], $P_{TxBB} = 0.62\ mW$ [84], $P_{RxBB} = 0.97.R_{Rx} + 8.16$ (mW) [84]
Signaling transmission times	$T_{BS}^{HOcmd} = 1$ms; $T_{UE}^{MR} = 1$ms; $T_{UE}^{HOconf} = 1$ms; $T_{UE}^{RACH} = 1$ ms (we use preamble format 0 according to the cell radius used in simulations [87])

3.3.2 Received Power Consumption Model

Analogous to Figure 8, Figure 9 shows a simplified overview of the BS and UE components included in the received power model, where P_{Rx} is the received power. The contribution of the HO mechanism towards the supply power is $P_{x,sup}$ that is necessary to retrieve the data.

The received power (in W) per signaling message s is obtained using the system-level simulator according to the following expression:

$$P_{x,Rx}^s = P_{x,Tx}^s . G_{i,j} . |h|^2 + P_n^s\,, \tag{9}$$

where x={*BS*, *UE*} and, $G_{i,j}$ is the total path gain for i^{th} UE and j^{th} t-BS (including distance-dependent attenuation, the angular antenna gain, and shadow fading), $|h|^2$ is the fast fading contribution and, finally, P_n^s is the additive white Gaussian noise contribution over the bandwidth of the signaling message s.

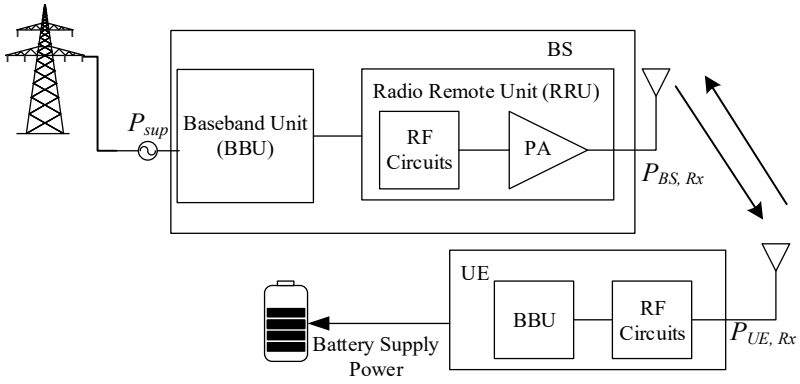

Figure 9. A simplified overview of the BS and UE components included in the received power model.

Now, some well-known power consumption models are applied for both the BS and UE, [83][84][86], in order to obtain the received power necessary to receive the data for each of the signaling messages. In particular, the supply power for the BS signaling s reception, $P_{BS,sup}^{s,Rx}$, can be written as:

$$P_{BS,sup}^{s,Rx} = P_{BS,Rx}^{s}/\eta + N_{TB}^{s}/N_{TB}^{DL} \cdot (P_{RF,BS} + P'_{BB}), \tag{10}$$

where $P_{BS,Rx}^{s}$ is the received power given by (9) and η accounts for the power amplifier efficiency. Equally, the supply power for the UE to receive the signaling message s, $P_{UE,sup}^{s,Rx}$, is given by:

$$P_{UE,sup}^{s,Rx} = P_{UE,Rx}^{s} + N_{TB}^{s}/N_{TB}^{UL} \cdot (P_{RF,UE} + P_{RxBB}(R_{Rx})), \tag{11}$$

where, $P_{UE,Rx}^{S}$ is the received power given by (9), and where the received power contribution to the RF part is also scaled by the portion of utilized resources by signaling s. P_{RxBB} is the received BBU power (see Table 2) where R_{Rx} is the received data rate that can be found as $R_x^s \cdot L_{TB}$.

Now, the time-averaged supply power can be written as:

$$\bar{P}_{x,sup}^{s,Rx} = P_{x,sup}^{s,Rx} \cdot T_x^s \cdot (N_s/\Delta T) = P_{x,sup}^{s,Rx} \cdot T_x^s \cdot R_x^s . \tag{12}$$

3.4 Simulation Analysis

This section provides a simulation evaluation for the DL-HO procedure in terms of HO performance metrics, signaling, and power consumption costs to find which part of the DL-HO scheme incurs higher signaling and power consumption costs.

3.4.1 Handover Performance Metrics

For the simulation evaluation, the considered simulation scenario is presented in Section 3.2. Herein, three HO performance metrics have been studied, namely: HOR, HOF ratio (HOFR), and ping-pong rate (PPR).

Figure 10 shows the HOR against various ISDs and UE speeds. It is clear from the graph that increasing the density of BSs (lower ISD, especially below 250m) results in an increase of HOR due to the increased number of cell borders that is expected. Also, the HOR increases with UE speed. Furthermore, at higher ISDs {750, 1000, 1250}m, the HOR increases because of the poor radio link conditions of the UEs located at the cell edge of the BSs.
Figure 11 presents the HOFR against the ISD for different UE speeds. An increase in HOFR is observed for both low and high ISDs. At low ISDs, the failures are due to adverse channel conditions because of excessive interference from nearby UEs. Moreover, high UE speeds contribute more to HOFR at low ISDs (125m, 250m, and 375m). We can argue that for small cells, higher UE speeds will cause moving away from the s-BS which may cause problems during HO. For larger cells, 1km and above, an increase in HOFR is again due to channel adversity. In this case, the UE speed impact is reversed as compared to the low ISD case because higher UE speed helps to escape from the cell border.

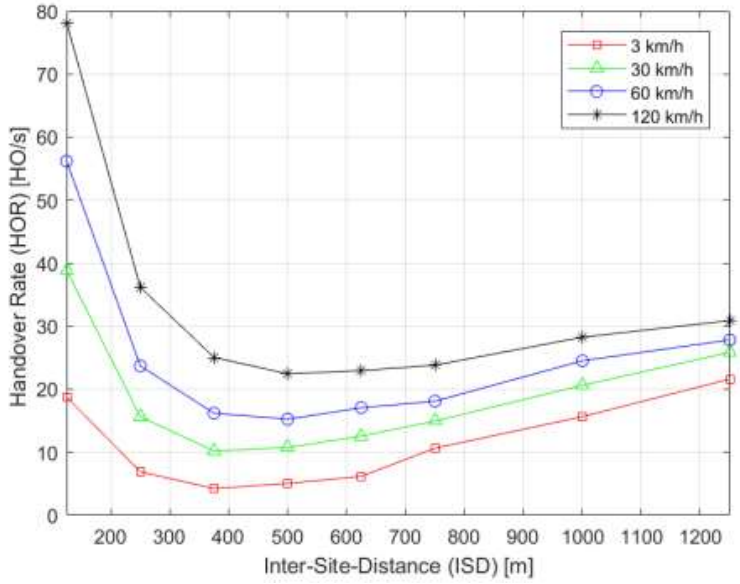

Figure 10. Handover Rate (HOs/s) against the ISD for different speed values.

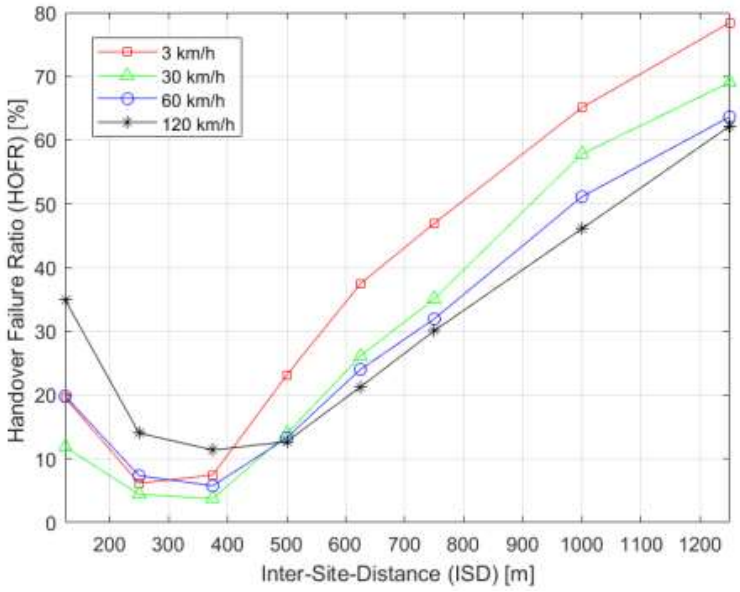

Figure 11. Handover Failure Ratio (HOFR) in % against the ISD for different speed values.

Figure 12 exhibits the HOFR breakdown per type F0 to F7. Overall, the failures are mostly concerned with UL transmission errors. For high ISDs, common failures are due to RLC MeasReport transmission error, RACH failure, and RLC HO confirm transmission errors which are due to the poor UL radio conditions for UEs close to cell borders in large cells. In particular, at medium to high ISDs, higher HO failures are noted for lower speeds, showing that low speed is not enough to "escape" from poor radio link condition areas. For small ISDs, F4 (T310 expiry before HOcmd reception) is very frequent because the UEs that transmit the MeasReport eventually move out of the s-BS coverage and thus the HO command, sent by the s-BS, cannot reach the UE. Similarly, for large ISDs, F5 (RACH failure after T304 expiry) is very frequent because the UEs transmitted power at the cell edge compromises the success of the HO.

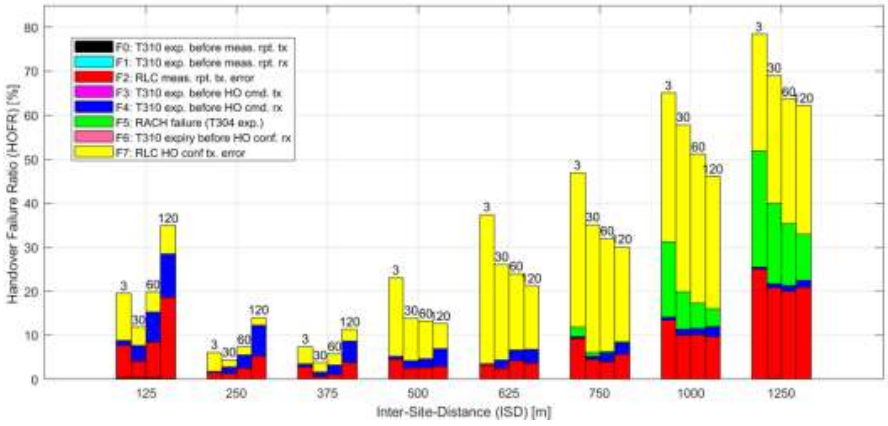

Figure 12. Handover Failure Ratio (HOFR) in % against the ISD for different speed values. HO failure type breakdown: F0…F7.

Figure 13 shows the PPR. Ping-pong events can appear because of the channel variability conditions and the consequence of HOFs to nearby BSs, and the subsequent efforts to reconnect the UE to nearby BSs even if not the most adequate at that time. As per the graph, both low and high ISDs have a high PPR due to channel quality impairments and subsequent HO failures (as already noted in Figure 10, Figure 11 and Figure 12).

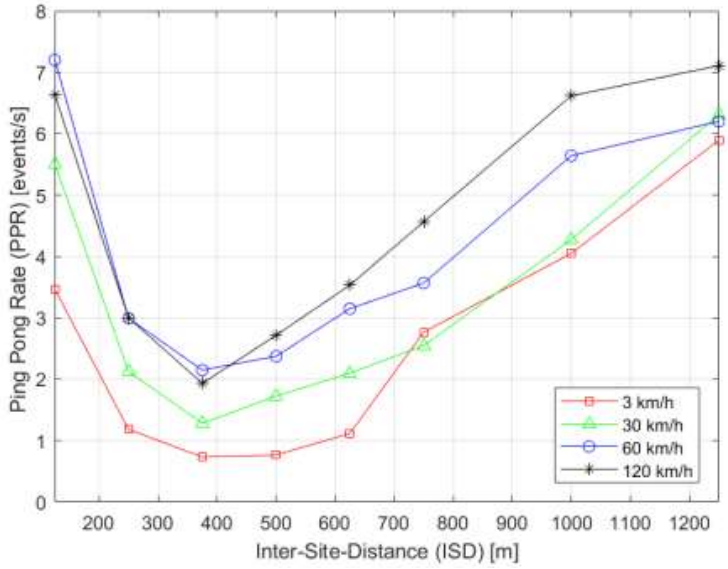

Figure 13. Ping-pong rate against ISD for different speed values.

3.4.2 Handover Signaling Rate Analysis

This sub-section shows the signaling rate analysis during the DL-HO procedure for the air-interface signaling: MeasReport, HOcmd, RACH, and HOconf. Simulations are performed as per the system model presented in Section 3.2 and the results are presented for various ISDs and UE speeds. An aggregate signaling rate analysis (i.e. the sum of all considered signaling rate transmissions) is shown in Figure 14. The plot exhibits that the signaling rate increases with speed especially at low ISDs (i.e. 125m) because of the high HOR, HOFR and PPR we noted in Figure 10, Figure 11 and Figure 13, respectively. Thus the highest speed experience a high signaling rate owing to successive signaling retransmissions. It is also clear from the graph that optimum cell size can be found (i.e. 500 m ISD in our case) around which an increase or decrease of the cell size brings the performance degradation in terms of signaling cost.

Figure 15 shows the percentage of the different considered air-interface signaling messages, averaged over all simulated cases considering different ISDs and UE speeds. The figure demonstrates that the signaling rate percentage is dominated by MeasReport transmission (37%). This is because of the UL transmission errors especially, the RLC MeasReport transmission error, we noted in Figure 12, for particular cell sizes. As a result, the MeasReport retransmissions degrade the performance in terms of increased signaling rate.

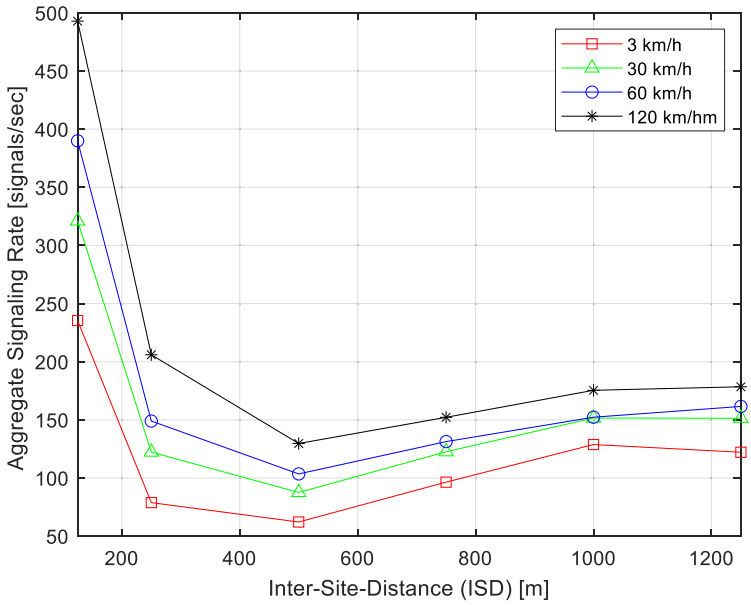

Figure 14. Impact of ISD and UE speed on the aggregate signaling rate.

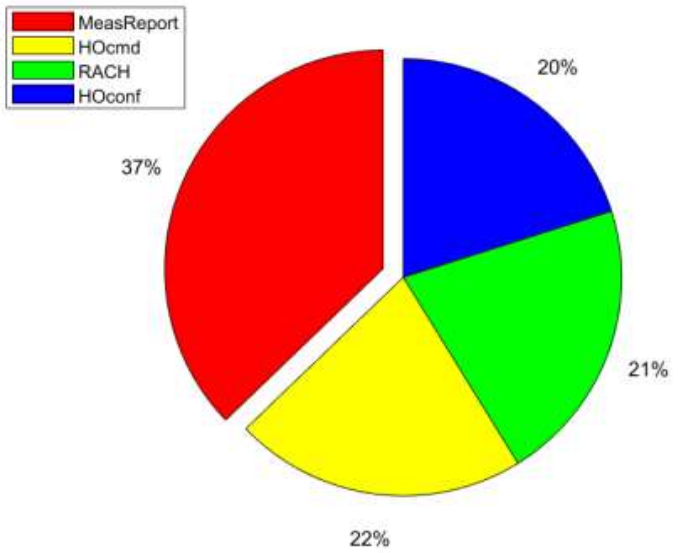

Figure 15. Percentage of signaling rate per type.

In Publication IV and Publication V, we found that increasing the TTT and offset values reduces the aggregate signaling rate significantly but at the cost of increased HOFs. On the contrary, low TTT and offset values have less HOF cases, as an early HO trigger prevents changing the radio link conditions [26].

3.4.3 Transmitted Power Consumption Analysis

In this sub-section, a simulation analysis of the average supply power consumption due to different HO signaling transmission is presented to find the main contributor to the transmitted power consumption.

UE Transmitted Power Consumption

Figure 16 shows the impact of varying ISD and UE speed on the average supply power consumption of the UE using (8), at fixed offset and TTT values. The highest UE transmitted power consumption is noted for the lowest ISD case then it reduces and, after that, it again starts increasing for high ISDs. This is because of high HOR, HOFR due to UL transmission errors and the high PPR we noted in Figure 10, Figure 12 and Figure 13, respectively for both low and high ISDs. The lowest power consumption is obtained for an optimum ISD case of 500m, under the simulated assumptions. This optimum ISD avoids the UL impairment issues arising for large ISDs (due to low UE transmitted power at the cell border) and small ISDs (due to high interference from nearby UEs). Furthermore, the power consumption increases with speed especially at low ISDs due to the high HOR we observed in Figure 10. Figure 17 describes the UE per-type signaling power consumption breakdown. It is found that the highest contributor to UE transmitted power consumption is the MeasReport transmission among other signaling. The MeasReport transmission is thus more detrimental to user battery lifetime.

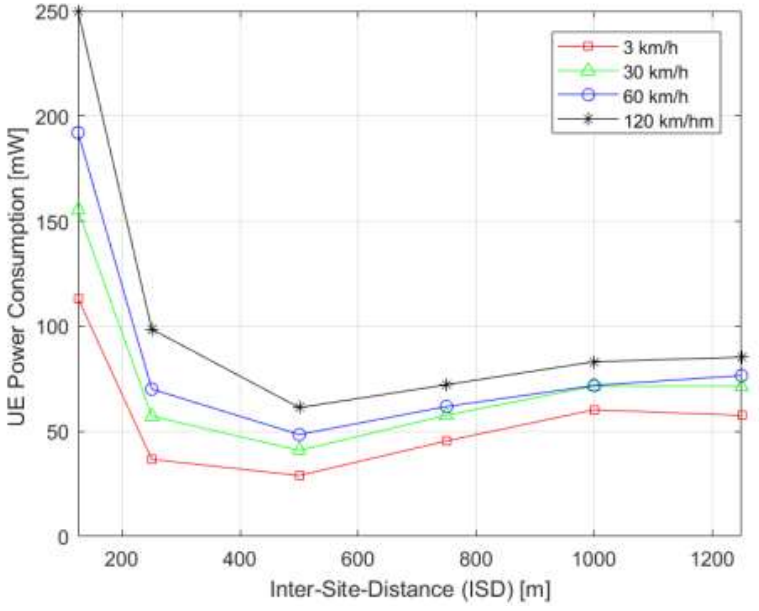

Figure 16. Impact of ISD and UE speed on the average supply power consumption of the UE, for offset= 1 dB and TTT= 32ms.

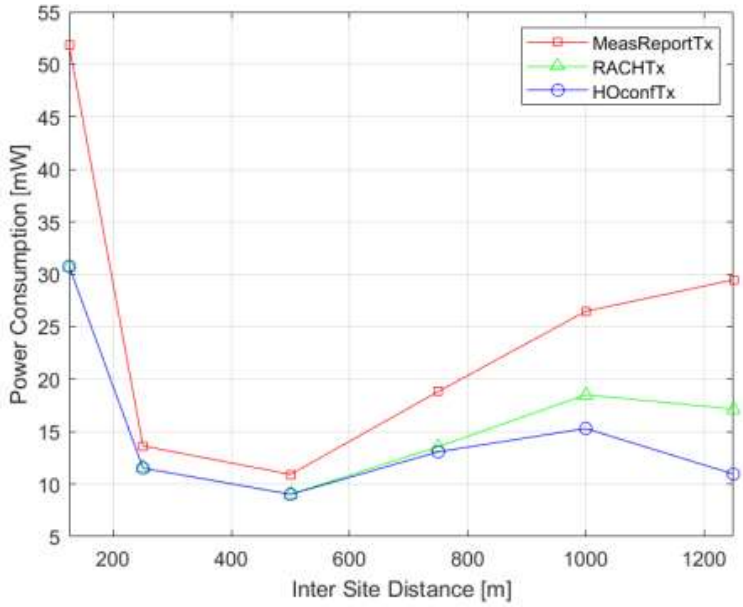

Figure 17. Impact of ISD on the average supply power consumption of various UE signaling messages transmission for speed= 3km/h, offset= 1 dB, and TTT= 32ms.

BS Transmitted Power Consumption

Figure 18 demonstrates the BS transmitted average supply power consumption due to the transmission of HOcmd signaling using (8). The trend of the graph by varying ISD and UE speed is similar to Figure 16 but the BS power consumption is much higher compared to UE power consumption which was expected. For an ISD of 500m a doubling of speed results in an approximate increase of 250 mW in the BS power consumption. The difference of BS power consumption between pedestrians (3km/h) and very high-mobility UEs (120 km/h) is highest at the lower end of the cell size interval corresponding to an increase of 135% and 100 % for an ISD of 250m and 500m respectively.

3.4.4 Received Power Consumption Analysis

In this sub-section, a simulation evaluation of the received average supply power consumption caused by the reception of different HO signaling messages is shown to discover the main contributor among various forms of signaling reception.

UE Received Power Consumption

Figure 19 shows the UE received average supply power consumption due to HOcmd signaling reception using (12). One trend of the graph shows that the smallest simulated cell size requires that the UE received power consumption exceeds 400mW, whilst all other schemes consume less than this. With the exception of the high mobility UEs (120km/h), all other ISD and UE mobility combinations lie below 250mW. Another trend exhibits that the UE received power consumption (for HOcmd) is higher than the transmitted power consumption

(for MeasReport, RACH, and HOconf), see Figure 16 and Figure 19. This is linked to two causes. Firstly, HOcmd requires a double number of TBs in comparison to other HO signaling schemes (see Table 2 for details). Secondly, high HOcmd delivery failures increase UE received power consumption especially at low ISDs which lead to successive signaling retransmissions, see Figure 12.

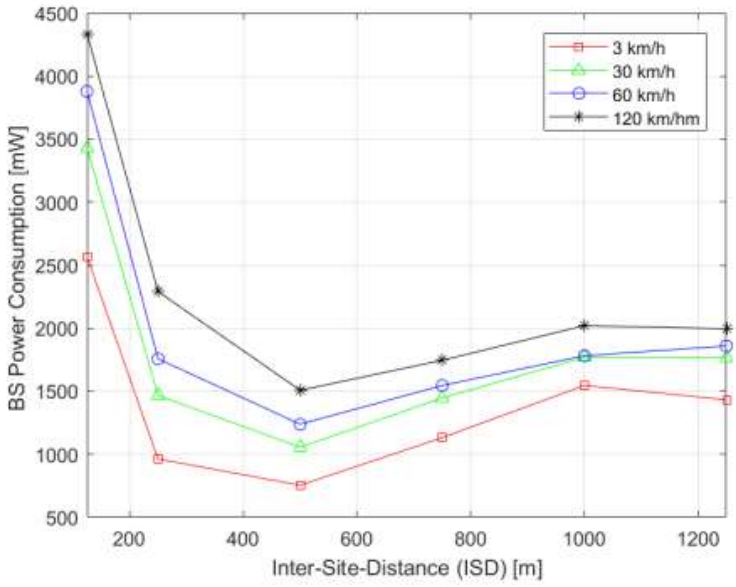

Figure 18. Impact of ISD and UE speed on the average supply power consumption of the BS, for offset= 1 dB and TTT= 32ms.

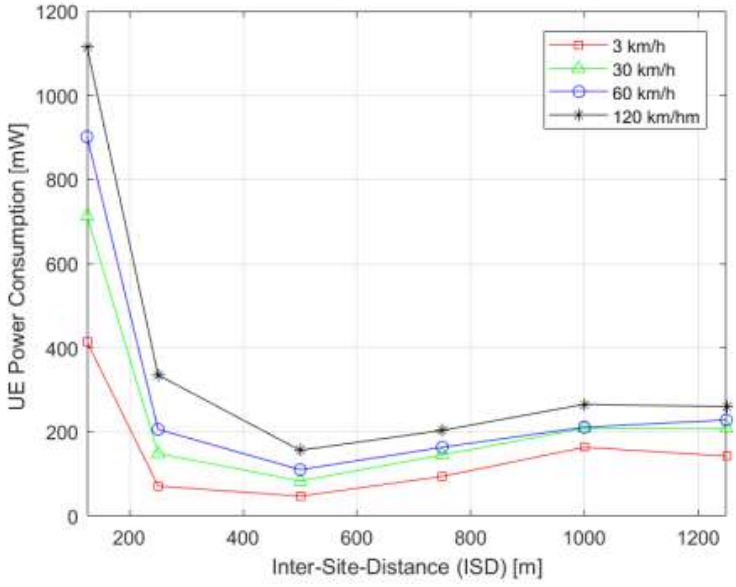

Figure 19. Impact of ISD and UE speed on the average supply power consumption of the UE received signaling messages, for offset= 1 dB and TTT= 32ms.

BS Received Power Consumption
Figure 20 demonstrates the BS received average supply power consumption due to MeasReport, RACH, and HOconf signaling reception using (12). The BS receives the signaling messages transmitted from the UE. The trend of the plot by varying ISD and UE speed is similar to Figure 19 but the BS power consumption is much higher in comparison to UE power consumption.

Figure 21 describes the BS per-type signaling power consumption breakdown. It is found that the highest contributor to BS received power consumption is the MeasReport reception among other signaling. Noteworthy, the results are in line with Figure 17 but the power consumption is much higher in comparison to Figure 17.

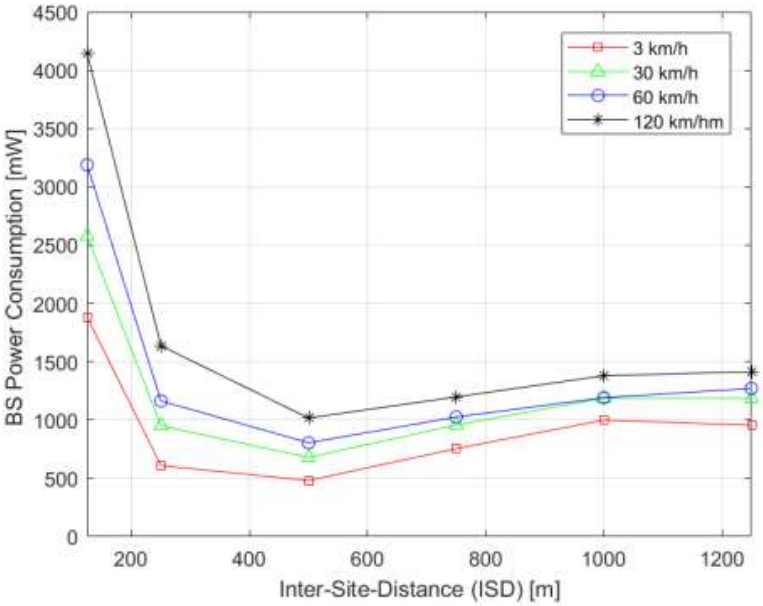

Figure 20. Impact of ISD and UE speed on the average supply power consumption of the BS received signaling messages, for offset= 1 dB and TTT= 32ms.

3.4.5 Power Consumption Analysis of Mobile Relays

This sub-section provides a simulation evaluation for UE and BS power consumption for simulation Scenario 1 presented in Section 3.2.1 with/without installing an MRN at the roof-top of a single bus. There are 12% on-board UEs and the remaining 88% are off-board UEs. Two speed values are simulated where the speed 30 km/h is shown with a “solid line” and speed 60km/h is presented with a “dashed line” in the following graphs. The two following case scenarios are simulated to have a fair comparison:

- **Case 1**: without MRN, i.e. all on-board UEs will perform their individual HO procedure with a macro BS.
- **Case 2:** with MRN, i.e. only the MRN will perform the HO procedure to the DBSs on behalf of the on-board UEs for group mobility.

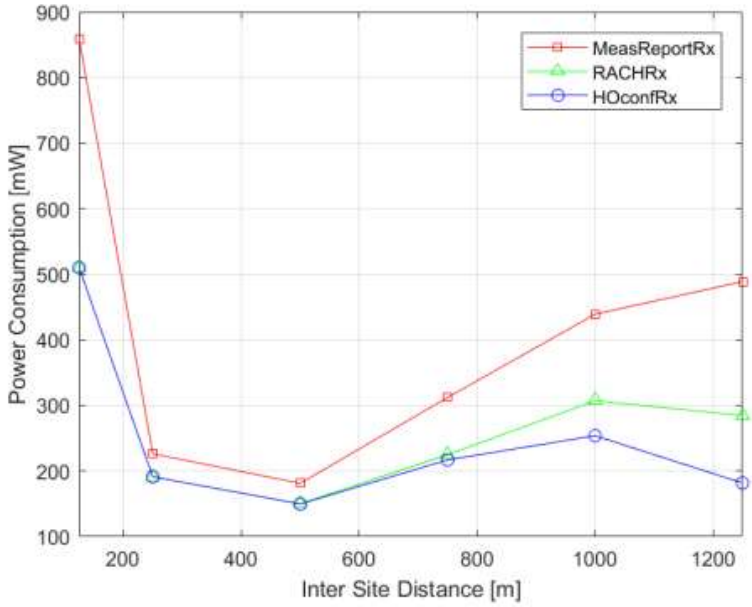

Figure 21. Impact of ISD on the average supply power consumption of various signaling messages reception at BS for speed= 3km/h, offset= 1 dB, and TTT= 32ms.

The total power consumption for both transmitted and received signaling at the BS or UE is computed using (8) and (12). Figure 22 shows a total UE power consumption, and Figure 23 displays the total BS power consumption at fixed TTT 64 ms and offset 3dB values. Overall, Case 2 outperforms in terms of power consumption due to the benefits of group mobility using the MRN. For Case 1, at high ISDs and 30 km/h speed, high power consumption is linked to the high PPR for this specific case that we noted in Publication VI. In short, the MRN deployment can reduce up to 14% of BS power consumption and 21% of UE power consumption for all the simulated cases of Case 2.

Figure 24 shows the MRN HOFR breakdown per type (F0 to F7) to identify the main causes of MRN HOFs to the DBSs. Mainly, the HOFs are linked to UL transmission errors i.e. RLC HO confirm transmission error (F7) is the highest among others. The RACH failure is common for large cell sizes due to the MRN poor UL radio conditions close to the cell borders. In the ISD 500m case, high failures are linked to low speed (i.e. 30 km/h) because the low speed of the bus is not enough to escape the MRN from the poor condition areas. Such types of failures create SPoF for on-board UEs and thus increases the HOR and the service interruption time. At a speed of 60 km/h, the ISD 500m is optimum in terms of lower SPoFs for the MRN out of the simulated cases. The analysis shows that we can further improve the HO performance by reducing the causes of MRN HOFs to DBSs.

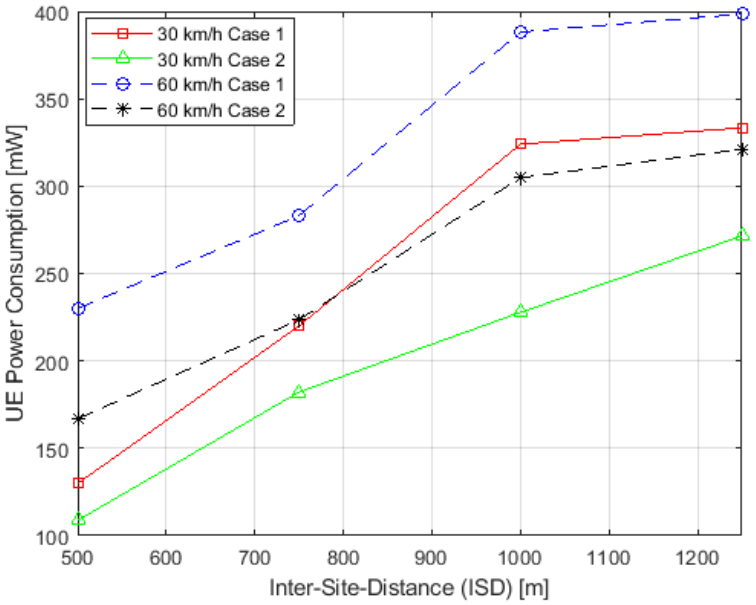

Figure 22. Impact of deploying the MRN on UE total power consumption.

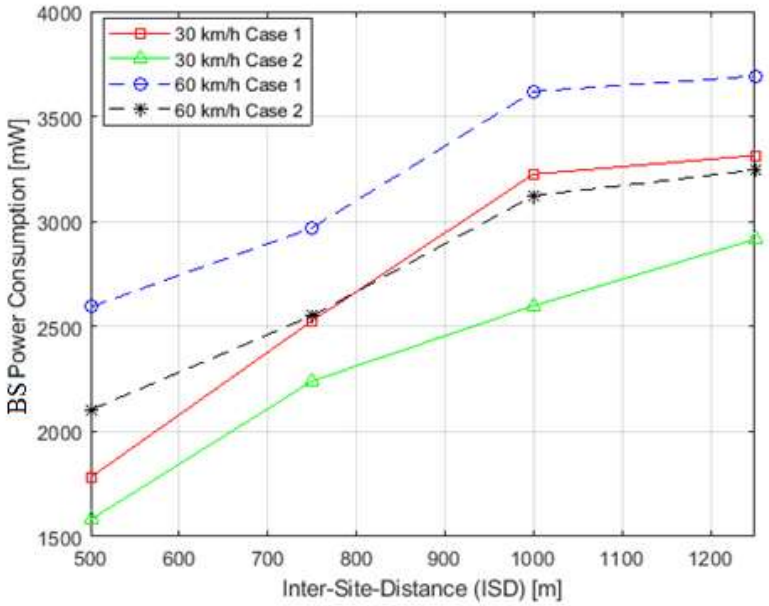

Figure 23. Impact of deploying the MRN on BS total power consumption.

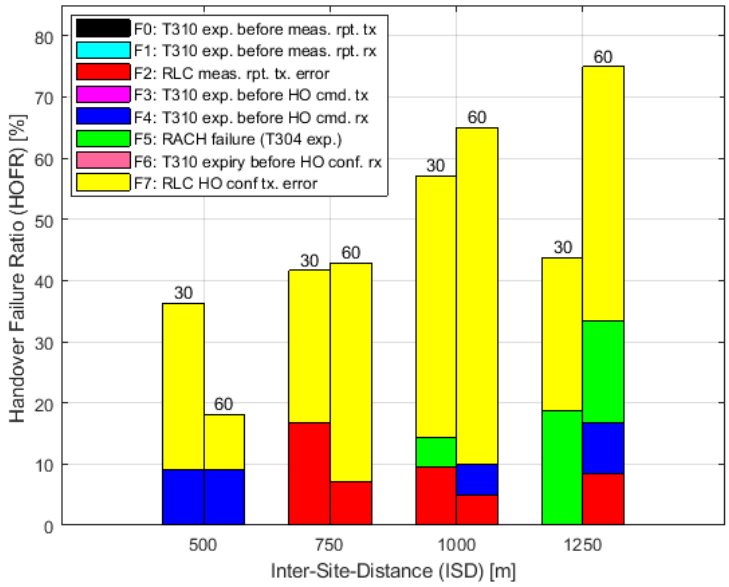

Figure 24. Impact of ISD and UE speed on MRN HOF ratio breakdown per type.

3.5 Discussion and Conclusion

The DL-HO simulation analysis shows that increasing BS densification directly impacts the DL-HO performance in terms of increased HOR, HOFR, and PPR. It is observed that the largest contributor to air-interface signaling overhead is the MeasReport transmission within the DL-HO procedure that is in line with the work presented in [22]. Also, the power consumption of the MeasReport for both transmission (from UE) and reception (at BS) is higher than the RACH and HOconf signaling. An optimum cell size (ISD=500m out of simulated cases) is found around which any increase or decrease of the cell size brings the performance degradation in terms of higher signaling and power consumption costs. Increasing the TTT and offset values reduces the aggregate signaling rate significantly but at the cost of increased HOFs, which is in line with the previous works considering HO parameter optimization for efficient HO [13][21][24][25][26][28][34][35][40][47]. In conclusion, DL-HO is problematic for future ultra-dense networks in terms of HO performance, higher HO signaling, and power consumption. An HO scheme that minimizes the DL RSs measurement, and HO-related air-interface signaling messages, especially MeasReport, would become more beneficial for future networks in terms of improving the user battery lifetime.

In addition, the simulation evaluation for the MRN demonstrates that the dominant SPoF cases of the MRN are linked to RLC HOconf transmission errors. Therefore, an HO procedure that can reduce the MRN HO signaling overheads has a great potential to reduce the HO delays, SPoF cases and provide uninterrupted services to on-board UEs.

Further investigations could address the implementation of the uplink power control feature, increase the number of active UEs per BS, consider the HetNets scenario where high-speed UEs are being served by macro BSs and include the fundamental “system ON” power to the power consumption model. The uplink power control feature has not been used in this work but this feature can further reduce the UE/MRN power consumption.

4. Energy-Efficient Handover based on Uplink Reference Signal

This section provides an overview of the UL-HO procedure for both LTE and NR. Modeling of the UL RSs for HO measurement purposes is discussed. This section also provides the performance of UL-HO in terms of HO performance, signaling cost, and energy efficiency in comparison to the DL-HO procedure.

4.1 Overview of Uplink Handover Procedure

In Chapter 3, we presented that both LTE and NR rely on DL RS measurement and subsequent reporting to the s-BS. In this Chapter, we propose an UL RS-based HO scheme (coined as UL-HO) to overcome the challenges we observed in the DL-HO procedure. We extend the applicability of UL RSs, in particular, the SRS defined in both LTE and NR (see [81][88]), for handover. The UL RSs are already used in current standards (e.g. for channel estimation, link adaptation, and beam management, etc.).

The UL-HO procedure is shown in Figure 25 in which the s-BS and nearby BSs receive the UL RSs transmitted by the UE, allowing the network to compute UL-RSRP. A central network controller process these measurements as shown in Figure 26, to decide which BS shall serve a given UE. If the UL-RSRP of a t-BS is higher than the s-BS by an "A3 UL-offset" and this condition is maintained during UL-TTT, the controller makes the HO decision and notifies the s-BS with the t-BS. Then, the s-BS transmits an HO request to the controller-suggested t-BS. The rest of the HO procedure remains the same as in LTE and NR starting from the HO preparation phase in Figure 1.

By reusing the UL channel measurements from UL RSs (needed in, e.g., massive MIMO operation) also for mobility purposes requires no extra signaling overhead. Another benefit of using UL measurements for UE mobility is that it is possible to improve the network performance by network-side upgrades without UE impact. The realization of the UL-HO scheme comes with the requirement that the time synchronization between the BSs receiving the UL RS should be within some specified upper bound. This requirement may already be in place to efficiently support other implementations such as TDD operation, joint uplink transmission, etc. in small-cell deployments with very short propagation times. In addition, in order for a neighboring BSs to be able to detect and measure the UL RS, it is also required that the configuration parameters (timing, frequency, code, etc.) of such an UL RS, which are set by the s-BS, are also shared with neighboring BSs. This can be effectively achieved via existing interfaces

(such as, for instance, X2 or S1 in LTE) and would only require some minor standard upgrades in defining the information elements to be communicated between the BSs. Furthermore, the detection of the UL RS is rather robust since it is, by design, a known signal transmission, with known time, frequency and code signatures and thus easily detectable and measurable at the neighboring BSs.

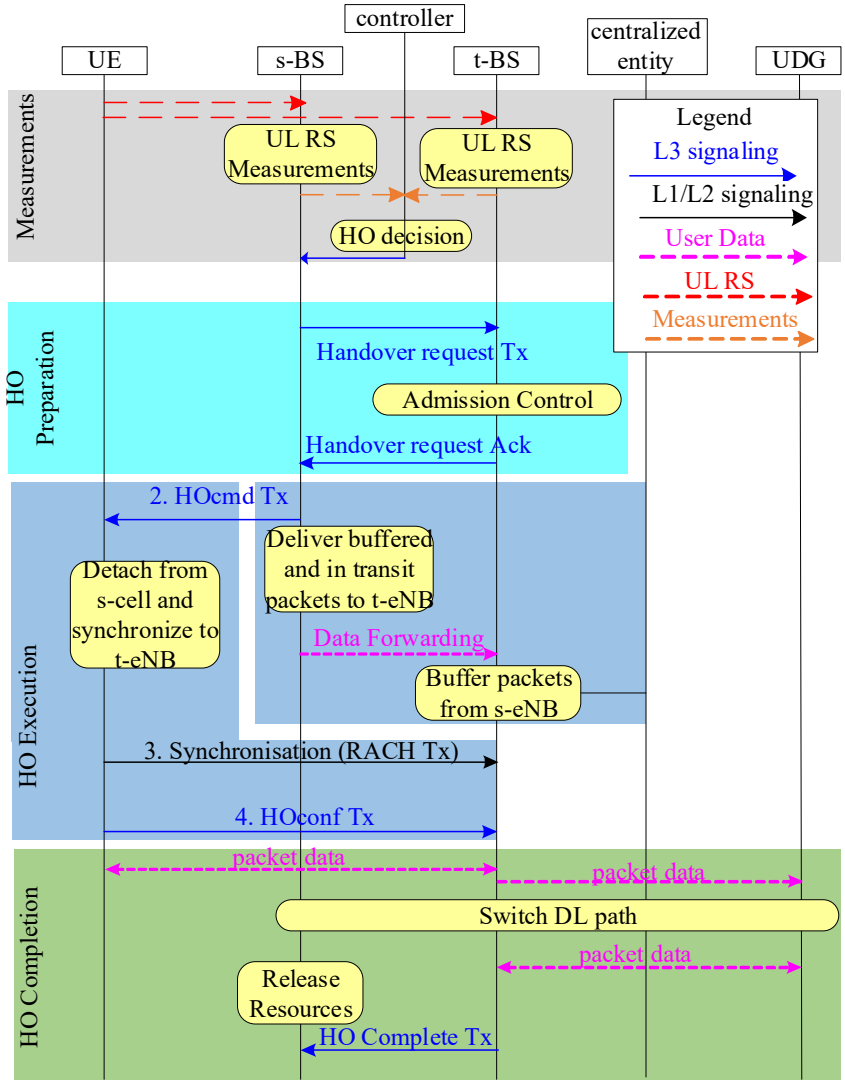

Figure 25. HO procedure based on uplink reference signal (adapted from [72][73][89]).

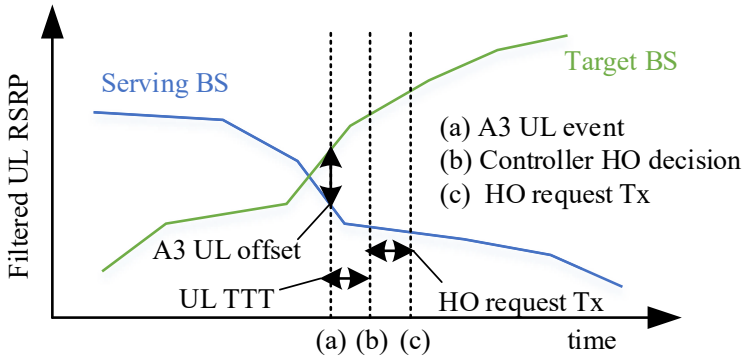

Figure 26. Network controller measurement processing.

4.2 Uplink Reference Signal Model

In this thesis, we utilize the SRS as an UL RS for HO measurement purposes [81][88]. In LTE and NR, SRSs can be utilized to estimate the UL channel to perform accurate link adaptation, maintain uplink synchronization, determine the channel quality information in the UL direction and support frequency selective scheduling. Each UE is individually configured with different periodicities, sounding bandwidths, sequence, and hopping patterns to achieve resource orthogonality. In addition, the BS configures the periodicity, sounding bandwidth, and frequency via higher-layer signaling on a cell-wide basis.

The considered numerical values for SRS parameters are shown in Table 3. The total bandwidth to be sounded (within the system bandwidth) is defined by the SRS bandwidth configuration parameter ($C_{SRS} \in \{0,1,\dots,7\}$) and the SRS bandwidth parameter ($B_{SRS} \in \{0,1,2,3\}$) along with the partial sounded bandwidth ($m_{SRS,b}$, with $b = B_{SRS}$) at each SRS transmission. The frequency hopping pattern followed by different SRS transmissions is defined by a hopping parameter ($b_{hop} \in \{0,1,2,3\}$) to sound a portion or the entire sounding bandwidth i.e. at $b_{hop} = B_{SRS}$, frequency hopping is done over the full sounding bandwidth. The subcarriers occupied by an SRS transmission bandwidth are defined by a comb parameter K_{TC}, i.e. $K_{TC} = 2$ assign a comb index $k_{TC} = \{0,1\}$ for odd and even subcarriers to multiplex SRS transmissions over the same bandwidth. Zadoff-Chu sequences are allocated to different UEs to provide code-domain multiplexing. To guarantee orthogonality in the code domain, a UE-specific sequence cyclic shift index ($n_{SRS}^{cs} \in \{0,1,\dots 7\}$) and a cell-specific sequence identifier (n_{ID}^{SRS}) are defined in the standards. SRS transmissions are configured with SRS periodicities (T_{SRS}) ranging from 2ms to 320 ms [82]. The SRS Configuration Index ($I_{SRS} \in \{0,1,..636\}$) calculates the different SRS periodicities. In this Chapter, we will simulate different SRS periodicities to find an optimum SRS periodicity value in terms of the lowest power consumption. Figure 27 presents the above mentioned SRS parameters for the case of two SRS transmissions.

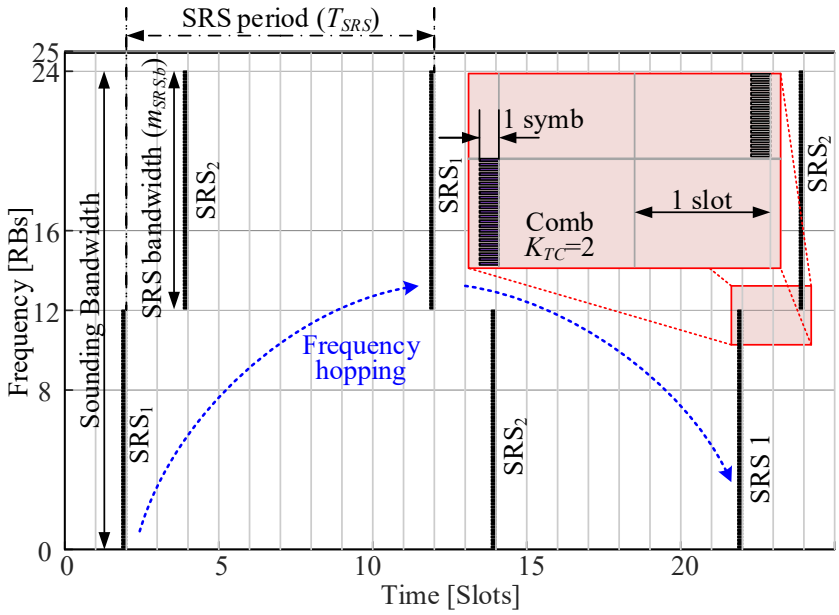

Figure 27. Example of two orthogonal SRS transmissions (SRS1 and SRS2 in the graph) along with main SRS design parameters.

Table 3. SRS parameters and values

Feature	Values
SRS periodicity (T_{SRS})	{5ms, 10ms, 20ms, 40ms, 80ms, 160ms, 320ms} [82]
Number of transmission combs (K_{TC})	2 [81]
Number of SRS antenna ports (N_a)	1 (used for sounding)
OFDM symbols per SRS resource	$N_{symb}^{SRS} = 1$
Cyclic shift (n_{SRS}^{cs})	{0, 1, 2,……,7} for K_{TC}=2 [81]
Bandwidth Configuration (C_{SRS})	7, choices {0, 1, 2, ……,7} [88]
SRS Bandwidth (B_{SRS})	$B_{SRS} = b = 1$ ($m_{SRS,0}$ =12 RBs)
SRS hopping parameter (b_{hop})	0 (hopping over entire bandwidth) [81]
SRS configuration index (I_{SRS})	$I_{SRS} = \{0,1,2,\ldots 636\}$, [82]

4.3 Simulation Analysis

This section provides the simulation analysis of the UL-HO scheme to quantify potential benefits in terms of HO signaling and power costs.

In Chapter 3, we found that the ISD 500m case is the optimum out of the simulated cases for DL-HO. Therefore, the following parameters were fixed for UL-HO, i.e. ISD to 500m, speed to 30 km/h, A3 UL-offset to 1dB and UL-TTT to 32 ms and varied the SRS periodicity values to find an optimum periodicity that reduces the power consumption during the HO to its minimal level.

4.3.1 Handover Performance Metrics

The impact of UL-HO on the HO performance metrics (i.e. HOR, HOFR, PPR) is shown in Figure 28 for SRS periodicities ranging from 5 ms to 320 ms. The graph shows that the HOR and PPR decrease with increasing periodicity values until an optimum SRS periodicity "40 ms" arrives. This way the UL-HO reduces the unnecessary HOs and PPs. After "40ms" periodicity cases, HOR and PPR start increasing because of the high SRS periodicity values. High periodicity means lower SRS transmission/reception rate, i.e. increasing the gap between UL-RSRP measurements. All HO signaling will eventually not be properly transmitted/received for this period. It may also happen, that the UE fails to HO to a neighboring cell and subsequent efforts to reconnect to the neighboring cells even if not the most adequate at that time, resulting in a high PPR and thus to high HOR. Notably, The UL-HO reduces the HOFR significantly in comparison to DL-HO. This is because no MeasReport transmission is required from the UE to BS in the case of UL-HO, thus the HO procedure completes before the UE loses its connection to the s-BS.

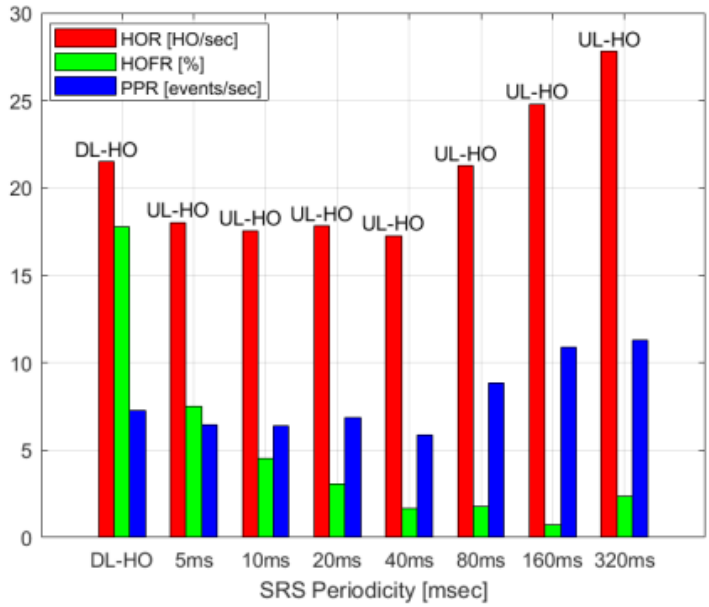

Figure 28. Comparison of DL and UL HO metrics, at fixed ISD= 500m, speed = 30km/h, DL/UL offset= 1 dB and DL/UL TTT= 32ms.

4.3.2 Transmitted Power Consumption

This section provides a comparison of DL-HO and UL-HO in terms of power consumption due to HO signaling messages transmitted from the UE/BS side.

UE Transmitted Power Consumption

In this sub-section, we consider HO-related air-interface signaling messages transmitted from the UE side namely, MeasReport Tx, RACH Tx, and HOconf Tx. Figure 29 shows the average UE transmitted supply power consumption

comparison for UL-HO and DL-HO. The graph exhibits that the UL-HO outperforms for all periodicity cases. This is because the UL-HO does not require the MeasReport signaling transmission from the UE side. The optimum SRS periodicity case of "40 ms" shows the highest reduction for the UE transmitted power consumption, 48% lower than the DL-HO case. After the optimum periodicity case, the UL-HO UE transmitted power consumption starts increasing because of the high HOR and PPR we noted in Figure 28.

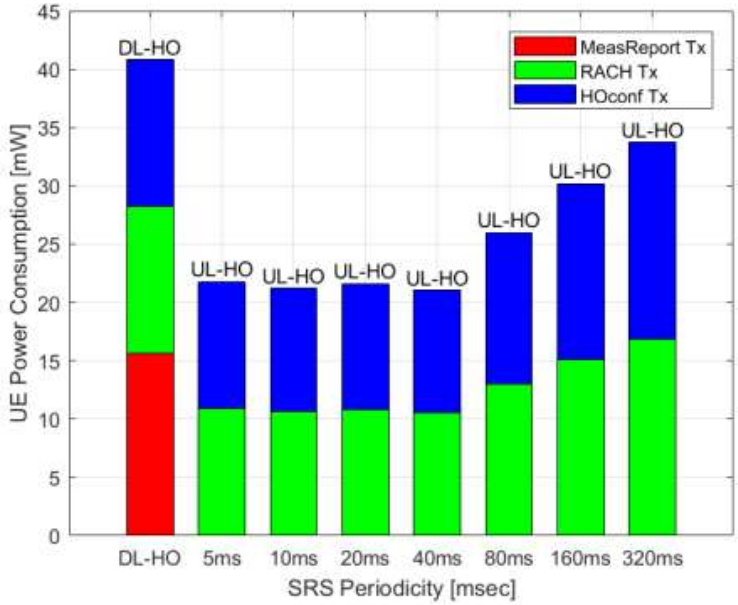

Figure 29. UE transmitted average supply power consumption comparison for DL-HO and UL-HO, at fixed ISD= 500m, speed = 30km/h, DL/UL offset= 1 dB, and DL/UL TTT= 32ms.

BS Transmitted Power Consumption

The average supply BS power consumption resulting from the transmission of the HO command is shown in Figure 30. The BS power consumption decreases for low SRS periodicity values then it starts increasing at high periodicity values because of high HORs due to the high PPR we noted in Figure 28. The UL-HO "40 ms" periodicity case shows the lowest BS transmitted power consumption, almost 17% lower than the DL-HO.

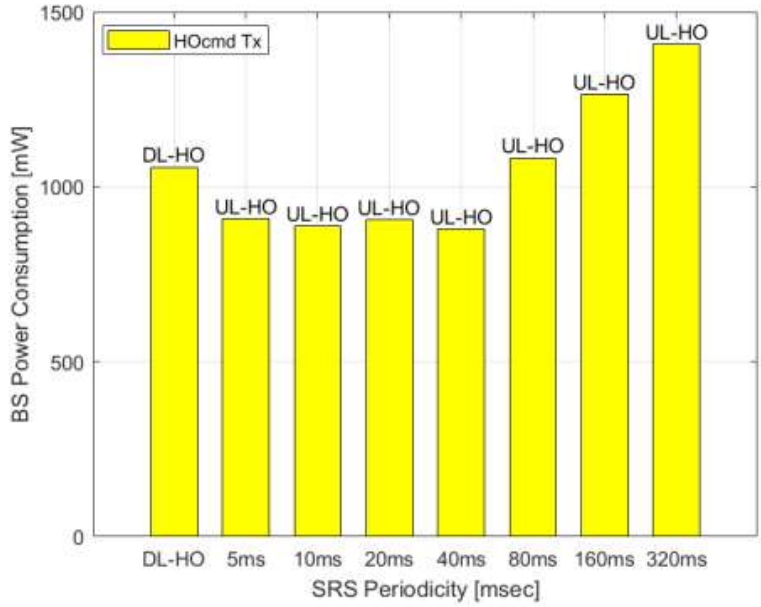

Figure 30. BS transmitted average supply power consumption comparison for DL-HO and UL-HO, at fixed ISD= 500m, speed = 30km/h, DL/UL offset= 1 dB, and DL/UL TTT= 32ms.

4.3.3 Received Power Consumption

This section provides a comparison of DL-HO and UL-HO in terms of power consumption due to the reception of signalling messages of the UE/BS. The HO signaling messages that are transmitted from the BS side are received at the UE and similarly, the messages transmitted from the UE side are received at the BS.

UE Received Power Consumption

The average supply UE power consumption resulting from the reception of the HO command is presented in Figure 31. The graph follows the same trend as we noted in Figure 30 but the UE power consumption is much lower than the BS power consumption we noted in Figure 30. The UL-HO "40 ms" periodicity case shows the lowest UE received power consumption, almost 27% lower than the DL-HO.

BS Received Power Consumption

Figure 32 exhibits the BS average supply power consumption due to HO-related signaling reception for both DL-HO and UL-HO. The plot presents that UL-HO outperforms for all periodicity cases, as no measurement report is received for this case. The lowest BS power consumption is found for the SRS periodicity case of "40 ms", which is practically half (49%) of the DL-HO.

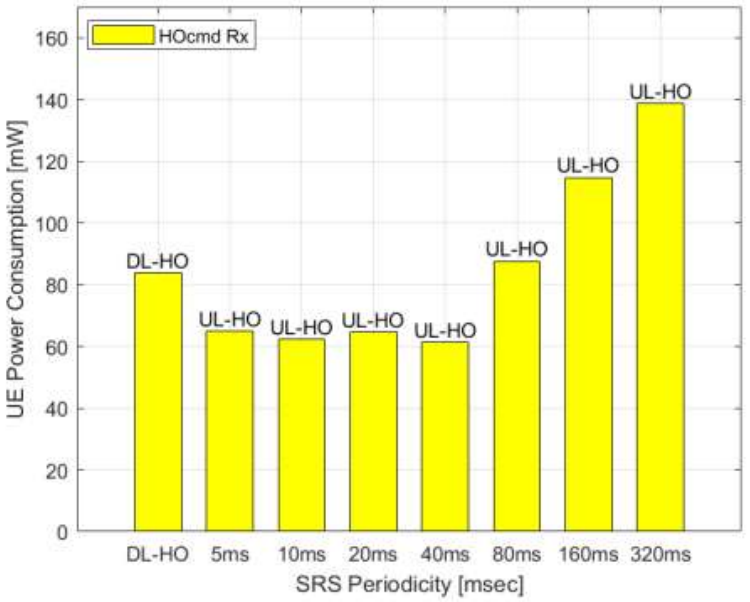

Figure 31. UE received average supply power consumption comparison for DL-HO and UL-HO, at fixed ISD= 500m, speed = 30km/h, DL/UL offset= 1 dB, and DL/UL TTT= 32ms.

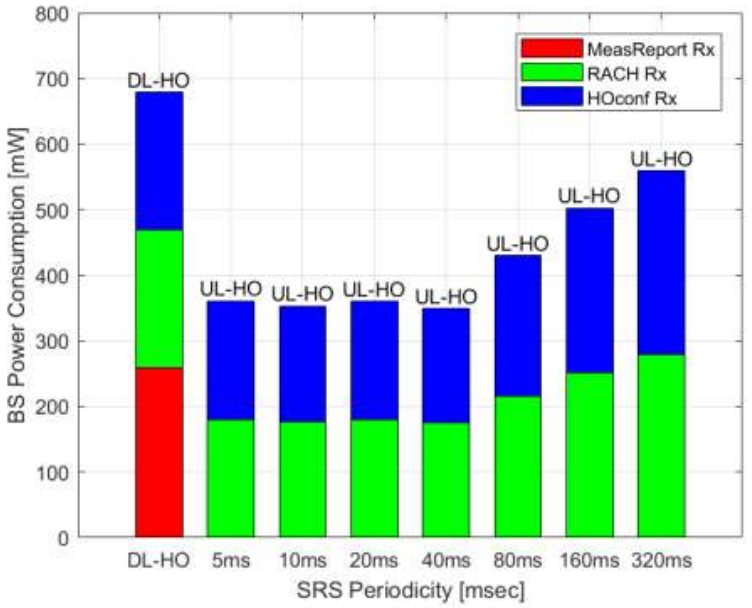

Figure 32. BS received average supply power consumption comparison for DL-HO and UL-HO, at fixed ISD= 500m, speed = 30km/h, DL/UL offset= 1 dB, and DL/UL TTT= 32ms.

4.3.4 Uplink Reference Signal Power Consumption

This section provides the power consumption comparison of DL RS and UL RS transmission and measurement at the UE/BS side. The details of how we calculate the DL/UL RS transmission and measurement are described in Publication VII. The signaling rate for the DL-RSRP and the UL-RSRP measurements are obtained using the system-level simulator. The average supply UE power consumption for DL RS measurements in comparison to UL RS transmission power consumption is shown in Figure 33. It is to be noted that the UL RSs are transmitted from the UE while the DL RSs are received at the UE. The graph shows the DL RS measurement has the highest power consumption because the UE has to measure the DL RS from both the s-BS as well as the neighboring BSs. In contrast, the UL RS transmission has the lowest UE power consumption as the UE only needs to send the SRS that is received at multiple BSs. The UE UL RS transmission power consumption practically remains consistent between 5ms and 20ms then it starts decreasing for high periodicities due to a lower number of UL RS transmissions. The UL-HO consumes almost four times less UE power in comparison to the DL-HO for the "40ms" periodicity case.
The DL RSs are transmitted from the BS side while the UL RS measurements are processed at the BS. The average supply BS power consumption for DL RS transmission in comparison to UL RS measurement power consumption is shown in Figure 34. For low periodicity values {5ms, 10ms, 20ms}, the power consumption of UL RS measurement is higher than the DL RS transmission because of the high number of UL RS receptions at multiple BSs. The UL RS measurement power consumption reduces with increasing periodicities due to fewer SRS transmissions. The UL-HO consumes half of the BS power in comparison to DL-HO for the "40ms" periodicity case.

4.3.5 Total Power Consumption

The total average supply power consumption for each air-interface HO signaling message (i.e. the sum of transmitted and received power consumption) is shown in Figure 35 where the percentage of power increase or decrease in comparison to DL-HO is also shown. The graph exhibits that the total power consumption shows a decreasing trend in comparison to DL-HO until a sweet-spot of "40ms" periodicity arrives, then it again starts increasing. After the 40ms periodicity case, the high power consumption is due to the frequent HOs we noted in Figure 28. The SRS periodicity case of "40 ms" shows the lowest total average supply power consumption, almost 30% lower than the DL-HO.

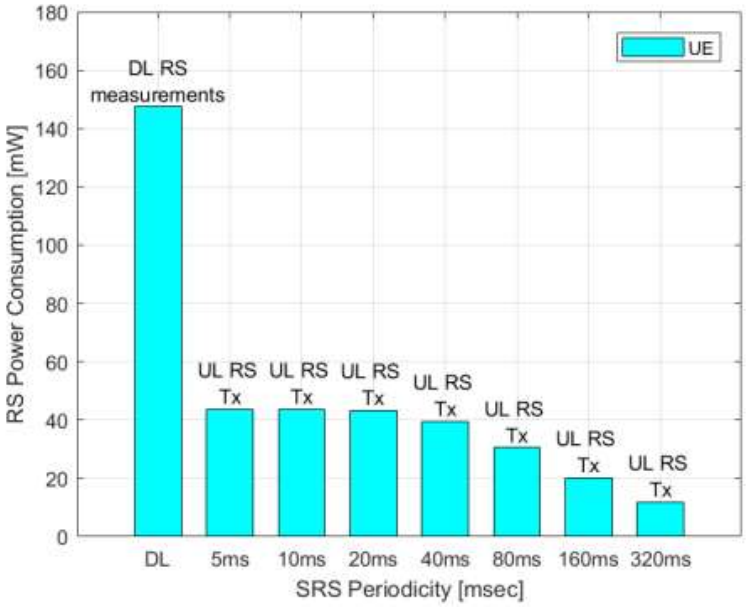

Figure 33. UE reference signal average supply power consumption comparison for DL and UL RS-based mobility, at fixed ISD= 500m, speed = 30km/h, DL/UL offset= 1 dB, and DL/UL TTT= 32ms.

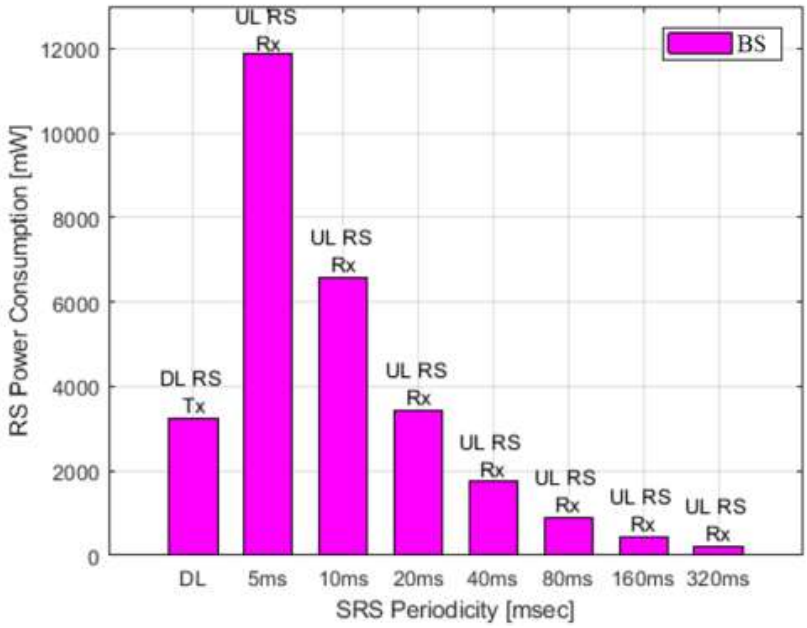

Figure 34. BS reference signal average supply power consumption comparison for DL and UL RS-based mobility, at fixed ISD= 500m, speed = 30km/h, DL/UL offset= 1 dB, and DL/UL TTT= 32ms.

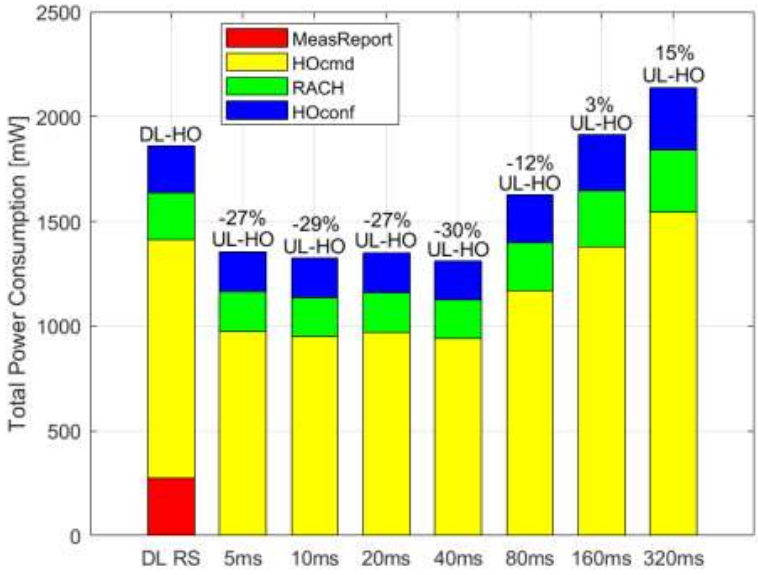

Figure 35. Total average supply power consumption comparison for DL-HO and UL-HO, at fixed ISD= 500m, speed = 30km/h, DL/UL offset= 1 dB, and DL/UL TTT= 32ms.

4.4 Discussion and Conclusion

In this Chapter, we found that the UL-HO measurement phase is more energy-efficient in comparison to DL-HO because no measurement report transmission is required, which is in line with the previous works in [70][89]. In the previous works [71][91][92], it was found that UL-HO can reduce UE power consumption and HOFs. However, our simulation analysis shows that the proposed UL-HO can reduce HOR, HOFs, and PPs rate in comparison to DL-HO if the SRS periodicity is carefully chosen ("40 ms" in this simulation scenario). Furthermore, the UL-HO reduces the average supply power consumption at both UE and BS sides, BS transmitted by 17%, UE transmitted by 48%, BS received 49%, UE received 27%, and total power consumption by 30% in comparison to DL-HO, for an optimum SRS periodicity case of "40 ms". We found that the UL RS transmission requires almost four times less power consumption while the UL RS measurement requires only half of the power consumption in comparison to DL-HO, at the "40 ms" periodicity case. This concludes that UL-HO is power-efficient at both UE and BS sides and it is beneficial since it reduces OPEX and environmental effects. Also, the UL-HO outperforms in comparison to existing techniques in literature, i.e. the reactive HO technique in [19] and early HO initiation in [15][21], as it significantly improves the HO performance and reduces the signaling overhead and power consumption. The benefits of using the UL-HO scheme come at the cost of some new requirements. The first requirement is that the time synchronization between s-BSs and several t-BSs need to receive the UL RS simultaneously. Secondly, the existing interfaces (e.g. X2 or S1 in

LTE) require some minor standard upgrades in defining the information elements to be communicated between the BSs and controller. Lastly, there is a need to coordinate UL RS resources between different cells to avoid pilot contamination, i.e. having different UEs sending the UL RS over the same resources thus inducing erroneous measurements.

5. Uplink Reference Signal based Energy-Efficient Handover for Mobile Relays and Mobile Small Cells

This section extends the discussion on how UL-HO can be applied to implement MSCs or MRs. The UL-HO measurement procedure for MRs is briefly described. Furthermore, the impact of varying on-board UEs cluster size on the UL-HO performance and the associated power consumption is analyzed. Finally, the performance of UL-HO for MSCs (in the form of MRs) in terms of signaling cost and energy efficiency is compared with DL-HO to identify the potential benefits.

5.1 Uplink Handover Measurement Procedure for Mobile Relays

The architecture Alt 1 MRN UL-HO measurement procedure is presented in Figure 36. The s-DBS and neighboring DBSs receive the UL RSs transmitted by the MRN, allowing the network to compute UL-RSRP. A central network controller process these measurements, to decide which DBS shall serve a given MRN. If the UL-RSRP of a t-DBS is higher than the s-DBS by an "A3 UL-offset" and this condition is maintained during UL-TTT, the controller makes the HO decision and notifies the s-DBS with the t-DBS. Upon successful reception of the potential t-DBS information at the s-DBS, an HO request is issued from the s-DBS to the t-DBS. The rest of the HO procedure is common to both DL-HO and UL-HO schemes starting from the HO preparation phase in Figure 3. The UL-HO scheme does not require a MeasReport to be transmitted from the MRN and received at the DBS in comparison to legacy DL-HO (see Figure 3 and Figure 36), thus it reduces the power consumption and OPEX.

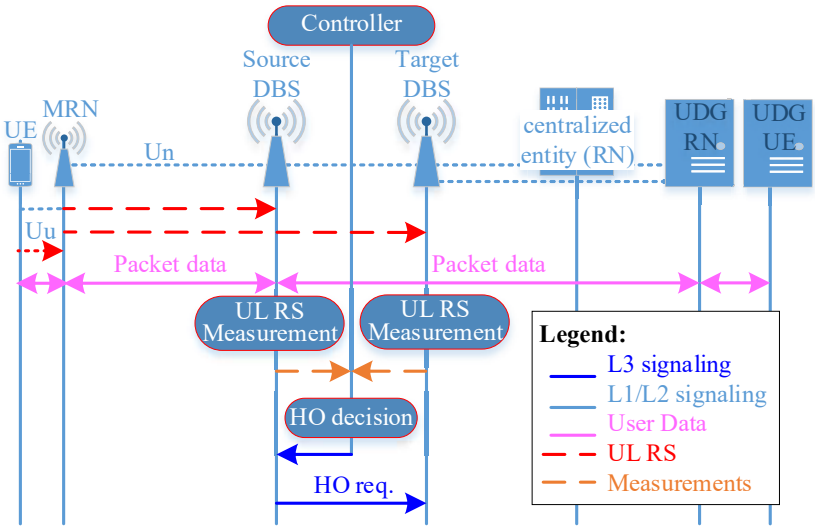

Figure 36. Architecture Alt 1 MRN proposed handover scheme with UL RS-based measurements (adapted from [72][73][74][89]).

5.2 Simulation Analysis

This section provides the performance of UL-HO for MRNs in terms of HO performance, signaling cost, and energy efficiency to compare it with DL-HO. This section also analyzes the impact of varying on-board UEs cluster size on UL-HO performance and the associated power consumption.

5.2.1 Mobile Relay Node Assisted User Clustering

The deployment scenario and the main simulations assumption for this subsection are covered in Section 3.2.1, Scenario 2, and Figure 7. This section provides the impact of varying on-board UEs cluster size on the HO performance metrics and the associated power consumption. A set of {12%, 24%, 36%, 48%} UEs out of 100 total UEs are traveling on three buses deployed across the scenario and the remaining off-board UEs are moving outside the bus, all over the scenario. The four following case scenarios are simulated:
Case 1: DL-HO without MRN
Case 2: DL-HO with MRN
Case 3: UL-HO without MRN
Case 4: UL-HO with MRN

Figure 37 shows the impact of varying on-board UE cluster size on the total average supply power consumption (i.e. addition of both transmitted and received power consumption). It is clear from the graph that the DL-HO cases (i.e. Case 1 and Case 2) have the power consumption due to MeasReport transmission/reception while the UL-HO cases (i.e. Case 3 and Case 4) do not require the measurement report transmission/ reception, which reduces the overall power consumption. The power consumption of HOcmd is higher than other

air-interface HO signaling because of the higher number of resources consumed (see Table 2 for details). For the low on-board UEs case (i.e. 12% UEs on-board), the UL-HO without MRNs (Case 3) provides better power consumption performance in comparison to DL-HO with MRNs (Case 2). For example, in the case of connected cars, the HO total power consumption can be reduced by only utilizing UL-HO, without deploying MRNs. The UL-HO scheme significantly reduces the power consumption in comparison to DL-HO because of the reduced number of HORs, HOFRs PPRs, and no requirement for MeasReport transmission/reception (see Publication VIII for details). Furthermore, increasing the on-board UEs cluster size reduces the total power consumption significantly for Case 4 in comparison to other cases (an approximate power saving of 780 mW in comparison to Case 1, for the 48% UEs on-board case). For example, in the case of buses and trains where we have a higher number of on-board UEs, the HO total power consumption can be reduced to its minimal level by utilizing the UL-HO scheme with MRNs.

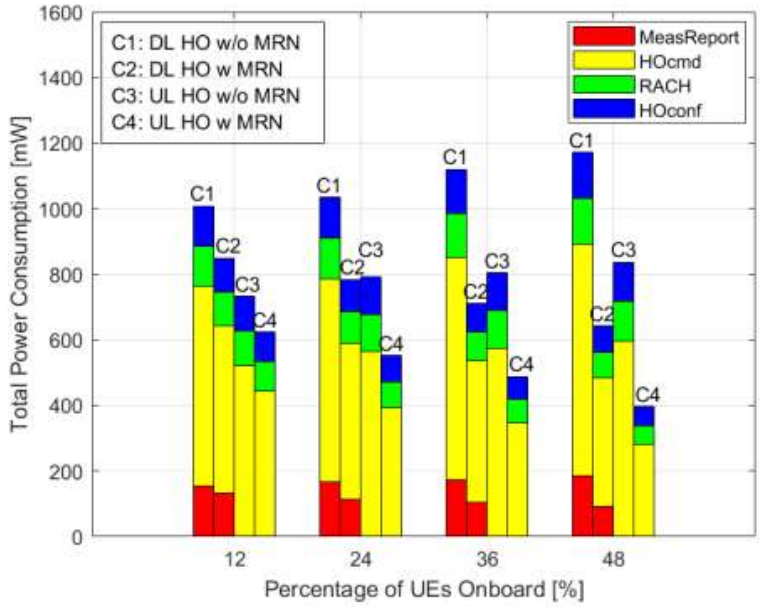

Figure 37. Impact of varying the cluster size of on-board UEs on the total average supply power consumption.

5.2.2 Uplink Handover Performance Evaluation for Mobile Relays and Group Mobility Scenarios

In this section, we provide a simulation evaluation of the UL-HO performance and the total power consumption in case of group mobility scenarios, with/without installing an MRN, in comparison to DL-HO. The deployment scenario and the main simulation assumptions for this and the following sub-section are covered in Section 3.2.1, Scenario 1, and Figure 6. A set of 24 UEs out of 200 total UEs are on board traveling on a bus at a fixed-trajectory and the remaining off-board UEs are moving outside the bus, all over the scenario. We motivate this

from the results we obtain in section 5.2.1 that the MRN is only suitable for a higher number of on-board UEs. Two case scenarios of UL-HO and DL-HO are simulated to have a fair comparison, DL/UL HO without MRN and DL/UL HO with MRN.

For the simulation evaluation, we assume that the DL-HO and UL-HO A3 event check occurs at each DL/UL RS periodicity (i.e. $T_{DLRS}/\mathrm{T_{SRS}} = \{20, 40, 60, 80\}$ ms) to have a fair comparison. Similarly, we assume that the number of samples of measurement updates to trigger the HO are $N_{samples} = 3$, the same number for both DL-HO and UL-HO cases. Also, the TTT is $N_{samples} * T_{SRS}/T_{DLRS}$, the ISD is fixed at 500 m, and the A3 offset is fixed at 3dB for both the DL-HO and UL-HO cases. In the next sub-sections, we will show the performance of DL-HO and UL-HO without MRN in Section 5.2.3, with MRN in Section 5.2.4, and all four aforementioned cases with/without MRN total power consumption in Section 5.2.5.

For DL-HO with MRN, we assume that the on-board UEs will not perform DL RS measurements from neighboring BSs as the MRN will perform the measurements from DBSs on their behalf. Similarly, for UL-HO with MRN, the on-board UEs will not transmit UL RSs to nearby BSs, only the MRN will do this on their behalf. In the case of MRN HOF to a DBS, the on-board UEs will perform their individual HO procedure with the nearby BSs. The off-board UEs are directly connected to BSs through their individual HO procedure for both UL-HO (see Figure 25) and DL-HO (see Figure 1) cases. In short, an individual UE HO is needed for all off-board UEs and on-board UEs only in case of an MRN HOF to a DBS.

5.2.3 Without Mobile Relay Node

In this section, two without-MRN cases are simulated namely, 'DL-HO w/o MRN' and 'UL-HO w/o MRN' for three speeds, {30, 60, 90} km/h, to find the benefits of UL-HO as a function of speed.

5.2.3.1 Handover Metrics

The impact of varying UE speed and DL/UL RS periodicities on the HOR, HOF rate, and PPR is shown in Figure 38, Figure 39, and Figure 40, respectively. One trend of the graphs shows that the HOR, HOF rate, and PPR increase as the UE speed increases for both DL-HO and UL-HO schemes. This is because UEs spend less time in the "HO region" as the speed increases and move out of the serving cell before the HO procedure completes thus causing more HOFs (see Figure 39) which consequently increases the HOR. The second trend shows that UL-HO can significantly reduce the HOF rate (see Figure 39). This is because of the fact that UL-HO eliminates the MeasReport signaling thus the HO procedure completes before the UE loses its connection with the s-BS, reducing the HOFs and consequently the HOR (see Figure 38). The third trend reveals that the low periodicities (i.e. 20 ms) have a higher HOR, HOF rate, and PPR. This is because of the fact that too many updates in measurements cause many A3 event evaluations consequently leading to unnecessary handovers and HOFs. However, the proposed UL-HO scheme can reduce the HOF rate and PPR (see Figure 39, and Figure 40 for details) especially at low periodicities, and consequently the HOR (see Figure 39). We observe a trade-off between HOFs and PPR at higher speeds (i.e. 60 km/h and 90 km/h) and high periodicities that reduce the UL-HO gain in terms of HOR (see for Figure 38 details). This trade-

off is in-line with the works presented in [93][94][95][96][97] that shows reducing the HOFs would increase the PPR. Also, high TTT values at high periodicities keep the UE connection with the s-BS for a longer time thus a significant reduction in HOR cannot be achieved even when the UL-HO eliminates the MeasReport signaling (i.e. TTT is three times the periodicity). In conclusion, the UL-HO without-MRN scenario can significantly improve the HO performance metrics if we optimize the periodicity to 20 ms, for all evaluated speeds. With the UL-HO scheme, the average reduction in the HOR is between 5% and 11%, HOF rate between 50% to 76%, and PPR between 3% to 26% in comparison to DL-HO, depending on the speed.

5.2.3.2 UE Power Consumption

The total UE power consumption is the sum of the MeasReport, RACH and HO confirm air-interface signaling message transmission and the HO command reception power consumption. Figure 41 exhibits the UE total power consumption as a function of speed and DL/UL RS periodicities. It is clear from the chart that the power consumption of UL-HO is always lower than the DL-HO for all simulated cases as it removes the power consumption part due to the transmission of the MeasReport. A significant reduction in UE power consumption is seen for the 20 ms periodicity case of all speeds because of the highest improvement the UL-HO brings in terms of HOR, HOF rate, and PPR (see Figure 38, Figure 39, and Figure 40 respectively) for this specific case. Overall, the UL-HO can reduce the UE power consumption by 15% to 25% in comparison to DL-HO, depending on the speed.

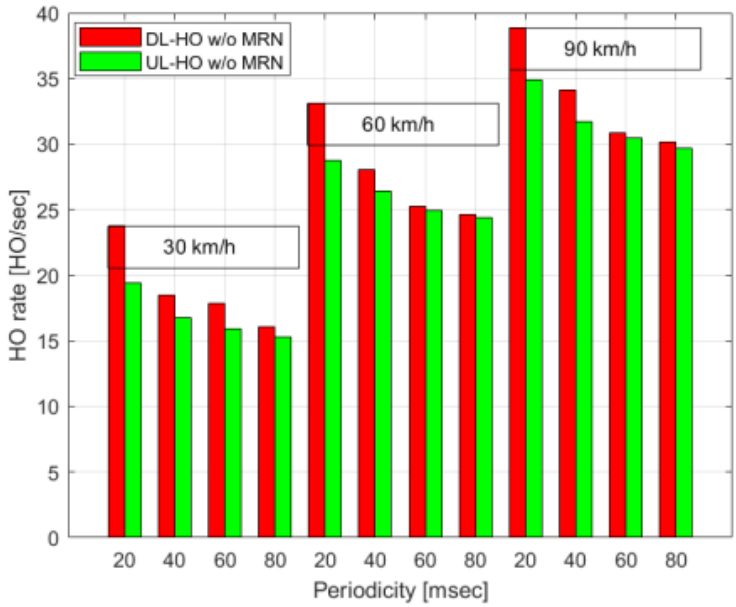

Figure 38. Impact of varying UE speed and UL/DL RS periodicity on HO rate (without MRN).

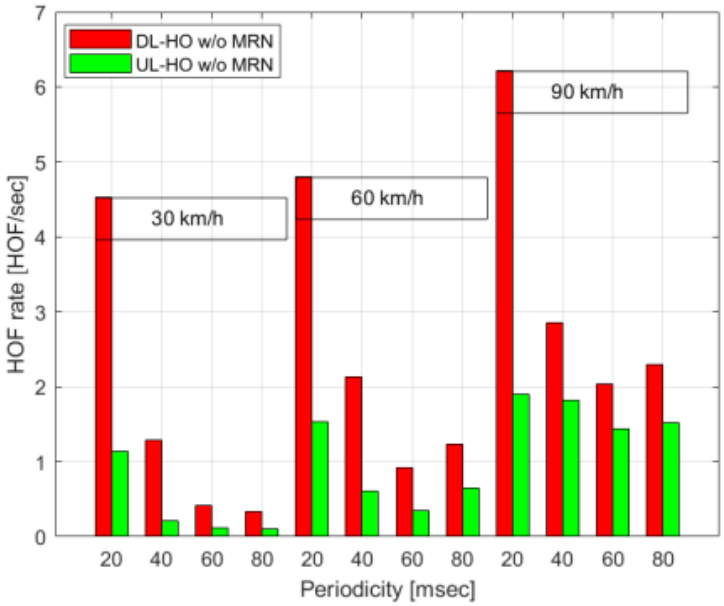

Figure 39. Impact of varying UE speed and UL/DL RS periodicity on the HOF rate (without MRN).

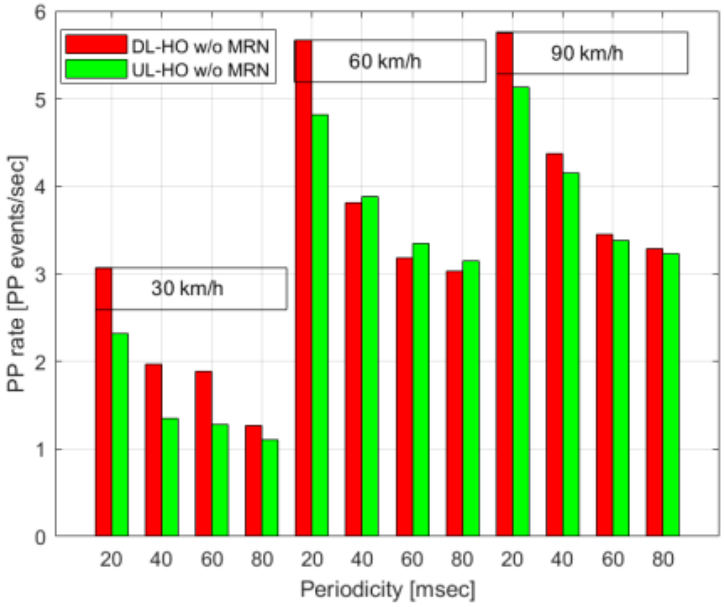

Figure 40. Impact of varying UE speed and UL/DL RS periodicity on PP rate (without MRN).

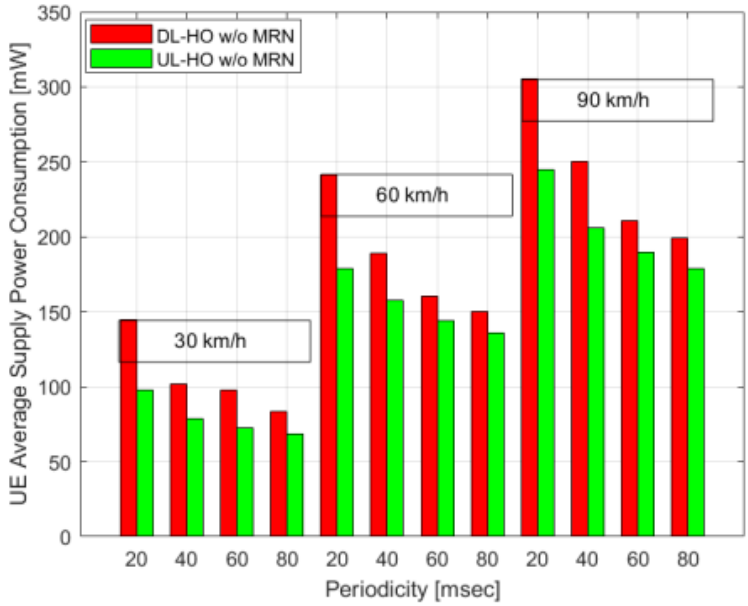

Figure 41. Impact of varying UE speed and UL/DL RS periodicity on UE total average supply power consumption (without MRN).

5.2.3.3 BS Power Consumption

The total BS power consumption is the sum of HO command transmission, along with the MeasReport, RACH and HO confirm air-interface signaling message reception power consumption. Figure 42 presents the BS average supply power consumption at different UE speeds and periodicities. The trend of the chart is the same as we noted in Figure 41 but the BS power consumption is much higher than the UE power consumption. It is apparent that the UL-HO can also significantly reduce the BS power consumption as it removes the power consumption part due to the reception of the MeasReport. On average, the UL-HO scheme provides an average BS power consumption reduction of 18% to 23% in comparison to DL-HO, depending on the speed.

5.2.3.4 Reference Signal Transmission and Measurement Power Consumption

The impact of varying the UE speed and DL/UL RS periodicity on the DL/UL RS transmission and measurement average supply power consumption is shown in Figure 43 which is the sum of DL/UL RS transmission and reception power consumption. The details of how we calculate the DL/UL RS transmission and measurement are described in Publication IX. It is to be noted that the RS power consumption remains the same for all speed values as it depends only on time (see Publication IX for details). As expected, the plot reveals that the power consumption reduces with increasing periodicities because of infrequent RS transmission. Overall, the UL-HO RS power consumption is almost 61% lower than the DL-HO case because of lower resource consumption.

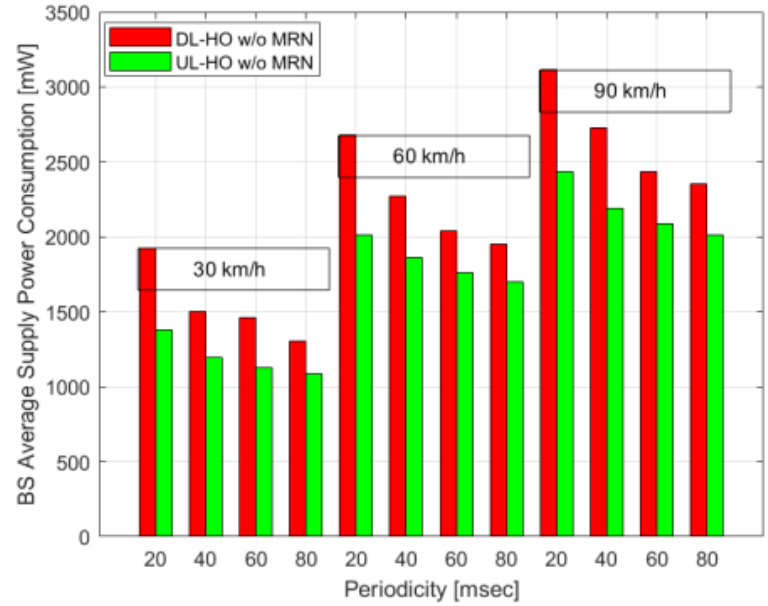

Figure 42. Impact of varying UE speed and UL/DL RS periodicity on BS total average supply power consumption (without MRN).

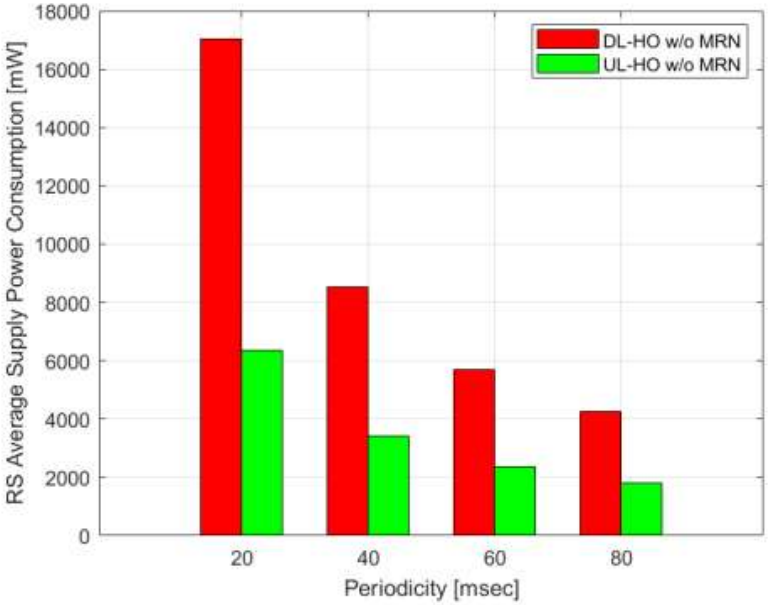

Figure 43. Impact of varying UE speed and UL/DL RS periodicity on RS total average supply power consumption (without MRN).

5.2.3.5 Total Power Consumption

We computed the total power consumption by adding both the UE and BS power consumption, i.e. the sum of Figure 41 and Figure 42 for various HO signaling over the air interface, namely: the MeasReport, the HOcmd, the RACH,

and the HOconf transmission and reception. Figure 44 presents the total average supply power consumption that clearly shows a significant reduction in total power consumption using the proposed UL-HO scheme. The reduction of the total power consumption using the UL-HO method is linked to getting rid of the MeasReport signaling, and the reduction of overall HOR (see Figure 38) and HOFs (see Figure 39). The highest reduction in power consumption is seen at the 20 ms periodicity case of the UL-HO scheme as the UL-HO reduces the HOR, HOFs, and PPR significantly for this specific case. However, the reduction in power consumption through UL-HO at high speed and high periodicities is lower because of the high PPR we noted in Figure 40. On average, the UL-HO scheme provides an average total power consumption reduction of 19% in comparison to DL-HO for all the simulated cases.

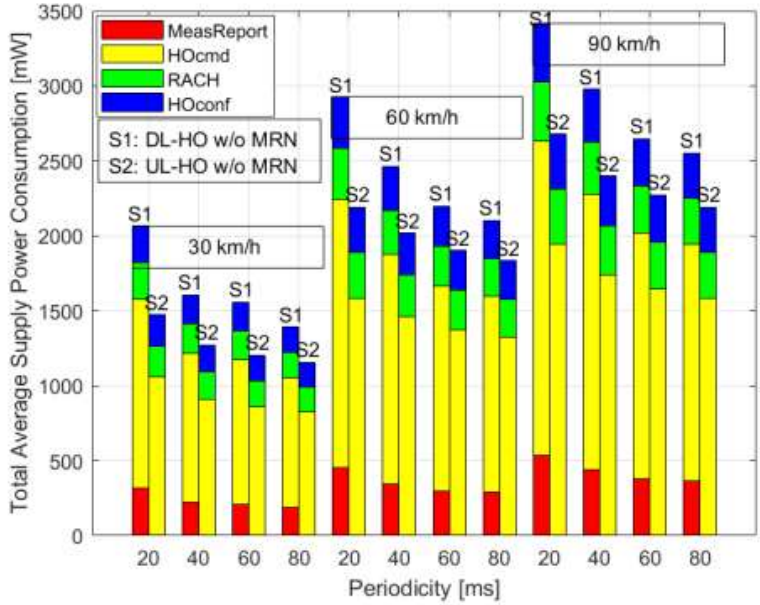

Figure 44. Impact of varying UE speed and UL/DL RS periodicity on the total average supply power consumption (without MRN).

5.2.4 With Mobile Relay Node

In this section, we will see the gains we achieve by using the MRN to service the on-board UEs for both the DL-HO and UL-HO.

5.2.4.1 Handover Metrics

The impact of varying UE speed and UL/DL RS periodicity on HOR (for all UEs), HOR (for on-board UEs only), HOF rate, and PPR is presented in Figure 45, Figure 46, Figure 47, and Figure 48, respectively when the on-board UEs are serviced through an MRN. Overall, the diagrams show that the HOR, HOF rate, and PPR are lower than the cases with no MRN. This is especially linked to the cell-edge users that now have good radio link conditions because of the connection with the MRN. Another trend in the graph shows that UL-HO still performs better in comparison to DL-HO. This is because the MRN-connected user in the case of DL-HO can still suffer from frequent HOs (see Figure 46) because of the MRN HOF to a DBS. However, the UL-HO scheme does not require the MeasReport signaling which reduces the HO delay, and the chances of MRN

HOF to a DBS, and thus, provides uninterrupted services for on-board UEs. So the UL-HO with MRN provides a higher gain in terms of reducing the HOR even at high speeds and high periodicities in comparison to the no-MRN case (see Figure 38 and Figure 45 for comparison) because of reduction in on-board UEs' HOR due to the deployment of an MRN. For the with-MRN case, we again reveal a trade-off between HOFs and PPs, similarly as we noted for the without-MRN cases. With the UL-HO scheme, the average reduction in the HOR is between 8% and 13%, HOF rate between 54% and 71%, and PPR between 10% and 22% depending on the speed.

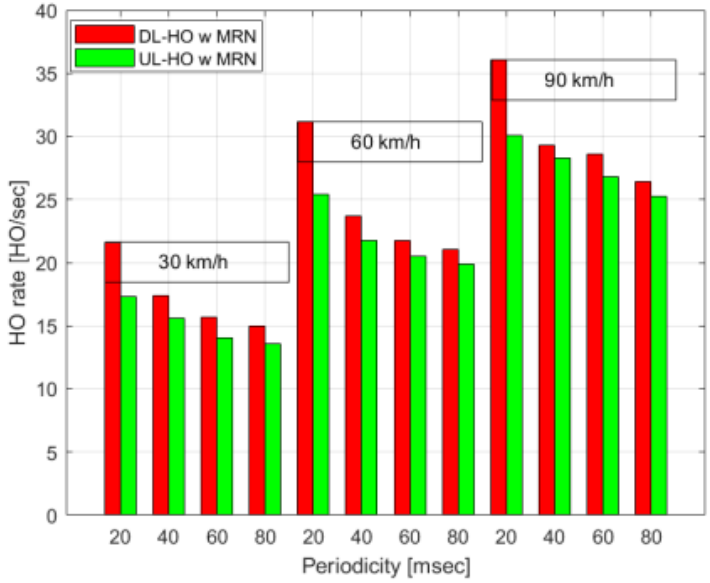

Figure 45. Impact of varying UE speed and UL/DL RS periodicity on HO rate (with MRN).

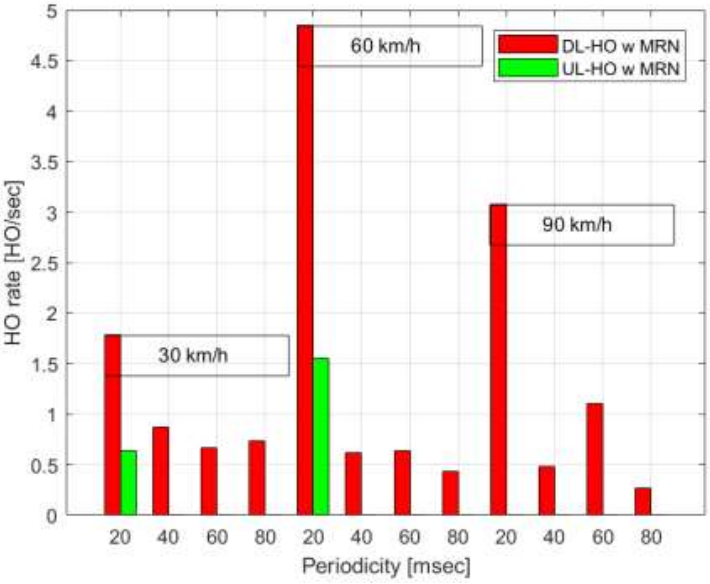

Figure 46. Impact of varying UE speed and UL/DL RS periodicity on HO rate for only on-board UEs (with MRN).

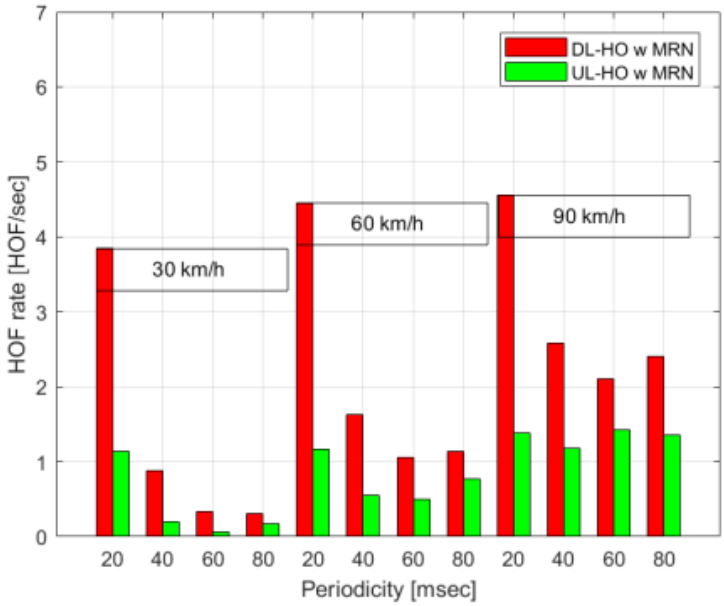

Figure 47. Impact of varying UE speed and UL/DL RS periodicity on the HOF rate (with MRN).

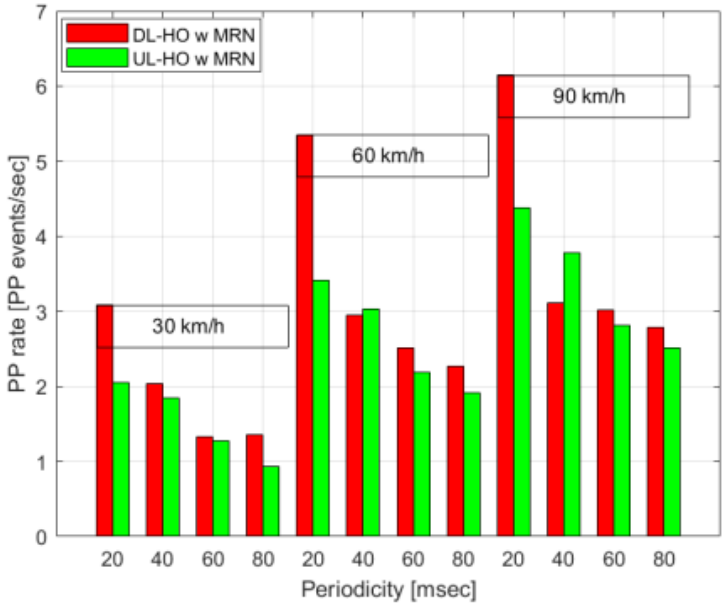

Figure 48. Impact of varying UE speed and UL/DL RS periodicity on PP rate (with MRN).

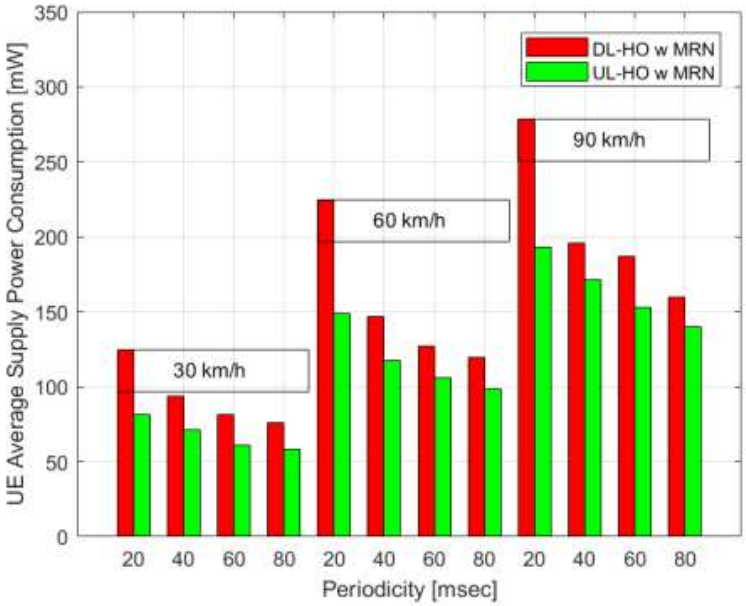

Figure 49. Impact of varying UE speed and UL/DL RS periodicity on UE total average supply power consumption (with MRN).

5.2.4.2 UE Power Consumption

Figure 49 provides the UE power consumption as a function of speed that shows the same trend as we noted in Figure 41 but deploying MRN herein significantly reduces the UE power consumption especially when we utilize the UL-HO procedure. This is because the MRN performs the group HO procedure on behalf of the on-board UEs and the UL-HO reduces the chance of MRN SPoF. Overall, the UL-HO scheme provides an average UE power consumption reduction of 20% to 28% in comparison to DL-HO, depending on the speed which is higher than the without-MRN case.

5.2.4.3 BS Power Consumption

Figure 50 presents the BS average supply power consumption at different UE speeds that also show the same trend as we noted in Figure 42 but the BS power consumption is reduced significantly because of the MRN deployment (see Figure 42 and Figure 50 for comparison). The graph shows that the UL-HO with-MRN case significantly reduces the BS power consumption, especially at low periodicities, i.e. at speed 30 km/h by around 500 mW, and at speed 60 km/h and 90 km/h by 800 mW in comparison to the legacy DL-HO method. On average, the UL-HO with-MRN scheme provides an average BS power consumption reduction of 20% to 24% in comparison to DL-HO, depending on the speed.

5.2.4.4 Reference Signal Transmission and Measurement Power Consumption

The RS power consumption is shown in Figure 51 that remains the same for all speeds because it is dependent on the time (i.e. how often we send or receive the RS). The trend of the graph is the same as depicted in Figure 43 but the RS power consumption is lower because of our assumption that the on-board UEs stop RS transmission/measurement when they are connected with an MRN to save energy. Overall, the UL-HO scheme provides an average RS power consumption reduction of 60% in comparison to DL-HO for all simulated cases.

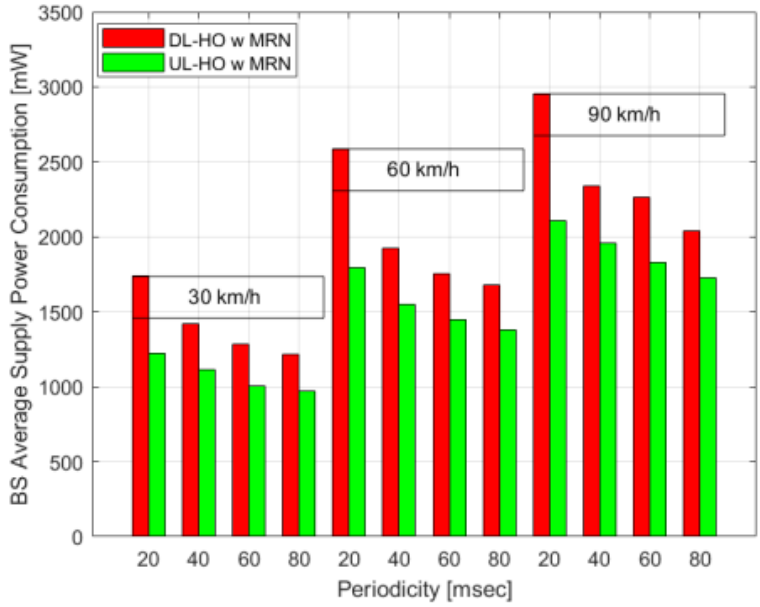

Figure 50. Impact of varying UE speed and UL/DL RS periodicity on BS total average supply power consumption (with MRN).

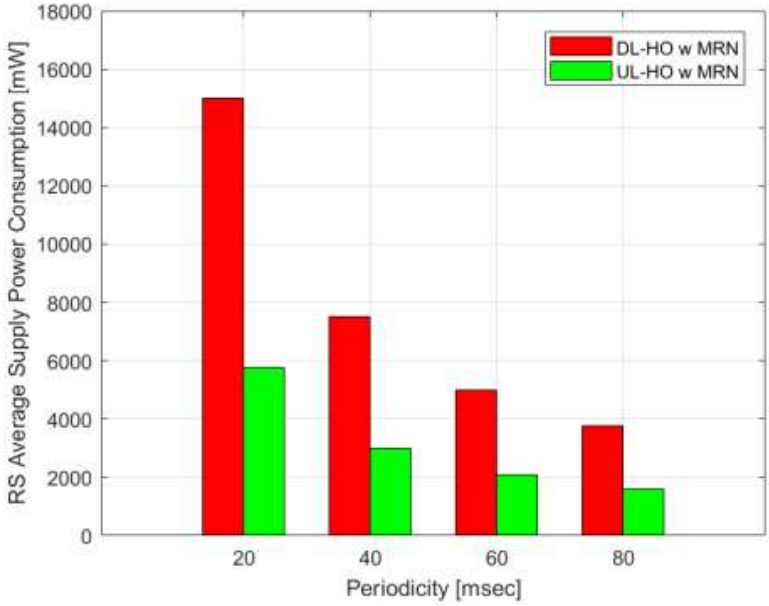

Figure 51. Impact of varying UE speed and UL/DL RS periodicity on RS total average supply power consumption (with MRN).

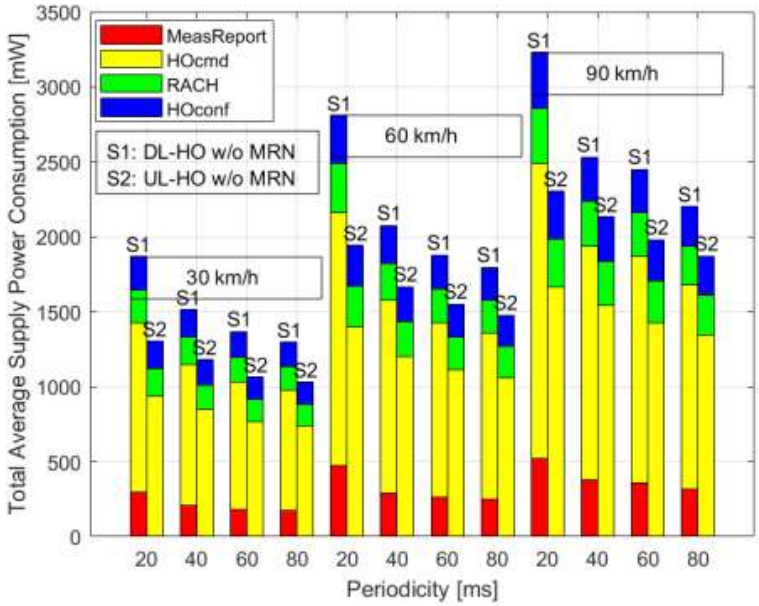

Figure 52. Impact of varying UE speed and UL/DL RS periodicity on total average supply power consumption (with MRN).

5.2.4.5 Total Power Consumption

Figure 52 presents the impact of a varying UE speed on the total average supply power consumption that shows the same trend as observed in Figure 44 with extra gains in terms of reducing the power consumption that we obtain by the deployment of the MRN. On average, the UL-HO scheme provides an average total power consumption reduction of 22% in comparison to DL-HO for all simulated cases.

5.2.5 Total Power Consumption With and Without MRN

The impact of a varying UE speed on the total average supply power consumption for both with-and without-MRN cases is presented in Figure 53. At both 30km/h and 90km/h speeds: S3 (UL-HO w/o MRN) outperforms S2 (DL-HO w MRN) for all periodicities. In this way, the UL-HO scheme saves MRN deployment and OPEX cost. Similarly, at speed 60km/h, S3 outperforms S2 at periodicities {20, 40}ms while other periodicities have also almost the same power consumption for both S2 and S3. Overall, the UL-HO with-MRN scheme has the lowest total power consumption for all speeds and periodicities. So, deploying an MRN with the UL-HO scheme seems to be the most attractive solution in terms of lowest power consumption, i.e. on average a 30% power consumption reduction in comparison to DL-HO without an MRN for all simulated cases.

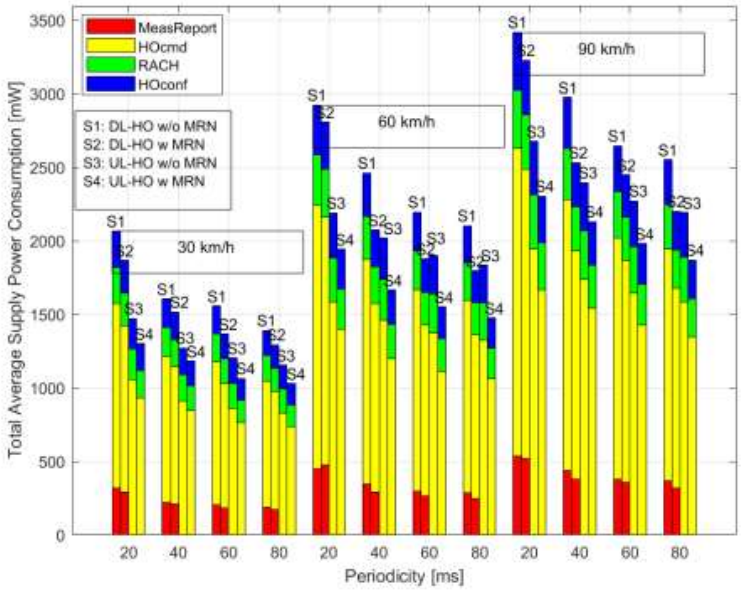

Figure 53. Impact of varying UE speed and UL/DL RS periodicity on total average supply power consumption (without and with an MRN).

5.3 Discussion and Conclusion

In the first part of this Chapter, it is observed that the MRN is one of the most feasible group HO solutions for a higher number of on-board UEs which is in line with the works presented in [52][58][59]. For less on-board UEs (i.e. 8 UEs per bus), the proposed UL-HO scheme, without MRN provides the same performance as in DL-HO with MRN, thus the UL-HO reduces the MRN deployment cost and the OPEX. The UL-HO with-MRN case can significantly reduce the power consumption for a higher number of on-board UEs (i.e. 48% on-board UEs case).

The second part of this Chapter extends the applicability of UL-HO for MRNs and group mobility (i.e. passengers traveling on a bus) scenarios. We found that the UL-HO scheme minimizes the HO delays and reduces the chance of the MRN single point of failure (SPoF) and thus provides uninterrupted services to the on-board UEs. Such improvements come because of no MeasReport transmission and reception over the air-interface [70][89], and thus the HO procedure completes before the MRN/UE loses its connection to the s-DBS/s-BS. The highest improvements in HO metrics has been observed for the scenario where both the MRN and the UL-HO procedure is utilized. The UL-HO shows significant improvement in HOR, HOF rate, and PPR especially at low periodicities (i.e. 20 ms) and thus the highest reduction in power consumption is seen for this specific case. Furthermore, a trade-off between the HOF rate and PPR shows that the UL-HO scheme significantly reduces the HOFs but at the cost of an insignificant increase in PPR, especially at higher speeds. In a scenario where

is cost reduction is the first priority, the UL-HO scheme is still a suitable candidate as it outperforms the without-MRN case in comparison to the DL-HO with-MRN case thus reducing the OPEX and MRN deployment cost. In the absence of an MRN, the UL-HO scheme can reduce the HOR by 5% to 11%, HOF rate by 50% to 76%, PPR by 3% to 26%, UE power consumption by 15% to 26%, and BS power consumption by 18% to 23% in comparison to DL-HO, depending on the speed. For the with-MRN case, the UL-HO scheme can reduce the HOR by 8% to 13%, HOF rate by 54% to 71%, PPR by 10% to 22%, UE power consumption by 20% to 28%, and BS power consumption by 20% to 24% in comparison to DL-HO, depending on the speed.

6. Conclusions and Future Work

In this thesis we found that the legacy HO procedure (DL-HO) for both LTE and NR is underperforming for future ultra-dense networks because of high MeasReport signaling, and high HOFs due to delay in the MeasReport delivery. Also we found that the DL-HO is not suitable for the future complex mobility scenarios where both the cells (i.e. MSCs implemented via MRN) and the UEs will be moving at a given speed. In MRN-enabled mobility scenarios, the aforementioned problems of the legacy DL-HO procedure cause the MRN HOF to the DBS especially at higher speeds that can further lead to an SPoF for on-board UEs resulting in a bad user experience. This thesis provides an UL-HO solution to cope with the problems of existing DL-HO. Using the proposed UL-HO scheme, the MeasReport signaling transmission/reception is not required, eliminating the aforementioned issues in the DL-HO. In this way, the UL-HO procedure completes before the UE/MRN/MSC loses its connection with the s-BS/s-DBS, reducing HOR, HOFR, PPR, SPoFs (in case of group mobility) and, most importantly, the power consumption due to the reduction in HO signaling. Therefore, the UL-HO scheme is effective for both dense networks and MSCs and should be used in future cellular networks.

A designer should take care of the following requirements while implementing the UL-HO scheme to the future cellular networks:

1. The UL-HO scheme applies to any radio access technology (incl. 4G, 5G, and 6G) that supports sounding reference signal (SRS).
2. Time synchronization between the BSs receiving the UL RS should be within some specified upper bound.
3. The UL RS configuration parameters (timing, frequency, code, etc.) set by the serving BS should also be shared with the neighboring BSs via existing interfaces (such as e.g. X2 or S1 in LTE).
4. The UL-HO scheme is sensitive to HO parameter selection (i.e. UL RS periodicity, and UL TTT). These parameters should therefore be chosen carefully considering various use cases.

The proposed UL-HO scheme can be applied to the future cellular network generations heading towards small-cell networks operating at higher frequencies and implementing a user-centric no-cell approach (UCNC) [98]. The target of the UCNC approach is to support massive connectivity while turning all UEs to cell-center UEs. The UCNC approach can be implemented in any cellular technology supporting a sounding reference signal (SRS), i.e. LTE and NR which makes our UL-HO scheme the most appropriate to be integrated with a

UCNC approach. In addition, future open radio access network (O-RAN) standard specifications target an RAN architecture based on a softwarized radio resource management (RRM) platform of functions including power-efficient HO as herewith proposed [99]. Such platforms will allow both LTE and NR to follow their own optimization and development, given their actual deployment worldwide. Furthermore, the introduction of Integrated Access and Backhaul (IAB) technology enables on-demand spectrum pooling between the access link and the backhaul link [73][100]. It is anticipated that the current static IAB nodes will evolve into mobile IAB nodes in future 3GPP releases, thus enabling the MCS concept. The proposed UL-HO scheme is very effective for MSCs deployments (especially in the form of MRNs) as it can reduce the MRN/MSC HOFs to the DBS. This makes the proposed UL-HO method more suitable for the MSCs to support power-efficient group mobility.

Future releases of 3GPP are looking for proposals that can especially reduce UE power consumption [101]. Our UL-HO solution is most appropriate as it can improve the user device's battery lifetime. Also, it is suitable to reduce the BS power consumption that can further reduce the OPEX and environmental effects. The proposed UL-HO solutions are being currently studied in 3GPP standardization [90][91][92] as an alternative solution for DL-HO. The simulation analysis in this work confirms that the UL-HO scheme is an excellent candidate for an energy-efficient HO procedure in future releases of the 3GPP standards heading towards higher frequencies, denser network deployments, and on-demand MSCs.

A UE-specific SRS periodicity selection procedure is suggested as a good future work topic, to improve the network performance and further reduce the power consumption (e.g. a UE closer to a cell border will have low periodicity). Also, an SRS power control procedure would be more beneficial to allocate the SRS power according to the UE's location (i.e. cell center, cell edge), to consequently save energy by allocating low SRS transmission power to the UEs/MRNs close to BSs/DBSs. Furthermore, the performance of UL-HO could be assessed in a multi-connectivity scenario and/or leveraging on IAB technology. We note that the implementation of the proposed UL-HO procedure is much easier in IAB technology. This is because the IAB network implements a separate distributed unit and control unit, so the control unit can act as a central network controller (i.e. the controller in Figure 25), potentially being able to process the UL RS measurements and decide which distributed unit shall serve a given UE.

References

[1] Cisco, “Cisco visual networking index: Global mobile data traffic forecast update, 2015–2020”, *white paper*, Feb 2016.
[2] Cisco, “Cisco visual networking index: Global mobile data traffic forecast update, 2017-2022”, *white paper*, Feb 2019.
[3] R. Arshad, H. Elsawy, S. Sorour, T. Y. Al-Naffouri and M. S. Alouini, “Handover Management in 5G and Beyond: A Topology Aware Skipping Approach”, *IEEE Access*, vol. 4, pp. 9073-9081, Dec 2016.
[4] K. Kanwal, “Increased Energy Efficiency in LTE Networks through Reduced Early Handover”, *PhD thesis*, University of Bedfordshire, 2017.
[5] K. Kanwal, G. Safdar, and M. Ur Rehman, “Energy Efficiency Led reduced CO2 Emission in Green LTE Networks”, in *EAI Endorsed Transactions on Energy Web and Information Technologies,* vol. 4, pp. 1-8, Oct 2017.
[6] T. Chen et al.,“Network Energy Saving Technologies for Green Wireless Access Networks”, *IEEE Wireless Communications,* PP. 30-38, Oct 2011.
[7] J. Rodriguez et al., “SECRET - Secure Network Coding for Reduced Energy Next Generation Mobile Small cells”, *IEEE Internet Technologies and Applications (ITA) conference*, pp. 329-333, 2017.
[8] G. P. Pollini, “Trends in handover design,” IEEE Commun. Mag., vol. 34, no. 3, pp. 82-90, Mar. 1996.
[9] D. L. Huff, “Advanced mobile phone service: The developmental system,” The Bell System Technical Journal, vol. 58, pp. 249–269, Jan 1979.
[10] M. Gudmundson, “Analysis of handover algorithms [microcellular radio],” in [1991 Proceedings] 41st IEEE Vehicular Technology Conference, pp. 537–542, May 1991.
[11] X. Yang, S. Ghaheri-Niri, and R. Tafazolli, “Evaluation of soft handover algorithms for UMTS,” in 11th IEEE International Symposium on Personal Indoor and Mobile Radio Communications. PIMRC 2000. Proceedings (Cat. No.00TH8525), vol. 2, pp. 772–776 vol.2, 2000.
[12] C.-C. Lee and R. Steele, “Effect of soft and softer handoffs on CDMA system capacity,” IEEE Transactions on Vehicular Technology, vol. 47, pp. 830–841, Aug 1998.
[13] M. T. Nguyen, S. Kwon and H. Kim, “Mobility Robustness Optimization for Handover Failure Reduction in LTE Small-Cell Networks”, IEEE Transaction on Vehicular Technology, vol. 67, no. 5, pp. 4672-4676, 2018.
[14] S. K. Ray, H. Sirisena and D. Deka, “LTE-Advanced Handover: An Orientation Matching-Based Fast and Reliable Approach”, IEEE conference on Local Computer Networks, pp. 280-283, 2013.
[15] K. Kanwal and G. A. Safdar, “Energy Efficiency and Superlative TTT for Equitable RLF and Ping Pong in LTE Networks”, Springer journal of Mobile Networks and applications, 2018.
[16] Y. Hussein, B. Ali, M. Rasid, A. Sali and A. Mansoor, “A novel cell-selection optimization handover for long-term evolution (LTE) macrocellusing fuzzy TOPSIS”, Elsevier journal of Computer Communications, pp. 22-33, 2016.
[17] S. Chaudhuri, I. Baig and D. Das, “Self organizing method for handover performance optimization in LTE-advanced network”, Elsevier journal of Computer Communications, pp. 151-163, 2017.
[18] Y. Li, B. Cao and C. Wang, “Handover Schemes in Heterogeneous LTE Networks: Challenges and Opportunities”, IEEE Wireless Communications, pp. 112-117, April 2016.
[19] A. Ulvan, R. Bestak and M. Ulvan, “The Study of Handover Procedure in LTE-based Femtocell Network”, IEEE Wireless and Mobile Networking Conference (WMNC), Third Joint IFIP, Oct 2010.
[20] J. Choi et al., “Handover Decision Algorithm Based on Available Data Volume in Hierarchical Macro/Femto Cell Networks,” Proc. 14th Int’l. Conf. Comm. and Electronics IEEE, pp. 145-149, 2012.
[21] H. Park, Y. Choi, B. Kim, and J. Lee, “LTE Mobility Enhancements for Evolution into 5G”, ETRI Journal, vol. 37, pp. 1065-1076, December 2015.
[22] K. Dimou, et. al., “Handover within 3GPP LTE: Design Principles and Performance”, IEEE VTC fall conference, 2009.
[23] X. Zhang, et al. “Multi-Slot Coverage Probability and SINR-Based Handover Rate Analysis for Mobile User in Hetnet”, IEEE Access, vol. 6, pp. 17868-17879, 2018.
[24] D. Perez, I. Guvenc and X. Chu, “Mobility Management Challenges in 3GPP Heterogeneous Networks”, IEEE Communications Magazine, pp. 70-78, Dec 2012.
[25] K. D. C. Silva, et al., “Adaptive Hysteresis Margin Based on Fuzzy Logic for Handover in Mobile Networks With Dense Small Cells”, IEEE Access, vol. 6, pp. 17178-17189, 2018.

[26] X. Gelabert, G. Zhou and P. Legg, “Mobility performance and suitability of macro cell power-off in LTE dense small cell HetNets,” IEEE 18th Int. Workshop Comput. Aided Modeling Design Commun. Links Netw. (CAMAD), pp. 99-103, Sep. 2013.
[27] Y. Song, P. Y. Kong and Y. Han, “Potential of Network Energy Saving Through Handover in HetNets,” IEEE Trans. Veh. Technol., vol. 65, no. 12, pp. 10198–10204, Dec. 2016.
[28] D. Xenakis, N. Passas and C. Verikoukis, “An energy-centric handover decision algorithm for the integrated LTE macrocell–femtocell network”, Elsevier journal of Computer Communications, pp. 1684.1694, 2012.
[29] M. M. Hasan, S. Kwon and J. H. Na, “Adaptive Mobility Load Balancing Algorithm for LTE Small-Cell Networks,” IEEE Trans. Wirel. Commun., vol. 17, no. 4, pp. 2205–2217, Apr. 2018.
[30] A. Ichkov, V. Atanasovski and L. Gavrilovska, “Analysis of Two-Tier LTE Network with Randomized Resource Allocation and Proactive Offloading,” Mobile Netw Appl, Springer, pp. 806–813, 2017.
[31] F. Guidolin et al., “Context-Aware Handover Policies in HetNets” IEEE Transactions on Wireless Communications, vol. 15, no. 3, pp. 1895-1906, March 2016.
[32] Z. Ali, et al.,”Machine learning based handover management for improved QoE in LTE”, IEEE/IFIP Network Operations and Management Symposium, 2016.
[33] H. Kalbkhani, et al., “QoS-Based Multi-criteria Handoff Algorithm for Femto-Macro Cellular Networks”, Springer Wireless Pers Commun, vol. 98, pp. 1435–1460, 2018.
[34] X. Xu, et al., “Modeling and Analyzing the Cross-Tier Handover in Heterogeneous Networks”, IEEE Transactions on Wireless Communications, vol. 16, vo. 12, pp. 7859-7869, December 2017.
[35] M. M. Hasan , S. Kwon and S. Oh, “Frequent-Handover Mitigation in Ultra-Dense Heterogeneous Networks”, IEEE Transactions on Vehicular Technology, vol. 68, no. 1, pp. 1035-1040, January 2019.
[36] K. Vasudeva, et al., “Analysis of Handover Failures in Heterogeneous Networks With Fading” IEEE Transactions on Vehicular Technology, vol. 66, Issue 7, pp. 6060-6074, July 2017.
[37] A. Taufique, “On Analytical Modeling of Mobility Signaling in Ultra Dense Hetnets”, PhD thesis, University of Oklahoma, 2018.
[38] NTT DOCOMO, Inc., “Enhanced Mobility State Estimation by Doppler Frequency Measurements,” Qingdao, China, 3GPP Standard Contribution (R2-124007), Aug. 2012.
[39] Y. Zhu, L. Ni and B. Li, “Exploiting mobility patterns for inter-technology handover in mobile environments”, Elsevier Journal of Computer Communications, pp. 203-210, 2013.
[40] M. Joud, M. Lozano and S. Ruiz, “User Specific Cell Clustering to Improve Mobility Robustness in 5G Ultra-dense Cellular Networks”, 14th Annual Conference on Wireless On-demand Network Systems and Services (WONS), pp. 45-50, 2018.
[41] O. Semiari, W. Saad, M. Bennis and B. Maham, “Caching Meets Millimeter Wave Communications for Enhanced Mobility Management in 5G Networks”, IEEE Transaction on Wireless Communications, vol. 17, pp. 779-793, Feb 2018.
[42] H. Zhang, W. Huang and Y. Liu, “Handover Probability Analysis of Anchor-Based Multi-Connectivity in 5G User-Centric Network”, IEEE Wireless Communications Letters, pp. 1-4, 2018.
[43] M. Alhabo and L. Zhang, “Unnecessary handover minimization in two-tier heterogeneous networks”, 13th Annual Conference on Wireless On-demand Network Systems and Services (WONS), USA, 2017.
[44] L. Sun, J. Hou and T. Shu, “Spatial and Temporal Contextual Multi-Armed Bandit Handovers in Ultra-Dense mmWave Cellular Networks”, IEEE Transaction on Mobile Computing, pp. 1-16, June 2020.
[45] M. Alhabo, L. Zhang and N. Nawaz, “A Trade-off Between Unnecessary Handover and Handover Failure for Heterogeneous Networks” 23th European Wireless Conference, 2017.
[46] M. Alhabo and L. Zhang, “GRA-based Handover for Dense Small Cells Heterogeneous Networks”, IET Communications, May 2019.
[47] M.Nguyen and S. Kwon, “Geometry-Based Analysis of Optimal Handover Parameters for Self-Organizing Networks”, IEEE Transactions on Wireless Communications, vol. 19, no. 4, pp. 2670-2683, April 2020.
[48] B. Yang, X. Yang, X. Ge and Q. Li, “Coverage and Handover Analysis of Ultra-Dense Millimeter-Wave Networks with Control and User Plane Separation Architecture”, IEEE Access, 2018.
[49] C. Lee, et. al., “Prediction-Based Conditional Handover for 5G mm-Wave Networks: A Deep-Learning Approach”, IEEE Vehicular Technology magazine, vol. 15, issue, 1, pp. 54-62, Mar 2020.
[50] A. Mukherjee, “Energy Efficiency and Delay in 5G Ultra-Reliable Low-Latency Communications System Architectures,” IEEE Netw., vol. 32, no. 2, pp. 55–61, Mar. 2018.
[51] 3GPP TS 22.261, " Service requirements for the 5G system; Stage 1 (Release 16)," V16.8.0, Jun. 2019.
[52] P. Fan, J. Zhao and C. L. I, “5G high mobility wireless communications: Challenges and solutions,” China Commun., vol. 13, no. 2, pp. 1–13, Nov 2016.
[53] Y. Liu, et. al., “Novel 3-D Nonstationary MmWave Massive MIMO Channel Models for 5G High-Speed Train Wireless Communications”, IEEE Transactions on Vehicular Technology, vol. 68, pp. 2077-2086, March 2019.

[54] Liu, et. al., “3D Non-Stationary Wideband Tunnel Channel Models for 5G High-Speed Train Wireless Communications”, IEEE Transactions on Intelligent Transportation Systems, pp. 1-14, Feb. 2019.
[55] J. Yang, et. al., “An Efficient MIMO Channel Model for LTE-R Network in High-Speed Train Environment”, IEEE Transactions on Vehicular Technology, vol. 68, pp. 3189-3200, April 2019.
[56] Y. Cao, et. al., “Enhancing Video QoE Over High-speed Train Using Segment-based Prefetching and Caching”, IEEE MultiMedia, June 2019.
[57] X. Ma, et. al., “Adaptive Optimization of Multi-Hop Communication Protocol for Linear Wireless Monitoring Networks on High-Speed Railways”, IEEE Transactions on Intelligent Transportation Systems, vol. 20, pp. 2313-2327, June 2019.
[58] M. Munjal and N. Singh, “Group mobility by cooperative communication for high speed railway”, Wireless Networks Springer, pp 1-10, Jan 2019.
[59] W. Li, et al., “Performance evaluation and analysis on group mobility of mobile relay for LTE Advanced system” IEEE VTC, pp. 1-5, Sep. 2012.
[60] P. Dat, et. al., “High-Speed and Uninterrupted Communication for High-Speed Trains by Ultrafast WDM Fiber–Wireless Backhaul System”, Journal of Lightwave Technology, vol. 37, no. 1, pp. 205-217, January 2019.
[61] Wa. Luo, R. Zhang and X. Fang, “A CoMP soft handover scheme for LTE systems in high speed railway”, EURASIP Journal on Wireless Communications and Networking, June 2012.
[62] Q. Luo, W. Fang, J. Wu and Q. Chen, “Reliable broadband wireless communication for high speed trains using baseband cloud” EURASIP Journal on Wireless Communications and Networking, Sept. 2012.
[63] A. L. Yusof, B. A. Bakar, N. Yaacob and M. A. Zainali, “Mobile Relay Handover Procedure in Train For 4G LTE-Advanced Network” Journal of Telecommunication, Electronic and Computer Engineering, vol. 9, No. 2-2, pp. 49-53, 2017.
[64] Y. Sui, A. Papadogiannis and T. Svensson, “The potential of moving relays a performance analysis,” IEEE VTC, 2012.
[65] Y. Sui, A. Papadogiannis, W. Yang and T. Svensson, “Performance comparison of fixed and moving relays under co-channel interference,” IEEE GLOBECOM Workshops, 2012.
[66] R. Ma, et. al., “FTGPHA: Fixed-Trajectory Group Pre-Handover Authentication Mechanism for Mobile Relays in 5G High-Speed Rail Networks”, IEEE transactions on vehicular technology, vol. 69, no. 2, pp. 2126-2140, Feb 2020.
[67] J. Zhoa, et. al, “High-speed based adaptive beamforming handover scheme in LTE-R”, IET Communications, vol. 12, issue 10, pp. 1215-1222, 2018.
[68] B. Lannoo, D. Colle, M. Pickavet and P. Demeester, “Radio-over-fiberbased solution to provide broadband internet access to train passengers [topics in optical communications]”, IEEE Communications Magazine, vol. 45, no. 2, pp. 56–62, Feb 2007.
[69] P. Sun, N. AlJeri and A. Boukerche, “An Energy-Efficient Proactive Handover Scheme for Vehicular Networks Based on Passive RSU Detection”, IEEE Transactions on Sustainable Computing, vol. 5 , Issue: 1 , pp. 37-47, 2020.
[70] H. Lundqvist, G. P. Koudouridis and X. Gelabert, “Joint tracking of groups of users with uplink reference signals,” IEEE 22nd International Workshop on Computer Aided Modeling and Design of Communication Links and Networks (CAMAD), pp. 1–5, 2017.
[71] Xu, Huichen, Xiangyang Wang, Wenxiu Liu and Wenbin Shao, “An Uplink Based Mobility Management Scheme for 5G Wireless Network.” IEEE International Conference on Communications (ICC), pp. 1–6, 2019.
[72] 3GPP TS 36.300, “(E-UTRA) and (E-UTRAN); Overall description; Stage 2 (Release 15)” V15.0.0, Section 10, pp. 93-143, Dec 2017.
[73] 3GPP TS 38.300, "NR; NR and NG-RAN Overall Description; Stage 2 (Release 15)," V15.5.0, Mar 2019.
[74] 3GPP TR 36.836, “Study on mobile relay for Evolved Universal Terrestrial Radio Access (E-UTRA); (Release 12), June 2014.
[75] A. Krendzel, “LTE-A Mobile Relay Handling: Architecture Aspects”, European Wireless, pp, 1-6, 2013.
[76] 3GPP TR 36.826, V11.3.0, “Relay radio transmission and reception for Evolved Universal Terrestrial Radio Access (E-UTRA); (Release 11), Jul 2013.
[77] K. Wehrle, M. Günes, and J. Gross, “Modeling and Tools for Network Simulation” Springer Berlin Heidelberg, 2010.
[78] 3GPP TR 36.814, “Further advancements for E-UTRA physical layer aspects (Release 9),” V9.0.0, Mar 2010.
[79] 3GPP TS 36.331, “E-UTRA Radio Resource Control (RRC); Protocol specification (Release 9)”, v9.2.0, Mar 2010.
[80] 3GPP TS 36.133, “Requirements for support of radio resource management (Release 9),” v9.15.0, Mar 2013.
[81] 3GPP TS 36.211, “Physical channels and modulation (Release 15),” v15.1.0, Mar 2018.
[82] 3GPP TS 36.213, “Evolved Universal Terrestrial Radio Access (E-UTRA); Physical layer procedures”, Table 7.1.7.2.1-1, Mar 2018.
[83] M. S. Mushtaq, S. Fowler and A. Mellouk. “Power Saving Model for Mobile Device and Virtual Base Station in the 5G Era.” IEEE International Conference on Communications (ICC), pp. 1–6, 2017.
[84] M. Lauridsen et., “An Empirical LTE Smartphone Power Model with a View to Energy Efficiency Evolution” Inter technology Journal, vol. 18, pp. 172-193, 2014.

[85] 3GPP R1-091791, “Handover performance in a Manhattan scenario,” Huawei, May 2009.
[86] H. Holtkamp, et. al., “A Parameterized Base Station Power Model”, IEEE Communications Letters, vol. 17, no. 11, pp. 2033-2035, Nov 2013.
[87] S. Sesia, I. Toufik and M. Baker. “LTE--the UMTS Long Term Evolution: From Theory to Practice”, (2nd Ed.) Wiley, 2011.
[88] 3GPP TS 38.211, “Physical channels and modulation (Release 16),” v16.1.0, Mar 2020.
[89] X. Gelabert, C. Qvarfordt, M. Costa, P. Kela and K. Leppänen, “Uplink Reference Signals Enabling User-Transparent Mobility in Ultra Dense Networks”, in proc. PIMRC, Sept 2016.
[90] 3GPP TR 38.804, “Study on new radio access technology: Radio interface protocol aspects,” March 2017.
[91] Qualcomm, “Comparative Power Analysis between UL and DL-based Mobility", 3GPP TSG-RAN WG1 #86bis, Oct 10-14, 2016.
[92] Sony, “UL Mobility in CONNECTED ACTIVE mode", 3GPP TSG-RAN WG1 #88, Feb 13-17, 2017.
[93] D. L. Perez, I. Guvenc and X. Chu, “Theoretical Analysis of Handover Failure and Ping-Pong Rates for Heterogeneous Networks”, IEEE International Conference on Communications (ICC), pp. 6774-6779, 2012.
[94] D. L. Pérez, I. Guvenc and X. Chu, “Mobility Management Challenges in 3GPP Heterogeneous Networks,” IEEE Communications Magazine, vol. 50, no. 12, Dec 2012, pp. 70–78.
[95] 3GPP TR 36.839, Evolved Universal Terrestrial Radio Access (E-UTRA); Mobility enhancements in heterogeneous networks, 2012.
[96] H. Chen, S. Jin, H. Hu, Y. Yang, D. López-Pérez, I. Guvenc and X. Chu, “Mobility and handover management”, in Heterogeneous Cellular Networks: Theory, Simulation and Deployment, Cambridge University Press, pp. 245–283, 2013.
[97] H. Park, et. al, “Is It Possible to Simultaneously Achieve Zero Handover Failure Rate and Ping-Pong Rate?”, Available online https://arxiv.org/ftp/arxiv/papers/1511/1511.00797.pdf , pp. 1-15, Sept 2020.
[98] J. Zhang et al., "PoC of SCMA-Based Uplink Grant-Free Transmission in UCNC for 5G," IEEE Journal on Selected Areas in Communications, vol. 35, no. 6, pp. 1353-1362, June 2017.
[99] O-RAN-WG1-O-RAN Architecture Description v1.0 - February 2020. (Available on-line at: https://www.o-ran.org/specifications)
[100] W. Lei, Y. Ye and M. Xiao, ” Deep Reinforcement Learning-Based Spectrum Allocation in Integrated Access and Backhaul Networks” IEEE Transactions on Cognitive Communications and Networking, Vol. 6, Issue: 3, pp. 970-979, Sept. 2020.
[101] 3GPP TS 38.840, " Study on User Equipment (UE) power saving in NR (Release 16)," V16.0.0, June 2019.
[102] J. Zander and S. Kim, “Radio Resource Management for Wireless Networks” , Appendix B: Simulation Models, Appendix C: RUNE Tutorial, Artech House, Norwood, U.S.A. 2001.
[103] M. Tayyab, X. Gelabert, C. Qvarfordt and G. Hui, “LTE UL Simulator Toolbox-A user’s guide”, Huawei internal simulator, Huawei technologies Sweden and Finland, 2019.
[104] A. Anpalagan, M. Bennis and R. Vannithamby, “Design and Deployment of Small Cell Networks”, Cambridge University Press, 2015.
[105] G. Zhou and P. Legg, “An Evolved Mobility Robustness Optimization Algorithm for LTE Heterogeneous Networks,” IEEE 77th Vehicular Technology Conference (VTC Spring), pp. 1–5, 2013.
[106] Z. Guohua, P. Legg and G. Hui, “A network controlled handover mechanism and its optimization in LTE heterogeneous networks,” IEEE Wireless Communications and Networking Conference (WCNC), pp. 1915–1919, 2013.
[107] C. Qvarfordt and P. Legg, “Evaluation of LTE HetNet deployments with realistic traffic models,” IEEE 17th International Workshop on Computer Aided Modeling and Design of Communication Links and Networks (CAMAD), pp. 307–311, 2012.
[108] G. P. Koudouridis, H. Gao and P. Legg, “A Centralised Approach to Power On-Off Optimisation for Heterogeneous Networks,” IEEE Vehicular Technology Conference (VTC Fall), pp. 1–5, 2012.
[109] G. Hui and P. Legg, “Soft Metric Assisted Mobility Robustness Optimization in LTE Networks,” International Symposium on Wireless Communication Systems (ISWCS), pp. 1–5, 2012.
[110] G. Hui and P. Legg, “LTE Handover Optimisation Using Uplink ICIC,” IEEE 73rd Vehicular Technology Conference (VTC Spring), pp. 1–5, 2011.
[111] P. Legg, G. Hui and J. Johansson, “A Simulation Study of LTE Intra-Frequency Handover Performance,” IEEE 72nd Vehicular Technology Conference - Fall, pp. 1–5, 2010.

Appendices

A1. Mobility Simulator Description

The in-house mobility simulator is based on an open-source RUNE simulator [102] but it has been evolved during the last ~9-10 years at Huawei Sweden and the last 3 years at Huawei Finland [103]. The simulator is advanced to the latest LTE DL-HO as well as the proposed UL-HO procedure and new metrics are included to compute signaling overheads and the power consumption for both DL-HO and UL-HO. This simulator is very important to analyze the complex mobility problems for LTE networks. Many research works have been published by Huawei using this simulator (i.e. some article publications using this simulator are [26][104][105][106][107][108][109][110][111]).

A1.1 Current Features of the LTE Mobility Simulator

The LTE system-level mobility simulator is a Frequency Division Duplex (FDD) and Time-based simulator with a 1-ms transmission time interval (TTI) granularity. Traffic sources at the IP level are web browsing, File Transfer Protocol (FTP), near real-time video (NRTV), VoIP (Speech), Gaming, Full Buffer, and Burst traffic. Packet Data Convergence Protocol (PDCP), RLC and MAC entities are also modeled. The physical layer is implicitly modeled using link-to-system curves, mapping the Signal-to-interference-plus-noise ratio (SINR) to bit error rate (BER). Shadow fading and fast fading are also considered. Both UL and DL transmissions are possible for the control plane, but user plane transmissions are either UL or DL. Only Intra-frequency (no inter-frequency/inter-RAT measurements) measurements are considered. Only the RRC_CONNECTED state (no RRC_IDEL state) is assumed. UE Measurement (using RSRP and reference signal received quality (RSRQ)), RACH model (based on LTE Release 8) and RLF are also implemented. In-sync and out-sync measurements are implemented, along with timers T310 and counters N310 & N311 as described in Figure 4. All of these features are presented in Fig. A1 and more details of the system simulation model are also presented in Publication II.

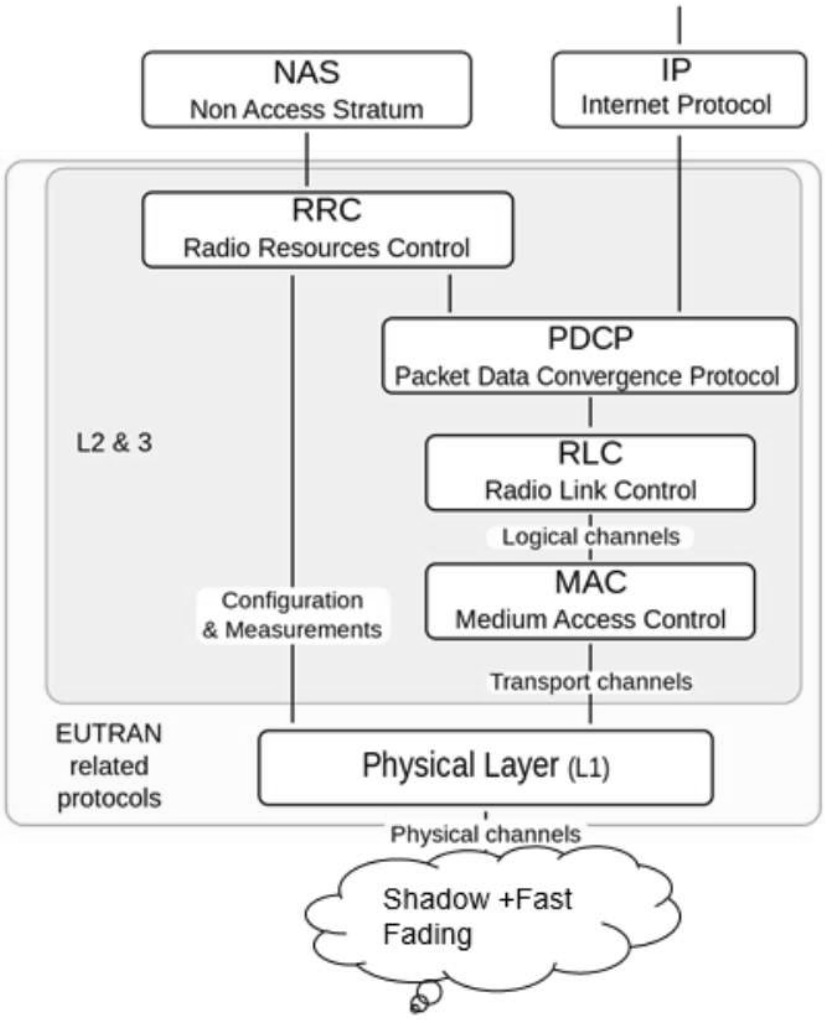

Figure A1. Current features of MATLAB based mobility simulator.

A1.2 Main Parameters and Structure of the Simulator

The main configuration parameters of the simulator include deployment, propagation, HO, UE, cell, channel and other related parameters as shown below:

Deployment Parameters:

- Cell radius
- Sector per site
- Number of sites
- Number of cells

Propagation Parameters:

- Antenna gain
- Antenna pattern (3D model)
- Path loss model
- Shadowing

HO Parameters:

- Time to trigger (TTT)
- A3 offset
- Filtering coefficient

UE Parameters:

- UE max. Power
- UE speed

Cell Parameters

- Inter site distance (ISD)
- eNB DL power
- eNB noise figure

Channel and Other related parameters

- Subcarrier spacing
- Bandwidth (5MHz FDD) at 2.1 GHz
- Simulation time (60s)
- Time granularity (1 ms)
- Position update interval

The structure of the simulator is shown in Fig. A2. The simulator initializes all of the parameters. If it is a time to move the UE, it updates the UE position, gain matrix and UE tracking set, otherwise, it starts monitoring the RLF directly. Then, it performs the UE measurement and updates the HO timer and traffic sources. Different procedures are performed at each layer level for both eNB and UE. Then the simulator handles the UL RRC and RRC reestablishment. Finally, the simulator checks if there are more TTIs to simulate, if not, it starts collecting the stats related to the HO procedure.

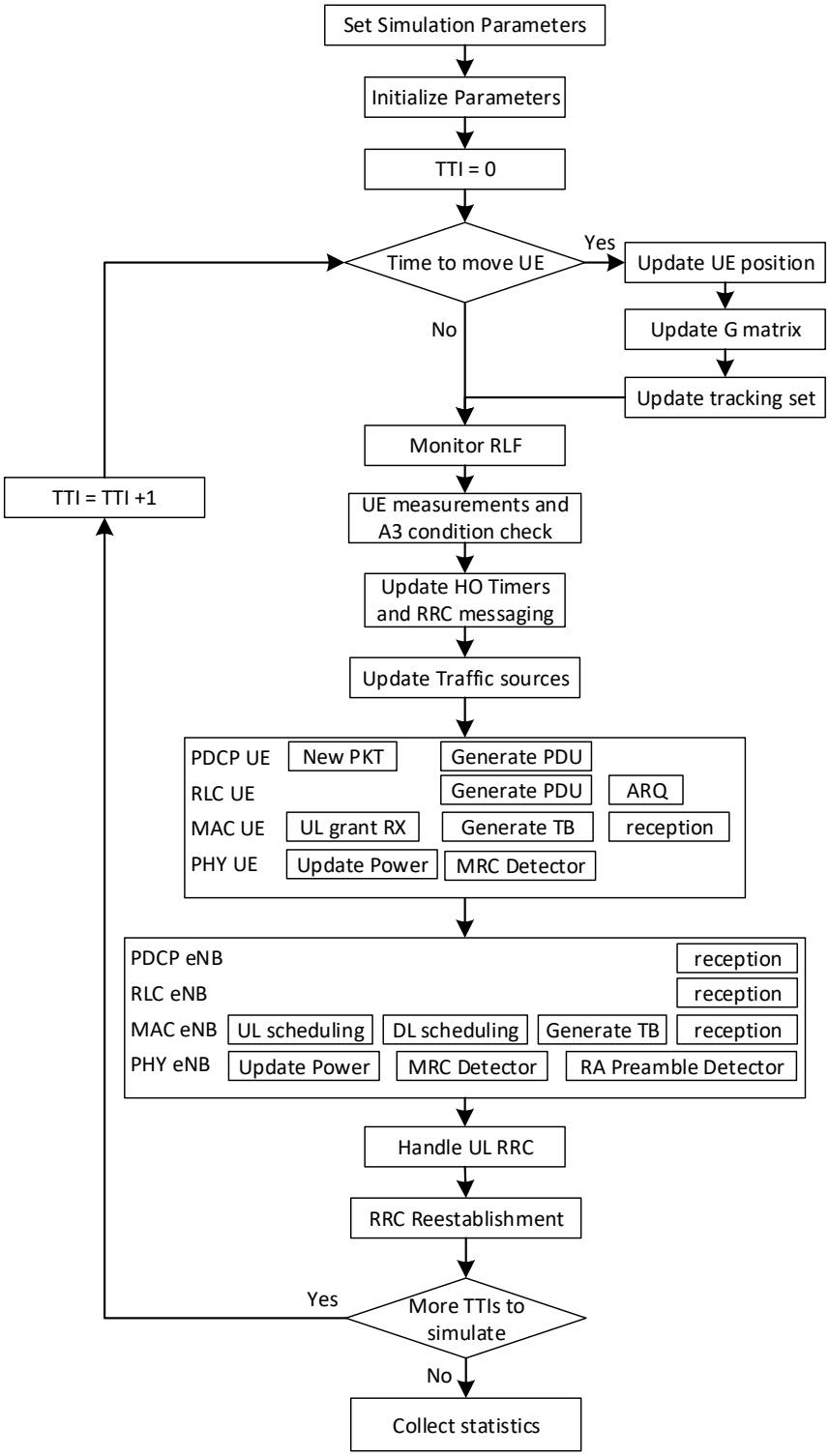

Figure A2. Structure of the mobility simulator.

A1.3 System Model

A cell wrap-around model for homogeneous interference conditions is considered. The main antenna orientation with three sectors per site is given by the black arrows in Fig. A3. In this figure, the number of sectors per site is three and the red circles show the site location. The number of cells (N) per cluster is 48 according to (1), where i and j are non-negative integers. In this example, $i = 4$ and $j = 4$.

$$N = i^2 + ij + j^2 \quad (1)$$

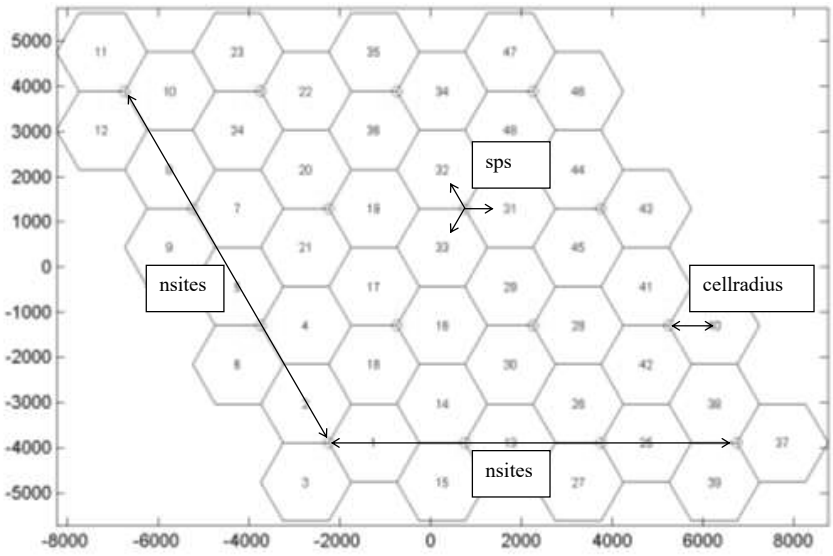

Figure A3. An example of the cell configuration.

A1.3.1 Distance Attenuation

The distance path loss is based on (2) where d is the distance between the transmitter and receiver given in kilometers as shown in Fig. A4. The figure shows that as the distance between transmitter and receiver increases, path loss increases.

$$L_{dB} = L_{const} + \alpha . log\ (d) \quad (2)$$

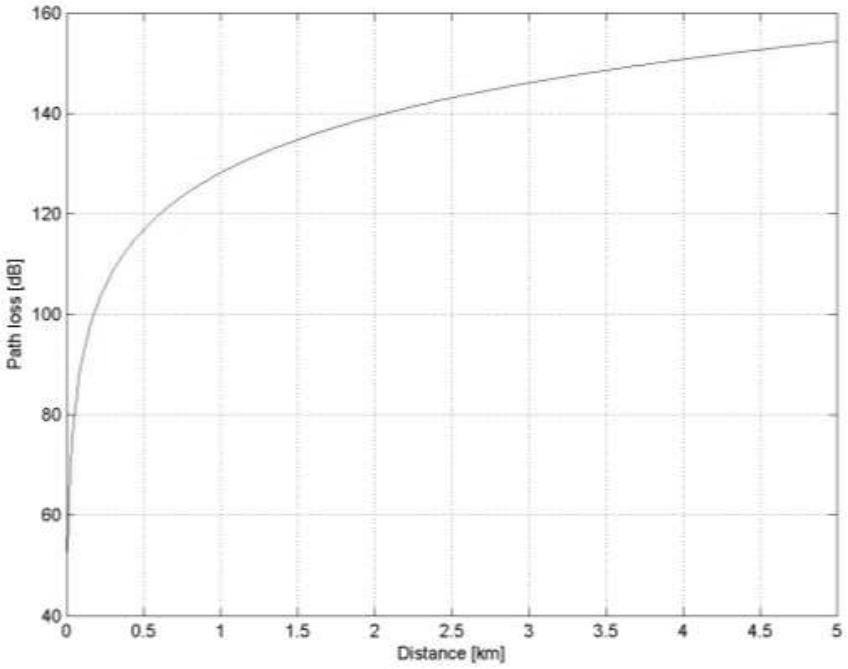

Figure A4. Example of the distance attenuation.

A1.3.2 Antenna Gain

In the simulator, the sites are equipped with three sectors. For a three-sector site, a directional antenna is used. The UEs are using an omnidirectional antenna with an antenna gain of 0 dB and therefore we have not considered the antenna direction or gain of the UE. The directional antenna pattern used for the eNB is shown in Fig. A5. Similarly, the omnidirectional antenna pattern for the UE is presented in Fig. A6. The antenna gain is calculated as the antenna gain vector at the angle of the UE's position. The angle is the difference between the main direction of the antenna and the direction between the eNB and the UE. The angular antenna gain can be calculated using Fig. A7.

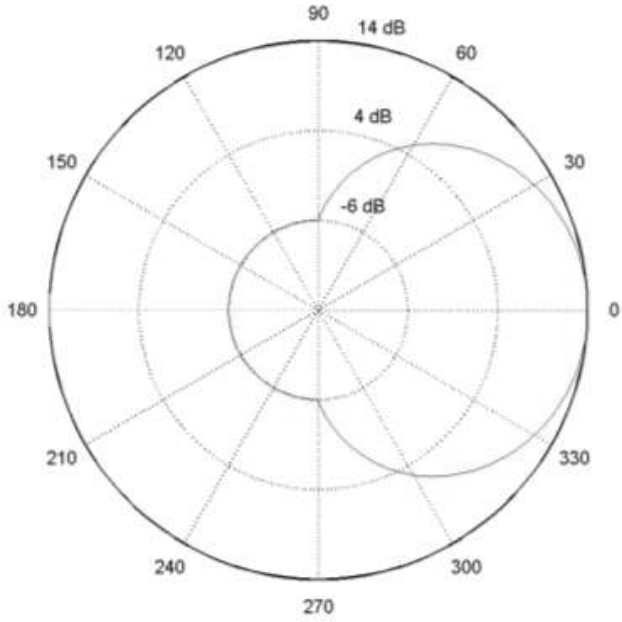

Figure A5. Directional antenna pattern.

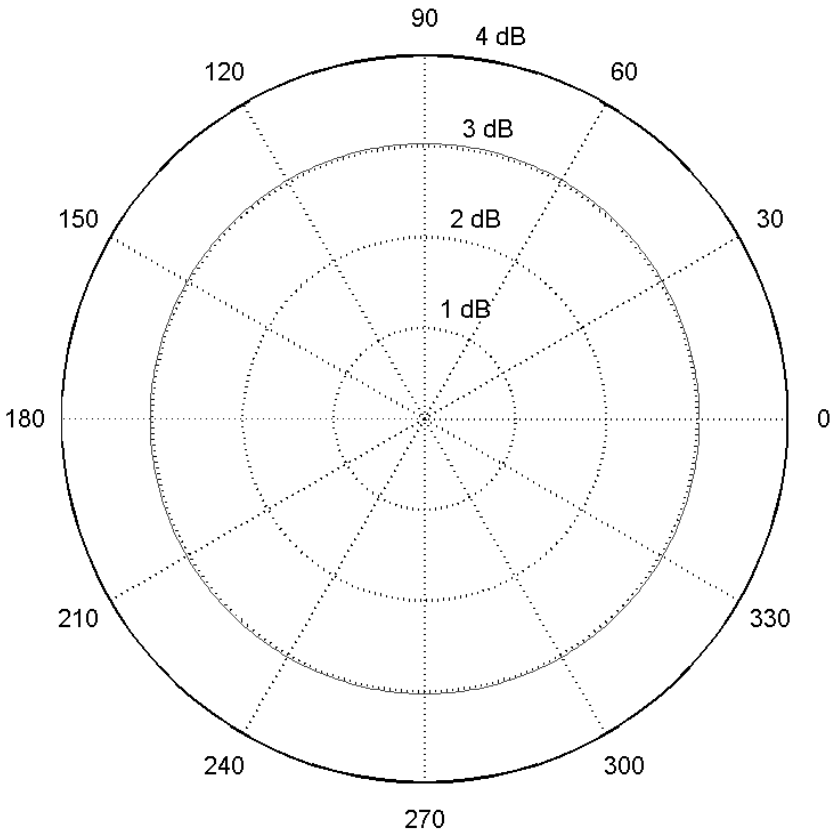

Figure A6. Omnidirectional antenna pattern.

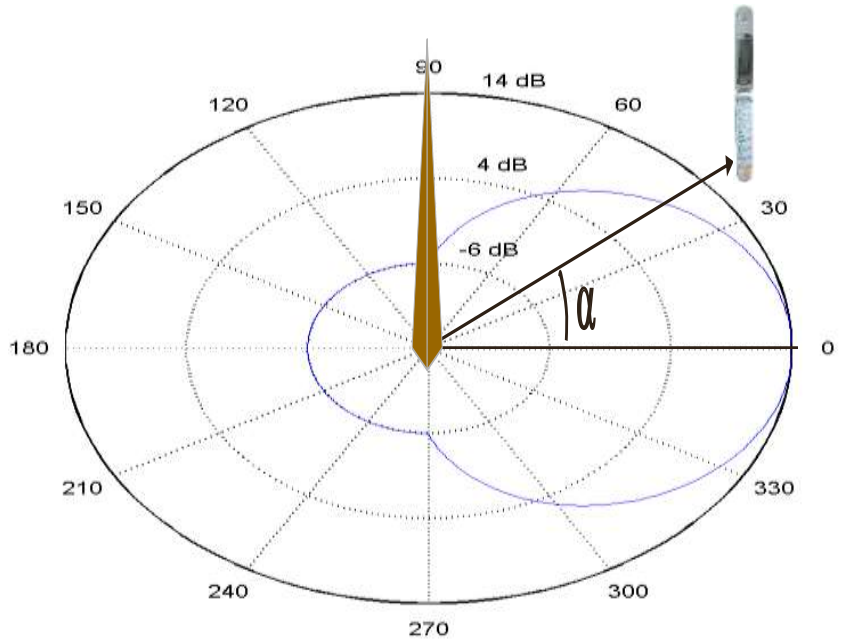

Figure A7. Angular antenna gain calculation.

A1.3.3 Wrap Around

A one-tier wrap-around model used in the simulator is shown in Fig. A8. Eight copies of the simulated area are added and the copy that gives the highest path gain, including both the distance attenuation and the angular antenna gain, is selected. The red arrow represents the selected copy of the cell that is used for calculating the received power to that cell.

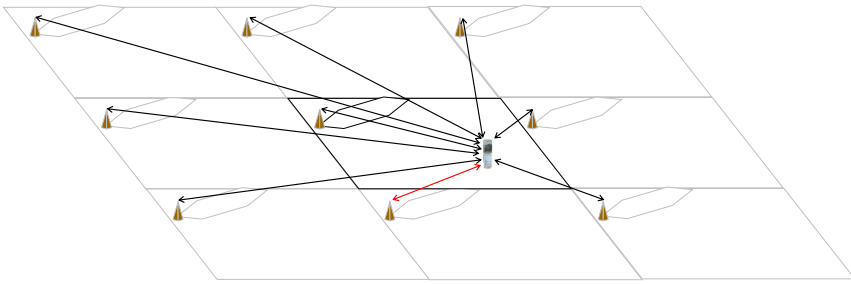

Figure A8. An example of the wrap-around technique.

A1.3.4 Shadow Fading

To generate the shadow fading of the different UEs that has a specific correlation in the area, a correlated log-normal map is generated with mean 0 and standard deviation 1 used as shown in Fig. A9.

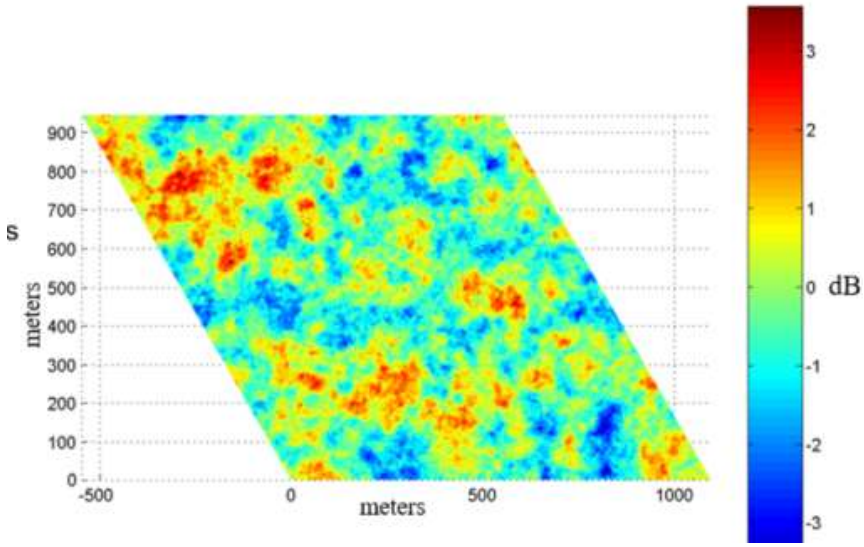

Figure A9. An example of shadow fading.

A1.3.5 Total Path Gain

The total path gain (in dB) is obtained with the values between each UE and each cell calculated as:

$$G_{i,j} = \max_{WrapAroungCopies}(G_{distance} + G_{antenna}) + G_{ShadowFading} \qquad (3)$$

Where, $G_{distance}$ is the path gain, $G_{antenna}$ is the antenna gain and $G_{ShadowFading}$ is the shadow fading gain. The UE position is wrapped into the geographical vicinity of the cell it is connected to.

A1.3.6 UE Models

A uniformly distributed position is given to the UE in the simulator that is a complex vector spanning the simulation area. In the simulator, the simulation area is a rhombic area spanning all the cells. The UE is also given an initial velocity and direction. With a certain period, the UE's position and velocity are updated according to the mathematical model presented in [102]. UE mobility possibilities in the simulator are:

- CONSTANT_SINGLE_SPEED_AND_DIRECTION
- CONSTANT_SINGLE_SPEED_AND_RANDOM_DIRECTION
- RANDOM_SPEED_AND_DIRECTION
- CONSTANT_MULTI_SPEED_AND_RANDOM_DIRECTION
- STREET_MOBILITY

The UE mobility model with RANDOM_SPEED_AND_DIRECTION is shown in Fig. A10. In this thesis, we used the CONSTANT_SINGLE_SPEED_AND_RANDOM_DIRECTION mobility model. UEs are moved on each specified "UE position update interval" according to the above mentioned mobility models. At each UE movement interval, the handover algorithm is also executed. After moving the UE it might do a handover to another cell that

has become better than the old cell, and to visualize the connection the UEs we will wrap the UE to the position with the shortest geographical distance from the new serving cell. Eight copies of the UE are generated and the position where the distance to the eNB is the shortest is selected.

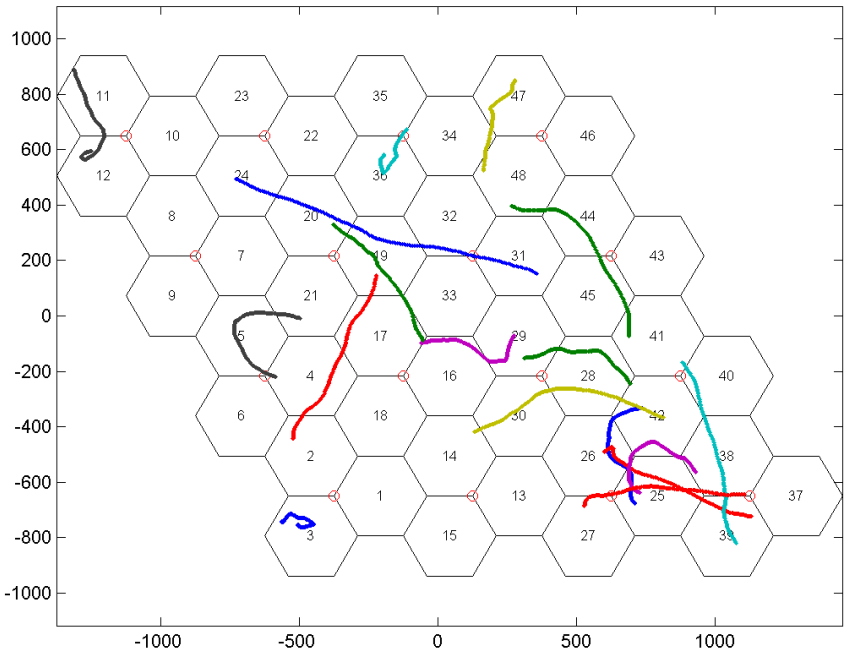

Figure A10. Example of UE mobility model.

A1.4 Link-to-System Mapping

As system-level simulation doesn't include the real link processing, a link-to-system level interface is needed to predict the instantaneous performance of the link layer. One of the most important models is how we map the system simulation channel quality results to an MAC PDU error probability, to feed the HARQ functionality with information. An overview of the interface is shown in Fig. A11.

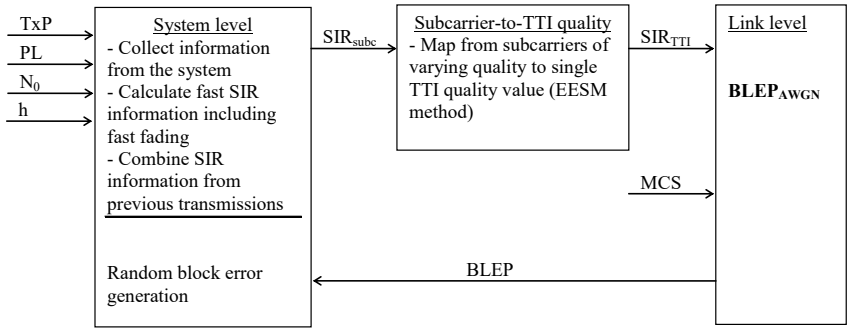

Figure A11. Link-to-system interface overview.

The inputs from the system simulations are the transmission power (TxP), path loss (PL), noise level (N_o) and fast fading (h) information which is used to generate a channel quality per subcarrier for the transmission of an MAC PDU. In Fig. A12, a simple model of how the signal quality is assessed in the simulation is shown. Each UE transmits and the signal is received by all eNBs in the network. The own signal is shown in the top row, where the received signal strength is calculated including both slow and fast fading. The interference is calculated using the power of each transmitting UE and the path gain. For some of the interferers, we also add fast fading information to the interference calculation. In the final stage, the signal information is divided with the sum of all interference contributions and also the noise per subcarrier to obtain the channel quality.

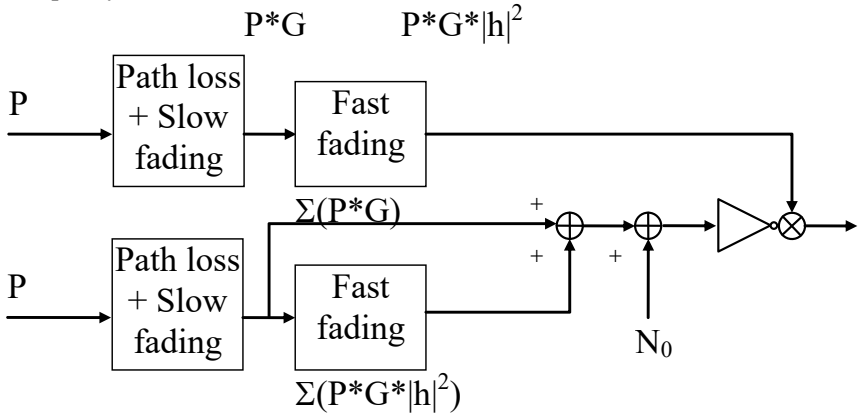

Figure A12. Channel quality calculation.

The fast fading information is obtained by extracting information in the time domain from a pre-generated complex channel response vector and through FFT, we get the frequency response of the channel. Correlated Rayleigh channel samples are generated. We can then apply different models, e.g.: ['VehA'; 'PedA'; 'PedB'; 'AWGN‘; ‘TU’]. A subset of the channel vector is shown in Fig. A13. Each new UE gets a pointer in this vector for the strongest received cell to obtain the current value of the channel. For each tap of the receiver, another pointer to the channel vector is added. The information from the channel response vector is extracted for each link and tap and multiplied by the power value of the tap. Then, using the delay values of the tap we calculate the frequency response from each of the active links. Combining the information from all the subcarriers that are involved in the transmission to generate an appropriate average transmission quality for this TTI is done using the Exponential Effective SIR Mapping function.

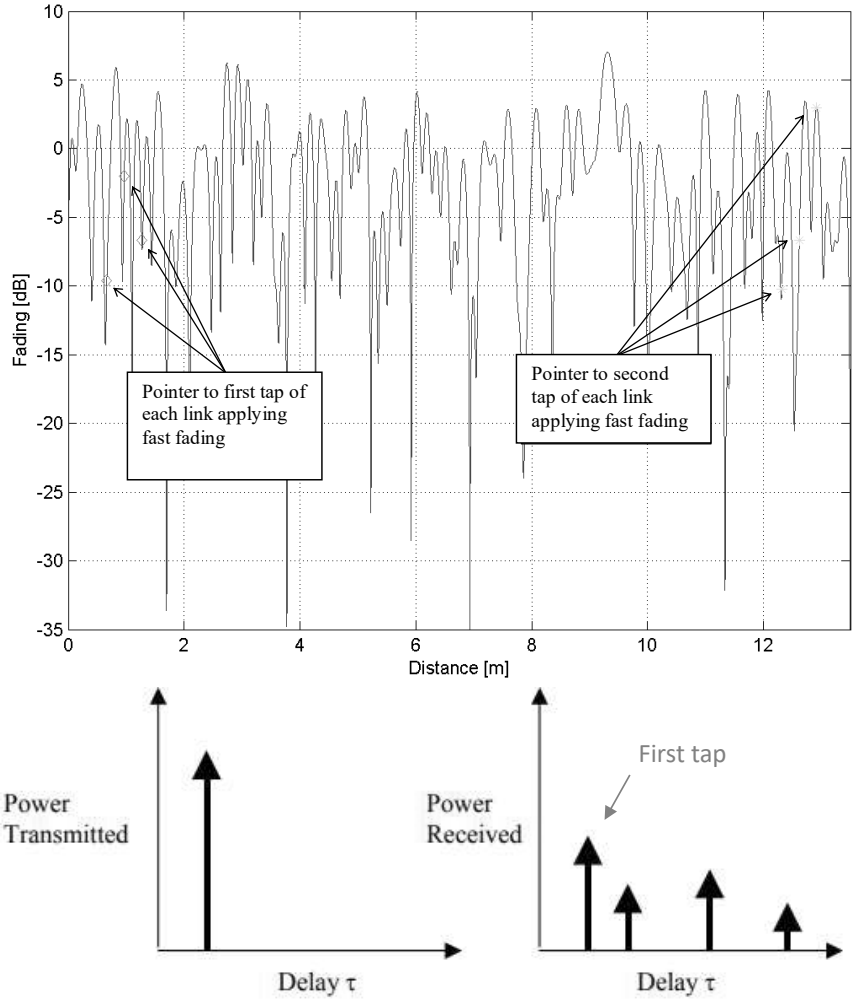

Figure A13. An example of the fast fading in the simulator.

As the link level curves are generated assuming a frequency flat channel response at a given SINR, an effective SINR is required to accurately map the system-level SINR to the link-level curves to determine the resulting block error probability (BLER). In our simulation platform, we use Effective Exponential SNR Mapping (EESM) as the mapping method. EESM provides a method of mapping post-processing SINR in a fading channel to one effective SINR in AWGN. The effective SINR is used to look up the BLER curve. The predicted BLER is close to the real link simulation results. The EESM method has been widely used and is effectively an averaging method where the SIR values are averaged in the dB domain. In Fig. A14, the link level results are plotted for different PRB sizes as an example of the lookup from the effective SIR value for the TTI to the error probability of the transmission. A random check (rand < BLER) then determines whether the MAC PDU was correctly received or not.

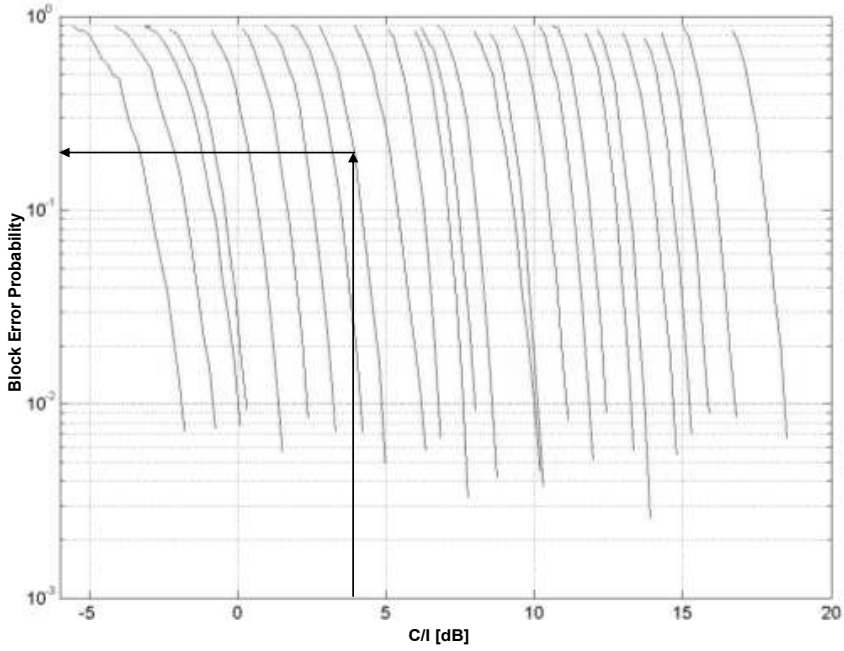

Figure A14. An example of link-to-system mapping using EESM method.

A1.5 HO Statistics

We can obtain the following statistics for HOs using this simulator:

- HO interruption time (HOIT)
- HO rate
- Mean time between HO (MTBH)
- Number of A3 events
- Number of TTT events
- Number of HOs
- Number of HO failure events
- Number of measurement reports
- Number of ping pongs
- Number of T310 reports
- Ping pong rate
- HO failure type breakdown: F0…F7
- Signaling rate
- Transmitted power consumption
- Received power consumption

The MTBH is the ratio between the total simulation time and the number of triggered HO events. HOIT is the time whereby the user plane is unable to deliver packets to and from the UE. The signaling rate provides the information of air-interface signaling transmitted/received during HO. The received power

consumption is calculated using the simulator considering shadow and fast fading and then the receiver power consumption model is used to calculate the supply average received power consumption.

A1.6 Simulator Calibration with 3GPP Calibrated Simulator

We calibrated our simulator with Huawei's internal 3GPP calibrated simulator in order to get comparable and trusty simulation results. Here we show the calibration results of our mobility simulator with a 3GPP celebrated simulator. We choose the 3GPP homogeneous macro 1 scenario [78] for calibration as given in Table 1. More detailed parameters for large-scale calibration are contained in Table 2:

Table 1. 3GPP case 1

Simulation Cases	Carrier frequency (GHz)	ISD (meters)	bandwidth (MHz)	Penetration Loss (dB)	Speed (km/h)	Additional Simulation Parameters
3GPP case 1	2.0	500	FDD:10+10	20	3	Table A.2.1.1-2

Table 2. Parameters for large-scale calibration

Parameter		Assumptions
Macro Cellular scenario		Case 1: 500m
Carrier Frequency / Bandwidth		2GHz / 10Mhz
Macro Cellular layout		Hexagonal grid, wrap-around ● HMesh:19sites, 3 cells per site, ● SMesh: 16sites, 3 cells per site,
UE distribution		Uniformly in geography area, Average 500 UEs/cell
Minimum distance between UE and macro eNB		35m (Considered in path loss calculation but not in UE distribution to keep consistency of both simulators)
TX power (Ptotal)	Cell	46dBm
	UE	23dBm
Antenna gain(horizontal) (For 3-sector cell sites with fixed antenna patterns)		$A_H(\varphi) = -\min\left[12\left(\frac{\varphi}{\varphi_{3dB}}\right)^2, A_m\right]$ φ_{3dB} = 70 degrees, A_m = 20 dB
Antenna gain	cell	14dBi
	UE	0dBi
Noise Figure	cell	5dB
	UE	9dB

Distance-dependent path loss for macro to UE		L= 128.1+37.6log10(R) for 2GHz, R in km
Lognormal Shadowing with shadowing standard deviation		0 dB/8 dB
Shadowing corre-lation	Between sites	0.5
	Between sectors	1.0
Shadowing correlation distance		50m
Penetration Loss		20dB

Path gain and geometry CDF are shown in Fig. A15 without shadow fading. Both the path gain and geometry CDF are almost the same for both simulators (i.e. mobility simulator used in this thesis and the 3GPP calibrated simulator). There is therefore no problem in the implementation of path loss calculation, network topology, antenna gain calculation, and UE distribution.

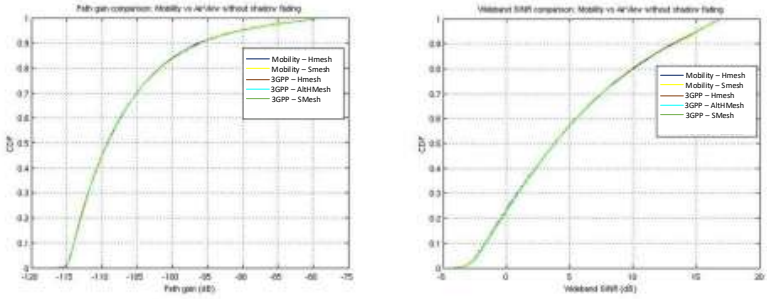

Figure A15. Large-scale comparison without shadow fading (Left: Path gain; Right: Geometry).

Path gain and geometry CDF are shown in Fig. A16 including shadow fading. Overall, there is around 2dB path gain difference between our mobility simulator and the 3GPP calibrated simulator. This is because of the shadow fading models used for calibration that are different in both simulators. The mobility simulator uses a shadow fading map, where the close UEs are considered with correlation. While in the 3GPP simulator, the UE shadow fading correlation is not considered. Other parameters are the same in both simulators. The mobility simulator geometry distribution is the same as the 3GPP simulator.

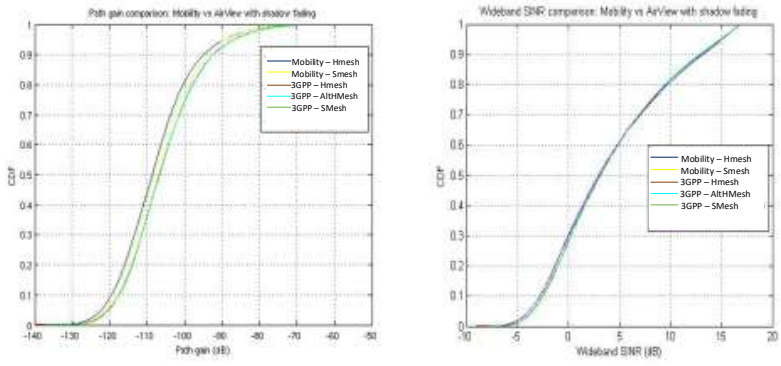

Figure A16. Large-scale comparison with shadow fading (Left: Path gain; Right: Geometry).

In conclusion, no big issue is found during the large scale calibration of the mobility simulator with the 3GPP calibrated simulator, with/without shadow fading. So there is no problem in the implementation of path loss calculation, network topology, antenna gain calculation, and UE distribution.

Aalto-DD 43/2021

ISBN 978-952-64-0319-9 (printed)
ISBN 978-952-64-0320-5 (pdf)
ISSN 1799-4934 (printed)
ISSN 1799-4942 (pdf)

Aalto University
School of Electrical Engineering
Department of Communications and Networking
www.aalto.fi

BUSINESS + ECONOMY

ART + DESIGN + ARCHITECTURE

SCIENCE + TECHNOLOGY

CROSSOVER

DOCTORAL DISSERTATIONS